NASA CR- 165,812

LANGLEY RESEARCH CENTER

3 1176 00501 5970

NASA Contractor Report 165812

USE OF TWO-DIMENSIONAL TRANSMISSION PHOTOELASTIC
MODELS TO STUDY STRESSES IN DOUBLE-LAP
BOLTED JOINTS

M. W. Hyer and D. H. Liu

VIRGINIA POLYTECHNIC INSTITUTE AND STATE UNIVERSITY
Department of Engineering Science and Mechanics
Blacksburg, Virginia   24061

NASA

National Aeronautics and
Space Administration

Langley Research Center
Hampton, Virginia 23665

NF01335

TABLE OF CONTENTS

LIST OF FIGURES

LIST OF TABLES

iv

LIST OF APPENDICIES

LIST OF SYMBOLS

c	calibration constant for photoelastic material, MPa/fringe (psi/ fringe)
C	distance from center of lead hole to isotropic point location, mm (in.)
D	hole diameter, mm (in.)
e	distance from the center of the second hole to the free-end, mm (in.)
E	distance between hole centers, mm (in.)
F	a function used to illustrate the finite-difference scheme
N	fringe order 0, ¹⸴, 1, 1½, ...
P	total tensile load applied to joint, N (lb) $P = P_1 + P_2$
P_1	load reacted by the lead hole, N (lb)
P_2	load reacted by the second hole, N (lb)
S	bearing stress, P/2Dt, MPa (psi)
t	thickness of inner lap, mm (in.)
W	width of joint, mm (in.)
x	coordinate perpendicular to joint centerline
y	coordinate parallel to joint centerline
Δx	increment in x-direction coordinate
Δy	increment in y-direction coordinate
θ	principal stress direction measure relative to + x direction
σ_1, σ_2	principal stresses, MPa (psi)
σ_x, σ_y, τ_{xy}	stress components in x-y coordinate system, MPa (psi)
σ_{gross}	gross stress, P/Wt, MPa (psi)

INTRODUCTION

For some time there has been an interest in the effects of through-the-thickness holes and other discontinuities in plates. From a practical point of view there is generally no way discontinuities in plates can be avoided. This is particularly true in regions where plates must be connected to other structural members. Because of associated stress concentrations, failure is most apt to occur at these discontinuities. Thus attention has been focused on regions of discontinuities, specifically connector regions. The work reported herein is a further study of connector regions. It is a study of stresses around multiple-hole connectors and of the influence of connector geometry on these stresses. The study concentrates on the stress distribution in two-hole connectors in a double-lap joint configuration. The two holes are in tandem, or series, and the joint is subjected to tensile loads along the line connecting the centers of the two holes. The load is transferred from one lap to the other by way of a snug-fitting pins. Figure 1 shows details of the joint configuration studied and introduces some of the nomenclature. The geometric quantities which were felt to influence the stress distribution in the joint were the width, W, of the joint, the hole diameter, D, the distance between the holes, E, and the distance from the second hole to the free end, e. For such joint configurations the thickness of the inner lap, t, is generally made twice the thickness of each of the outer laps. This is done to maintain a balance of stiffness in the joint.

A motivating factor for this study was a previous experimental

1

study [1,2] of double-lap double-hole joints fabricated from graphite-epoxy fiber-reinforced composite material. The material was quasi-isotropic and of the many joints tested to failure, a high percentage of joints failed in net-section tension at the lead hole in the thicker inner lap. This effect was practically independent of joint width or hole diameter and is typical of the failure of brittle materials. (In this discussion lead hole refers to the hole in a particular lap which reacts the applied load first. The term second hole refers to the other hole in tandem. Obviously the lead hole for the inner lap is the second hole for the outer laps and vice versa.) For brittle materials, like fiber-reinforced composites, no yielding occurs and high net-section loads lead to a sudden catastrophic failure. For ductile materials, such as aluminum, the danger of net-section failure is lessened by the yielding of the materials. When one area of a loaded structural component is overstressed, the material yields and transfers some of the load to another region of the component. The question arises as how possibly the geometric parameters associated with the joint design can be chosen to minimize net-section stresses, thereby avoiding catastropic net-section tension failures of brittle materials. The work presented here is aimed at answering this question. The work is not intended to answer the question specifically but rather it is intended to clarify the picture of the stress distribution around the holes in isotropic materials. This stress distribution can then be used with a failure criterion pertinent to isotropic composite materials, such as the ones promoted in [3], and information regarding failure can be obtained. The study here is strictly experimental, using two-dimensional isotropic

transmission photoelastic models of the joints to determine the stresses.

This report describes the philosophy behind using photoelastic models, as opposed to analytical techniques, and discusses some of the philosophy of the particular models used here. Some aspects of the models are felt to be unique and deserve attention. The machining of the models was an important aspect of the study and a portion of this report is devoted to discussing that facet. The fixtures used to load the joints were of the type normally associated with tensile testing. However, the loads needed to be transmitted to the photoelastic model in such a fashion as to establish a known uniform far-field stress away from the region of interest, namely the connector region. The mechanism to transmit the loads smoothly and the rest of the experimental equipment are described.

An indication of typical photoelastic data obtained from the models is illustrated. While presenting these photoelastic data, the presence and importance of a photoelastic isotropic point is discussed. This isotropic point was not necessarily expected to occur. However it occurred and it was located on the model centerline partway between the two holes. By the nature of the joint stresses, the location of this isotropic point between the holes was related to the percentage of total load reacted by each pin in the joint. Generally the problem of determining the reaction at each hole is a statically indeterminate one. Without resorting to strain (or displacement) measurements, determining the reaction at each hole is impossible. As illustrated, the isotropic point can be used to circumvent this problem. A separate experiment is

3

required, however, and this experiment is described.

After these discussions, attention is given to obtaining numerical results. Since photoelastic data yield only information concerning the principal stress difference and the principal stress direction, other information is needed to obtain the complete picture of the plane-stress stress field in the connector region. The approach taken here was to use an overdetermined solution of the plane-stress equilibrium equations in finite-difference form. These equations together with the photoelastic data gave the desired stress state. That approach is described and the governing equations are presented.

Finally the discussion centers on the stresses within the joint, the primary goal of this study. The effect of geometry on some peak stresses, the stress distributions at the net-section, the stress distributions along the model centerline, and other important trends are presented in the body of the text.

It should be noted that certain commercial materials are identified in this paper in order to specify adequately which materials were investigated in the research effort. In no case does such identification imply recommendation or endorsement of the product by NASA, nor does it imply that the materials are necessarily the only ones or the best ones available for the purpose. In many cases equivalent materials are available and would probably produce equivalent results.

REVIEW OF PAST WORK AND MOTIVATION FOR PRESENT APPROACH

Past studies of through-the-thickness holes can be categorized into two general problem areas: open holes, and; filled or loaded holes. The former problem area, while receiving much attention over the years, is not of interest here. The latter category is quite pertinent to the study of connectors, particularly those studies of loaded holes. The main issue with the loaded holes, and how they relate to connectors, is the loading on the hole. Basically the issue is centered on how the load is transferred from one part of the connector, through the pin, rivet, or bolt, and into the other part of the connector. If a plane-stress stress analysis is conducted, variations of loading through the thickness of the connector must be ignored. This is usually done. One of the early investigators to address the hole loading issue was Bickley [4]. Bickley studied the stresses in an infinite plate loaded at a hole by forces in the plane of the plate. The forces acted radially and circumferentially at the hole edge. Bickley used a plane-stress stress-function approach to determine the stresses due to point forces, pressure loadings, and shear tractions acting on the hole. In the study the magnitudes of the pressure and shear loads could vary with circumferential distance around the hole. The most often quoted of the loadings Bickley investigated was the cosinusoidal radial loading over 180° of the hole. This was meant to conveniently represent the forces of a pin, bolt, or rivet bearing against the hole. Many other investigators have since used this loading to represent pin action in a hole, several as recently as the last few years, e.g. [5]. These recent applications

5

have been in the context of fiber-reinforced composite materials.
Knight [6] addressed issues similar to Bickley's but was concerned
primarily with the effects of finiteness of the plate. This is a more
practical problem and he used superposition of special solutions to find
the effects of finite width. Solutions were chosen in such a way that
the superposed stresses cancelled each other on boundaries known to be
traction-free. Theocaris [7] also used this approach to study the
problem. The interest in the analysis and design of connectors has
inspired design guides, codes, and rules-of-thumb. Reference [8] is a
typical example of this sort of documentation.

The earlier papers were based on rigorous elasticity analyses while
later papers (not necessarily cited) have used finite-element analyses.
There were many questions concerning the various assumptions in the
theoretical approaches, particularily the assumptions regarding how a
pin actually transmits a load to a hole. Is the loading actually
cosinusoidal over half the hole? What about the effects of friction
between the pin and the hole? Is pin flexibility important? These
questions led to several experimental approaches to the problem. Using
photoelasticity, Coker and Filon [9] studied the stresses near the edge
of a hole in a pin-loaded plate. They purposely chose a large enough
plate so finite-width effects were not important. From the photoelastic
data they matched coefficients in Bickley's infinite plate stress
function. They studied only one model geometry and, except for a few
anamolies in the results, their findings gave a good indication of the
stress magnification effect at the hole. Bickley actually presented

a comparison between his theoretical predictions and these photoelastic results. The comparison is quite good. Frocht and Hill [10] used oversized aluminum specimens, with strain gauges, and photoelastic models to determine the stresses near the edge of a pin-loaded hole. They presented stress concentration factors as a function of the ratio of the hole diameter to specimen width and as a function of pin tolerance in the hole. Two important findings of their study were: (1), stress concentration factors increased with increasing clearance between the pin and the hole, and; (2), for snug-fitting pins, maximum stresses did occur at the net-sections.

In a series of papers, several groups of investigators looked at stresses around holes in pinned connectors using photoelastic techniques. Jessop, Snell, and Holister [11] studied the stress distribution around a circular hole in a flat bar under simple tension. The hole was filled by snug-fitting pins of varying Young's moduli. They found that compared with an unfilled hole, the maximum tensile stress at the net-section was reduced by 15% for all geometries tested. In addition, varying Young's modulus of the pin had little effect on the stress distribution. In these studies Young's modulus of the pin varied from a factor of 1 to a factor of 30 times as great as the Young's modulus of the connector material. These same investigators later studied the effects of varying amounts of pin/hole interference on peak stresses and found that the greater the interference, the lower the stress concentration factor [12]. The diameter of the hole relative to the width of the bar also had an effect on the stress concentration factor. The interpretation of their finding needs to be clarified

7

because the total peak stress generally increased with increasing inter-
ference fit. However, if the stresses were divided into a mean stress
around the hole, due to the interference fit, and a stress around the
hole due to the far-field applied stress, then the stress concentration
factor due to the applied stress decreased with increasing interference
mean stress. These three authors found the same phenomena when exam-
ining the stresses around holes which were actually loaded by a pin
[13]. An interesting phenomena which was revealed in their studies was
the existence of a nonlinear relation between the peak stress and ap-
plied load. This nonlinearity was a function of the interference level.
Lambert and Brailey [14], using photoelasticity, studied this effect and
concluded that friction between the pin and the hole edge, and sep-
aration of the pin and the hole at high loads were responsible for the
nonlinear relation. That work addressed the whole complicated issue of
interaction between the bolt and connector material and is felt to be
valuable. Lambert and Brailey [15] continued to study the effect of
interference on the stresses in pinned connectors. Cox and Brown [16]
also pursued these types of investigations. Theocaris [17] used the
pin-loaded hole as an application of his electrical analogy method for
the evaluation of principal stresses along stress trajectories. The
purpose of his work was not so much the study of pin-loaded connectors
as it was the study of the analogy method. Thus his results are limited
but they follow the same trends Coker and Filon [9] found.

Continuing the optical approach, Nisida and Saito [18] used an
interferometric method coupled with photoelasticity to investigate

stresses around a pin-loaded hole. They presented data on the radial stress distribution around the hole and concluded that a cosinusoidal loading did not adequately represent the effect of the pin. However, a close examination of their data reveals that for the cases they studied, the cosinusoidal distribution is a very good first approximation. More recently Oplinger, Parker, and Katz [19] used Moiré interferometry to study the stresses around the pin-loaded hole in a composite plate.

With the advent of composites, as indicated by the last reference, the interest in stresses around connector holes continued and in fact grew. Much of the concern has been with the prevention of the previously mentioned catastrophic failures. However, since the failure mechanisms in composites are somewhat statistical in nature and not fully understood, much of the experimental work to date has centered around actual ultimate-strength tests. In these tests the joints are loaded to failure and the failure load is the quantity of primary interest. This is in contrast to the experimental studies concerned with the details of stress distribution around the loaded holes in isotropic homogeneous materials. Some of this lack of investigation, however, is due partly to the lack of a photoelastic material which accurately represents a composite material. Also some of the failure mechanisms in composites are three-dimensional in nature and these effects are difficult to measure experimentally.

Full-scale testing-to-failure of composite materials is costly in terms of material and time. Thus some of the earlier analytical methods were reimplemented and applied to composites. In addition, many new approaches were used. The introduction of anisotropy into the problem

9

greatly complicates the analysis and so many of the new approaches were approximate in nature. Among these are the finite-element method, both displacement-based and hybrid, the boundary integral method, collocation, and finite-difference. There is no need to review all the important work in this area. One was mentioned earlier, i.e. [5]. An excellent review of all work up to 1978 involving connectors for composite materials was written by Garbo and Ogonowski [20]. Since then Soni [21] studied failure modes of composite connectors using finite-elements. Recently Crews, Hong, and Raju [22] studied the stresses around pin-loaded holes in finite-width orthotropic laminates. They used finite-element analyses, modeling a frictionless steel pin to load the hole. Some results from their work will be discussed later. A study of wooden connectors, which are orthotropic, was conducted by Wilkinson [23]. He used a finite-element analysis to model a rigid steel pin in a wooden joint, including the effects of friction between the wood and steel. The analysis, a plane-stress analysis is quite rigorous and is accompanied by experimental measurements using strain gages and Moiré interferometry.

As with isotropic materials, a vast majority of all work with composites connectors has dealt with single-pin connectors. Thus there is a need to investigate multiple-pin connectors. Because of the lack of yielding in composite materials, the need is more urgent for these materials than it is for ductile materials. As with single-pin connectors, there are several approaches which can be used to study stresses in multiple-hole connectors. These methods are both experimental and theoretical. It is important to remember that no single approach should

be used exclusively and, in fact, different methods need to be used as a cross-check. If one were concerned only with isotropic materials, there are many arguments that can be made for using a photoelastic approach. First, within the context of the model, the photoelastic approach gives an exact solution. There are no approximations or assumptions about friction, or lack thereof, between the pin and the hole. The issue of pin flexibility is automatically resolved. The same is true for the issue of a cosinusoidal loading. With multiple-pin connectors, one concern is the amount of load transferred to a particular pin. As mentioned previously, the problem is statically indeterminate. If the stiffness in the inner and outer laps is the same and the tolerances of all pins in their holes are identical, the load is distributed evenly among the holes. With the two-pin connector at hand this means each hole reacts 50% of the total applied load. With an analytical model, some assumptions regarding the pin/hole tolerance must be made. With photoelastic models the tolerance problem is inherently a part of the model. If typical machine-shop tolerances are maintained in making the model, the effects of slight differences in tolerances among holes will in actual joints be represented and no assumptions need to be made.

Another advantage of photoelastic models is that if the appropriate optical equipment exists, the approach is quite inexpensive. Isotropic model materials are readily available and require minimal machine forces, making the models easy to work with. The effects of model geometry can be easily studied by remachining a single model or by taking advantage of the relatively inexpensive material and machining several models. Even if the appropriate optical equipment does not exist, set-

11

ups to obtain some quantitative information can be constructed without too much cost. Photoelasticity is also a whole-field measurement technique. Much can be learned from the density and the shape of the fringe patterns without resorting to quantitative analysis of the fringe data. By simply observing the fringe patterns, the effects of a geometry change in the model can be quickly assessed.

Finally, despite the fact that the vast majority of photoelastic work in the past has been with isotropic photoelastic materials, orthotropic photoelastic materials do exist and may become more common in the future [24,25]. Characterization of these materials, both elastically and optically, is still an area that needs investigation. However, eventually problems will be solved using these materials. The composite connector problem is one area that should be investigated with orthotropic photoelastic materials when they become available. Thus, some of the experience gained by fabricating and testing joint models for isotropic materials can be applied to the fabrication and testing of joint models of orthotropic photoelastic materials. In addition, many stacking sequences of composite materials exhibit in-plane isotropic elastic behavior. The usual relation between Young's modulus, Poisson's ratio, and the shear modulus does not hold but the material properties are not a function of in-plane orientation. Thus, information gained from isotropic photoelastic models can be used to aid in the analysis and design of components fabricated from these quasi-isotropic composite materials. With these ideas in mind, a study of the stresses in two-pin connectors using isotropic photoelastic models was initiated. Appendix A presents a brief overview of the photoelastic technique as it is used

12

in this study.

DESIGN AND FABRICATION OF THE MODELS

Since many of the composite bolted specimens tested in the pre-
viously mentioned study [1,2] failed in the inner lap, the ideal situa-
tion in the present joint study was to be able to determine the stresses
in the inner lap. Thus the goal was to design models so that the stress
state in the inner lap of a loaded joint could be measured. The general
philosophy for such an experimental design is illustrated in fig. 2.
This design required the outer laps to be transparent and to not affect
the observation of the inner lap stresses. However, all transparent
materials exhibit some degree of photoelastic response, commonly called
birefringence, when subjected to stress. Glass, for example, exhibits
very little birefringence, while some plastics made especially for
photoelastic model-making exhibit a large birefringent response. Since
in a double-lap joint both the inner and outer lap are subjected to
stresses, the problem called for using two transparent materials, one
which exhibited a high degree of birefringence and one which exhibited
very little birefringence. Another restraint on the material selection
was to use materials with similar elastic properties. However it is the
in-plane stiffnesses of the joint laps which are important and having
identical Young's moduli is not essential. Cross-sectional areas can be
chosen to compensate for differences in Young's moduli of the two
materials. Poisson's ratio mismatch was not felt to be important but
having similar values of the ratio for the two materials would give a
more accurate representation of an actual joint. Finally, to study the

effects of geometry, several models would be involved. Thus the selected materials needed to be easy to work with. The workability of the material was in the context of cutting, drilling, and the machining of the material.

Several materials came close to meeting all of the above requirements. The materials finally chosen for the model were PSM-1[1] for the photoelastic inner lap and Acrylite[2], and acrylic for the outer lap. The PSM-1 is a polycarbonate material specifically for photoelastic model making and Acrylite is a commonly available plexiglass material. The PSM-1 material is available in several thicknesses as is the Acrylite. More importantly, the PSM-1 material is at least an order of magnitude more sensitive to the photoelastic effect than is the acrylic. Figure 3 shows a PSM-1 disk and an Acrylite disk subjected to the same compression loads. It is obvious the PSM-1 is much more sensitive to the photoelastic effect. From the manufacturer's data, Young's moduli for the materials were taken to be: 2.76 GPa (400,000 psi) tension and compression for the PSM-1, and 3.27 GPa tension, 2.96 GPa compression (475,000 psi tension, 430,000 psi compression) for the Acrylite. Poisson's ratio for each material was about 0.38. Based on these figures, the elastic properties of the PSM-1 and the Acrylite were assumed to be the same.

The most serious concern in the model design was the modeling of the actual connector. Although pins have been used in many studies, bolts and rivets are most commonly used in actual joints. Bolts are usually used in conjunction with washers. Rivets have heads which cover about the same area as a washer. In either case a through-the-thickness

---

[1]Photoelastic, Inc. Raleigh, NC 27611
[2]American Cyanamid, Wayne, NJ 07470

normal stress is produced around the hole as the bolt is torqued or the rivet head is formed. The normal stress, through Poisson's ratio, would add or subtract from the load-induced stresses in the plane of the joint. In addition, friction between the washer or rivet head and the joint surface could affect the load transfer to the joint. Through this friction some of the load would be reacted into the joint through shear (between the washer or rivet head and the surface of the outer lap, or between the laps) instead of all the load being transferred through bearing on the hole edge. Both the through-the-thickness stress and the shearing-in of part of the load are felt to increase the load carrying capacity of the joint. Ignoring these effects would be conservative. Thus the connectors in photoelastic models were represented by snug-fitting acrylic dowels. With dowels, as opposed to rivets, or bolts, the through-the-thickness effects and the shearing effects were absent. However, because of the lack of the nut or a rivet head, viewing of the stresses to the edge of the hole was possible. Using acrylic dowels, Young's modulus of the dowels was the same as Young's modulus of the joint material.

The polariscope to be used in the study was a split-bench model with columnating lens 305 mm (12 in.) in diameter. The load frame available for the study could accomodate a model 1.2 m (48 in.) long. These polariscopes dimensions dictated overall model size but other aspects of the model had a bearing on model design. The most difficult portion of the model to analyse would be the area around the hole. The larger the diameter of the holes, the easier it would be to determine the stresses in those regions. In addition, certain geometric or dimen-

16

sional portions were important. Joint width-to-hole diameter ratios of up to 8 were to be tested. The joints were to have a distance between hole centers of up to 6 hole diameters and the holes were to be up to 3 hole diameters from the free end of a lap. Thus the largest model had to be at least 12 hole diameters long and up to 8 hole diameters wide.

A final consideration in model design was the method of applying the tensile load to the joint. In actual joints in both the inner and outer laps, at some distance away from the two holes, a uniform state of stress exists. The value of this stress can be computed from a simple force/area calculation. It is the interruption of this uniform stress by the holes which cause weaknesses in joints. When testing actual joints or models of joints, care must be taken to insure a somewhat uniform state of stress exists away from the holes. If this condition is not enforced, the stress distribution associated with this nonuniform state of stress could interact with the stress distribution produced by the holes themselves. With such a situation the stress distribution in the joint could be incorrectly assessed. To avoid introducing spurious stress distributions, specimens can be designed long enough so that the actual joint region takes up, say, the central third of the specimen, the outer third on either side of the joint region being used to allow a uniform state of stress to develop between the load introduction and the test holes. The long specimen approach, though desirable, can be costly both due to material costs and to machining costs. Thus the approach taken here, mainly to avoid machining as opposed to excessive material usage, was to use long aluminum load-introduction doublers. The idea was to generate a uniform stress state in the doublers and attach them,

17

with many small bolts, to the joint model three or four hole diameters away from the test holes. With many small bolts connecting the doubler to the joint, the uniform stress state would suffer only a localized perturbation in the zone around the small connectors.

Taking into account all of the aforementioned factors, the hole diameter on all models was chosen to be 22.2 mm (0.875 in.). The largest model tested, accounting for the maximum width, maximum distance between holes, and maximum distance to the end of the specimen, was 177 mm (7.00 in.) wide. For this largest model the hole centers were 133 mm (5.25 in.) apart and the free ends of the laps were 66.7 mm (2.63 in.) from the center of the second hole. Figure 4 shows the geometry of the largest model as well as the geometry of the load introduction doublers. The tensile load from the load frame was transmitted to the joints by a single 9.77 mm (0.375 in.) connector at the end of each doubler. For both the inner and outer laps, the distance from the row of small connector bolts to the center of the lead holes was 82.6 mm (3.25 in.). An aluminum spacer, machined to be the same thickness as the inner lap, actually connected the outer laps to the doubler through a second set of small bolts. The inner lap was 6.35 mm (0.25 in.) thick while the outer laps were each 3.18 mm (0.125 in.) thick. The thickness of the PSM-1 inner lap varied insignificantly over the area of the model while the Acrylite outer laps varied up to 20% in thickness. The load introduction doublers were designed to be used with all of the model geometries tested.

The actual making of the models produced some concerns. These concerns were: (1), maintaining accurate tolerances of the specified

18

dimensions; (2), insuring accurate alignment of the holes along the model centerline; (3), insuring identical hole placement and hole diameter in all three laps and; (4), minimizing heat-induced stresses from the drilling and cutting operations. After much consideration, it was decided to machine all three pieces simultaneously as a sandwich. The major effect of this was to insure alignment of the holes. In addition, to minimize the machining stresses around the test holes, the holes were machined while the three layers were submerged in a coolant. To begin the machining of the joint, the three laps were clamped together and the long sides of the model were machined parallel to each other. Then the rows of small connector holes were drilled in the clamped sandwich, perpendicular to the long edges. A flat, open, tray-like tank was mounted on a milling machine and the three pieces placed in it. Precision steel pins protruded from the bottom of the tank and were used with the small connector holes to maintain the original alignment of the three laps. The laps were again clamped lightly together and the tray filled with coolant. The two test holes were then machined with an offset cutter. The coolant used throughout the machining operation was a water-soluable coolant. Figure 5 shows the actual machining operation. In this photograph the three laps are clamped onto the bottom of the coolant tank and one of the test holes is being machined. Figure 6 shows a finished joint model with the aluminum doublers attached and ready to be tested. Figure 7 shows all the models used in this study. In these last two photographs a 305 mm (12.0 in.) ruler is present for size comparison.

The values of 4, 6, and 8 were chosen for the ratios of joint

19

width-to-hole diameter, i.e. W/D = 4, 6, and 8. The three longest models (at the left in fig. 7) had a distance of 6 hole diameters between the centers of the two holes (E = 133 mm (5.25 in.)) and a distance of three hole diameters from the center of the second hole to the free end of the specimen (e = 66.6 mm (2.62 in.)). The three medium length models (at the center in fig. 7) had a distance of two hole diameters from the center of the second hole to the free end (e = 55.6 mm (2.19 in.)) while all other dimensions were the same as the longest model's. The three shortest models (at the right in fig. 7) had a distance of four hole diameters between the centers of the holes (E = 88.7 mm (3.50 in.)) and two hole diameters between the center of the second hole and the free end (e = 66.6 mm (2.62 in.)). The three joint widths, W, were: 178 mm (7.00 in.), 133 mm (5.25 in.), and 88.9 mm (3.50 in.). Table 1 summarizes the dimensions of all the models tested.

The measurements and calculations for this study were made in U.S. Customary Units. Dimensional numerical values are given in both SI and U.S. Customary Units.

TYPICAL EXPERIMENTAL RESULTS AND THE EXISTENCE
OF A PHOTOELASTIC ISOTROPIC POINT

Figure 8 illustrates the long wide model in the loading frame. The loading frame was a hand operated screw-type frame and was fitted with a load cell to monitor the loads on the models. The cell was located above the model and is visible in the figure. Dead-weight loadings were periodically used to check the calibration of the load cell. Since the polariscope was a split bench model and since the models with their doublers were quite large, the load frame was mounted on castors so it could be rolled in and out between the halves of the polariscope. This arrangement made it simple to work on the models while they were in the load frame and made it easy to change models in the frame. The polariscope light source was a 250-watt mercury vapor source. The source was fitted with a filter so that in addition to viewing the model with white light, monochromatic light of the sodium green wavelength, 571 nm (22.5 $\times$ 10^{-6} in.), could be used.

The viewing of the model and the taking of photoelastic data were accomplished by a variety of methods. The main goal of all the methods was to be able to determine accurately the geometric location of all the fringes. Three methods to do this emerged as the most convenient. Enlarged black and white photographs of the model as a whole served as a permanent record of the fringe pattern generated in a specific model subjected to a specific loading. Using scribe marks on the specimens, these photographs provided accurate information on the fringe locations. Figure 9 shows the dark-field fringe pattern in the medium length narrow

model subjected to 1121 N (250 lb.) tensile force. The free end of the
inner lap is at the bottom of the photograph and is clearly visible.
The near perfect symmetry, about the vertical centerline, of the fringe
pattern in the figure is typical of the symmetry observed in all tests.
This indicated that in the plane of the model the joint was subjected to
pure tensile loads with no side-to-side bending induced by the loading
frame or the aluminum doublers. This also indicated the good alignment
of the two test holes. The symmetry was evident in all tests.

For a more detailed look at the fringe patterns, a traveling tele-
scope was used. The telescope could focus on a small region of the
model, such as a region below the lead hole. The location and number of
the higher order fringes could then be recorded. Figure 10 shows a
typical close-up view of the fringe pattern using the telescope. This
photograph shows the fringes near the bottom hole in the long narrow
model. Notice that the symmetry of the fringe pattern is generally
preserved even at this scale. In addition, a region on the hole bound-
ary containing a singular point is visible and is illustrated in the
figure. This singular point is characterized by the fact that the
isochromatic fringes emanating from either side of the point on the hole
boundary diverge in opposite directions.

The third way of obtaining information from the model was to pro-
ject the image of the fringe pattern onto tracing paper. The fringe
images, as well as an outline of the model, were traced on the paper and
the fringe locations determined from this tracing. This method was used
more for recording the location of the isoclinic fringe pattern than it
was for studying the isochromatic fringe patterns. It was more conven-

22

ient to record the location of the isochromatic fringe patterns with either of the two photographic methods described. Knowing fringe location is important. It is necessary to know the locus of points for a particular fringe; or, it is necessary to know the fringe information at given locations. Both approaches to data acquisition yield the same information but one or the other is a necessary step in the photoelastic technique.

One of the most interesting aspects of this study was totally unexpected. When the image shown in fig. 9 was first seen it was viewed with white light. An unusual feature was immediately apparent. The small circular spot on the model centerline, about one-quarter of the distance between the holes, was actually black. Except for the corners and this spot, all fringes were colored. This black spot, a fringe of order zero, indicates either an isotropic point or a singular point. These are explained as follows.

The photoelastic effect, as it is being used in this study, measures the differences in the numerical value of the principal stresses. The number of fringes times a calibration constant gives the numerical value of the difference in principal stresses,

$$\sigma_1 - \sigma_2 = cN, \tag{1}$$

c being the calibration constant in Pa/fringe (psi/fringe) and N being the fringe order. The fringe order being zero implies

$$\sigma_1 - \sigma_2 = 0, \tag{2}$$

which requires either

$$\sigma_1 = \sigma_2 = 0 \tag{3}$$

23

or

$$\sigma_1 = \sigma_2 = ? \tag{4}$$

The former case is referred to as a <u>singular point</u>, that is, both principal stresses are zero. This can occur on the boundary or in the interior of the model. As was just pointed out, singular points existed on the hole boundaries of the joint models. This is because the pin separated from the hole (lost contact) over a region of the hole. Thus the radial and shear stresses on the hole were zero in that region. In addition, the circumferential stresses changed sign around the circumference of the hole and passed through zero at some point. This zero point was in the region where the dowel had separated from the hole. A point of zero stress occurred and so both principal stresses were zero, eq. 3. The second case, eq. 4, is referred to as an <u>isotropic point</u>, so-called because the principal stresses, though unknown, are equal. At an isotropic point a state of hydrostatic-like stress state exists. With a hydrostatic stress, the stresses being either tensile or compressive, the stresses are the same in all directions and hence the term isotropic.

It was hypothesized that the vertical location of the isotropic point, relative to the distance between the hole centers, depended on the percentage of total load reacted by each hole. If the hypothesis were true, the isotropic point location would be a very convenient way to assess load transfer. To test the hypothesis, the outer laps of the first model tested were removed and a scheme to load each hole independently was devised. This apparatus is shown in fig. 11. The plexiglass dowels were inserted into the holes of the inner lap and a hanger,

24

utilizing dead weights and attached to the bottom dowel, was used to load the bottom hole a known amount. The loading screw mechanism at the top of the load frame actually translated the model up and down as the screw rotated. A flexible braided-wire harness was fixed to the sides of the load frame and was looped over the top dowel. As the model was translated up by loading screw, the harness loaded the top hole while the dead weights loaded the bottom hole. The load cell registered the total load and knowing the dead-weight load on the bottom hole, the load on the top hole could be computed. To help locate the isotropic point on the model, a grid, marked to the resolution of 2.54 mm (0.1 in.), was scribed on the model's centerline. With the ability to vary each hole load independently, the vertical location of the isotropic point was determined for a variety of load conditions. Its location versus hole loading was determined for low and high total load levels; for constant total load and variable upper and lower hole loads; for constant lower hole load and variable upper and total hole loads; interchanging the two dowels; and various other conditions. In each case, the location of the isotropic point had the same very specific relation to the percentage of load reacted by each hole. Figure 12 shows the movement of the isotropic point as a function of hole loading. It is clear the percentage of load on each hole affects the position of the isotropic point. Figure 13 represents experimental data for some of the many conditions tested. Plotted on the vertical axis is the nondimensional distance of the isotropic point, C, from the center of the top hole. The horizontal axis represents the proportion of total load, P, reacted by the lead hole, P_1. The data from all conditions clustered tightly about a

relationship which appeared to be slightly nonlinear. The nonlinearity was felt to be due to the changes in the contact area of the pin in the hole as the load level in each hole changed. This is a geometric nonlinearity. (Note: The data shown in fig. 13 is not for the particular joint shown in fig. 9 or the joint shown in fig. 12.)

Thus as shown in fig. 14, with the plexiglass laps back in place and having run a series of experiments to produce a curve as shown in fig. 13, the location of the isotropic point could be observed. Working backwards, the percentage of load reacted by each hole could be determined. For each of the nine models tested, data as in fig. 13 was obtained. Then with the outer laps in place, the percentage of load reacted by each hole was recorded for each model at the load level used to record photoelastic data. Table 2 presents the load and stress levels used for testing each model and indicates the load proportioning characteristics.

DETERMINATION OF STRESSES

As mentioned at the beginning, the primary goal of this study was to provide an accurate picture of the stress state in the inner lap of the model. It was not necessary to compute the stresses at every point in the model but certainly it was required to know the stresses at a large number of points around the two holes. To have a complete picture of the stress state at a point in a plane-stress condition, three quantities must be known. The most logical quantities, and the ultimate interest in this case, are the two normal stresses and the shear stress. Referring to fig. 1 and using the usual nomenclature for stress, these three stresses are σ_x, σ_y, and τ_{xy}. There are other quantities which, if known, would lead to knowing the stress state at a point. For example, if one knew the sum of principal stresses, the difference of principal stresses, and the principal stress direction, then the three stresses could be uniquely determined. Since in transmission photo-elasticity only the difference in principal stresses and the principal stress directions are known, the obtaining of σ_1 and σ_2, or ultimately σ_x and σ_y, requires a knowledge of a third quantity. Several approaches have been used by researchers to provide a third condition. One method requires measuring the change in thickness of the model as the loads are applied. Since the change of thickness of a model is proportional to the sum of the principal strains, various mechanical and optical methods have been applied to measure this change. For isotropic elasticity, using the elastic properties of the model material, the sum of principal

27

stresses can be determined from the sum of principal strains. Another approach, introduced by Post [26], utilizes the fact that σ_1 can be made to produce one set of fringes and σ_2 can be made to produce a second set of fringes. The viewing of these two sets of fringes provides the needed information. Since in isotropic elasticity the sum of the principal stresses satisfies Laplace's equation, the electrical analogy of Theocaris [17] and the analytical approach of Dally and Erisman [27] have been used to obtain the sum of the principal stresses as a third known quantity. A fourth method, and the one used here, relies on information obtained from the plane-stress equilibrium equations to provide a complete picture of the state of stress at a point. The key to this method is that the stresses obtained from the photoelastic data are made to satisfy the plane-stress equilibrium equations. Two popular versions of this technique are the shear-difference method [28], and the integration of the equilibrium equations along principal stress directions [29]. This latter approach was pioneered by Filon [9]. The shear-difference method is also an integration of the equilibrium equations so both approaches rely on known boundary data (or known data elsewhere) to obtain numerical values of the stresses. The shear-difference method is subject to large error because generally the integration proceeds along paths quite far from the known boundary data. Unless some other stress information is known along the integration path, the numerical errors of approximate integration can accumulate. With Filon's method, since the principal stress directions are usually curved paths, the integration is along a curved path. The method is more accurate than the shear-difference approach but generally there is

28

interest in stresses along lines other than these curved paths and so the application is limited. Filon's method works well along lines which are lines of symmetry for both the loading and model geometry because these lines of symmetry are generally principal stress directions.

To be able to determine the stresses at arbitrary points in the model with a minimum of error, an approach originally presented by Berghaus [30] was adopted. The method uses the finite-difference form of the plane-stress equilibrium equations, the photoelastic fringe data, and the boundary conditions as set of overdetermined equations which are solved in the least-square sense. The solution of the equations are the three stress components which satisfy, in a least-square sense, equilibrium, the photoelastic data, and the boundary conditions. The overdetermined technique as it is used here is different from the version Berghaus reported but credit that investigator with the basic idea. An explaination of the approach follows.

Referring to the joint nomenclature in fig. 1, the equilibrium equations which applied in this situation are,

$$\frac{\partial \sigma_x}{\partial x} + \frac{\partial \tau_{xy}}{\partial y} = 0 \tag{5}$$

$$\frac{\partial \tau_{xy}}{\partial x} + \frac{\partial \sigma_y}{\partial y} = 0 \ . \tag{6}$$

The photoelastic data can be represented by

$$\sigma_1 - \sigma_2 = cN \tag{7}$$

$$\theta \ (\text{principal stress direction}) = \text{known} \tag{8}$$

The photoelastic equations can be put in another form, namely,

$$\sigma_x - \sigma_y = cN \cos(2\theta) \tag{9}$$

$$\tau_{xy} = \frac{cN}{2} \sin(2\theta) \tag{10}$$

These equations are the result of applying a stress transformation from principal stress coordinates to the x-y coordinates. With this usage, θ is the angle the principal stress directions make relative to the x-axis of fig. 1 (+θ goes from +x to +y). In the nomenclature of photoelasticity, the principal stress direction, θ, is often referred to as the the isocline parameter. It should be pointed out that eqs. 5-10 are valid at every point in the model. Finally, the boundary data consists of knowing one, two, or three of the three stresses at a selected point or a locus of points in the model.

The photoelastic and the boundary conditions are algebraic equations while the equilibrium equations are partial differential equations. The exact solutions to the equilibrium equations are generally not obtainable in domains with complicated boundaries. Thus some form of discretization, e.g. finite-element or finite-difference, is required to obtain appoximate solutions. The finite-difference discretization of the equilibrium equations are a set of algebraic equations which have as unknowns the stresses at discrete points in the model. Applying the photoelastic equations and the boundary conditions at these same points provide more algebraic equations relating the stresses at these points. All of these equations can then be solved for the stresses.

As is well known, the finite-difference scheme relies on the approximation of the derivative of the function at a point by using values of the function in the neighborhood of the point. The three common methods of approximation are referred to as the forward dif-

30

ference, the backward difference, and the central difference. Referring to fig. 15, the forward difference for the evaluation of the first derivative of some function F(x) at point x = x_i is given by

$$\left.\frac{dF}{dx}\right|_{x=x_i} \simeq \frac{F_{i+1} - F_i}{\Delta x} \qquad . \qquad (11)$$

The backwards difference is given by

$$\left.\frac{dF}{dx}\right|_{x=x_i} \simeq \frac{F_i - F_{i-1}}{\Delta x} \qquad (12)$$

while the central difference is given by

$$\left.\frac{dF}{dx}\right|_{x=x_i} = \frac{F_{i+1} - F_{i-1}}{2\Delta x} \qquad (13)$$

A more comprehensive treatment of the finite-difference formulation can be obtained in [31]. With the finite-difference approach, interest centers on the values of the function at a discrete number of points. Extending this notion to two-dimensions and to the problem at hand, the finite-difference representation of the equilibrium equations depends on writing the partial derivatives of stresses in terms of stresses at discrete points in a two-dimensional grid. Figure 16 shows such a grid superimposed on a joint model. With the particular partial differential equations to be approximated in this problem, and with the particular geometric properties of the regions to be analyzed, the finite-difference equations take on a different form from one point to the next in such a grid. For example, at point A in fig. 16, the finite-difference representations of both $\partial/\partial x$ and $\partial/\partial y$ must use the forward

31

difference. The equilibrium equations at such a point i,j take the form

$$\sigma_{x_{i+1,j}} - \sigma_{x_{i,j}} + \frac{\Delta x}{\Delta y}\left(\tau_{xy_{i,j+1}} - \tau_{xy_{i,j}}\right) = 0 \tag{14}$$

$$\tau_{xy_{i+1,j}} - \tau_{xy_{i,j}} + \frac{\Delta x}{\Delta y}\left(\sigma_{y_{i,j+1}} - \sigma_{y_{i,j}}\right) = 0 \tag{15}$$

Along line AB, but not including points A or B, $\partial/\partial x$ can be represented by the central difference while $\partial/\partial y$ must be represented by the forward difference. The equilibrium equations at this type of point i,j then take the form

$$\sigma_{x_{i+1,j}} - \sigma_{x_{i-1,j}} + \frac{2\Delta x}{\Delta y}\left(\tau_{xy_{i,j+1}} - \tau_{xy_{i,j}}\right) = 0 \tag{16}$$

$$\tau_{xy_{i+1,j}} - \tau_{xy_{i-1,j}} + \frac{2\Delta x}{\Delta y}\left(\sigma_{y_{i,j+1}} - \sigma_{y_{i,j}}\right) = 0 \tag{17}$$

For an interior point, say E, both derivatives can be represented by the central difference. The equilibrium equations for such a point i,j then become

$$\sigma_{x_{i+1,j}} - \sigma_{x_{i-1,j}} + \frac{\Delta x}{\Delta y}\left(\tau_{xy_{i,j+1}} - \tau_{xy_{i,j-1}}\right) = 0 \tag{18}$$

$$\tau_{xy_{i+1,j}} - \tau_{xy_{i-1,j}} + \frac{\Delta x}{\Delta y}\left(\sigma_{y_{i,j+1}} - \sigma_{y_{i,j-1}}\right) = 0 \tag{19}$$

For the point i,j the photoelastic equations become

$$\sigma_{x_{i,j}} - \sigma_{y_{i,j}} = cN_{i,j}\cos(2\theta_{i,j}) \tag{20}$$

$$\tau_{xy_{i,j}} = \frac{cN_{i,j}}{2}\sin(2\theta_{i,j}) \quad . \tag{21}$$

where $N_{i,j}$ is the isochromatic fringe number at the point and $\theta_{i,j}$ is the principal stress direction, relative to the x-axis, at the point.

.

.

The boundary conditions are expressible as one or more of the following relations at the points i,j which are on the boundaries of the grid region:

$$\sigma_{x_{i,j}} = \text{known}, \quad \sigma_{y_{i,j}} = \text{known}, \quad \tau_{xy_{i,j}} = \text{known} \qquad (22\text{-}24)$$

For example, in fig. 16, the first and third of these equations would be enforced (with the stresses set to zero) at each grid point on line AD.

The two equilibrium equations, the two photoelastic equations, and the boundary conditions constitute a set of linear algebraic equations for the three stresses in the grid. With this scheme there are always more equations than there are unknown stresses. For example, if region ABCD in fig. 16 represents a 6 x 5 grid, there would be 30 x 3 unknown stresses. There would be 30 x 2 equilibrium equations, 30 x 2 photo-elastic equations, and 5 x 2 boundary conditions ($\sigma_x = \tau_{xy} = 0$ on AD). This represents 130 equations for 90 unknowns, an overdetermined set of equations. These equations can only be satisfied in the least-square sense. An advantage of the least-square method, however, is that certain equations can be weighted to have more influence on the solution. For example, in fig. 16 it is known with certainty that the side AD is traction free. Thus instead of using

$$\sigma_{x_{i,j}} = 0 \quad \text{and} \quad \tau_{xy_{i,j}} = 0 \qquad (25\text{-}26)$$

along that edge, the equations can be weighted to be

$$5\sigma_{x_{i,j}} = 0 \quad \text{and} \quad 5\tau_{xy_{i,j}} = 0 \ . \qquad (27\text{-}28)$$

This approach causes these known conditions to have a stronger influence

on the solution. Other uses of this weighting of known conditions are discussed later.

Rather than solve for all of the stresses in the model at one time, by using one large solution grid superimposed on the model, the model was broken into zones. This idea is shown in fig. 17. A system of zones was established around each hole. The stresses were determined in a zone-by-zone fashion, starting with zone 0 and proceeding with zones 1, 2, 3, 4, and 5 in that order. There were several reasons for adopting this zone scheme. The primary reason was that it kept the problem tractable. Instead of solving for the stresses at, say, 400 points (1200 unknowns) simultaneously, the stresses in one zone were computed and examined for their plausibility. If the stresses did not seem reasonable, looking for possible errors was relatively easy since only the data from a certain region of the model were involved. If the computed stresses in the first zone looked reasonable, stresses in the second zone were computed and checked, and so forth for the other zones. Another advantage of this approach was that the mesh size in each zone could be different to reflect steep stress gradients. Variable mesh finite-difference schemes could be used but this zone approach was much simpler. Also with this scheme the grid size in, say, zone 5 could be refined and the stresses recomputed without having to recompute the stresses in all the other zones. Since the fringe patterns were symmetric about the centerline, only one-half of the model was analysed. The fringe data were taken from just one-half of the model. An alternate approach would have been to gather data from both the left and right sides of the model and then average it. The averaged data could

then have been used to do the one-half model analysis. This approach involved more data gathering and the effort was not felt to be warranted.

The zone concept and the overdetermined nature of the governing equations were a key to having confidence in the computed stresses. This confidence is traceable to the solution of the first zone, a zone which represented a cross-section of the joint. For zone 1 associated with the lead hole

$$\int_{-W/2}^{W/2} \sigma_y dx = P_2 , \tag{29}$$

where P_2 is the load transferred to the second hole. The value of P_2 for each model was determined from the total applied load and the isotropic point location, Table 2. For a zone 1 below the second hole

$$\int_{-W/2}^{W/2} \sigma_y dx = 0 \tag{30}$$

for all models. By approximating the integrals using Simpson's rule and using the values of σ_y at the various grid points across the joint width, a check on global equilibrium was possible. This type of calculation was done as a first step in the stress analysis but then these integrals, in discretized form, could be used as additional algebraic equations to be enforced in a least-square sense. Since there was a high degree of certainty in these integral equations, the algebraic representation of them could be weighted to influence the solution. Actually, the stresses computed in zone 1 before enforcing the integral equilibrium equations came quite close to satisfying equilibrium anyway.

35

This provided confidence in the stress analysis.

The stresses of zone 1 calculations provided a firm basis on which to base the other zone's calculations. Using zone 1 calculations to help compute the stresses in the other zones was accomplished by considering the stresses at the upper grid points in zone 1 as boundary conditions on the lower grid points in zones 2, 3, and 5. For zones 3 and 5, with their finer meshes, stresses at grid points between the grid points of zone 1 were needed. The stress values at these intermediate zone 3 and 5 grid points were determined by using a cubic spline interpolation between the known stresses at the zone 1 grid points.

Cubic spline interpolation was used in one other facet of this numerical scheme. The photoelastic equations, eqs. 20 and 21, require the isochromatic fringe value, $N_{i,j}$, at every point in the grid. Looking at fig. 2 with the superimposed grid in mind, it is obvious the integer and half-order fringes would rarely intersect a grid point. Thus the fractional fringe orders at each grid point were needed. Rather than use some scheme such as Tardy compensation, a cubic spline was used to interpolate the fringes at the grid points. This interpolation was based on the known x and y coordinates of the integer and half-order fringe points on the model.

To this point in the discussion the determination of the principal stress directions has not been mentioned. To compute the stresses at every point in the grid, the principal stress direction at each point, $\theta_{i,j}$, must be known. Whereas the acrylic outer laps had little influence on the isochromatic fringe pattern of the inner lap, the outer laps strongly influenced the isoclinic fringe pattern. There was no way the

36

principal stress directions of the inner lap could be determined with the outer laps in place. Fortunately the equipment used to determine the variation of isotropic point location could be utilized. This was done as follow: With the outer laps in place and the model loaded, the isotropic point location was noted. The model was unloaded and the outer laps removed. Then the model was reloaded with the apparatus shown in fig. 11. By adjusting the load on each hole, the isotropic point location was made to coincide with the location it had when the outer laps were in place. The principal stress directions at each grid point could then be determined directly from the polariscope mechanism designed to do this. There was concern that the independent hole-loading apparatus did not produce the same hole loading as the outer laps did. This concern was in the context of contact area and distortion of the acrylic dowel within the hole. It appeared, however, that the principal stress directions were not as sensitive to these parameters as were the isochromatic fringes. Small variations in the percentage of load reacted by each hole and variations in the total load level did not significantly change the principal stress directions. This was fortunate because it was felt there was no alternative to determining principal stress directions. Appendix B shows typical values of N and θ at the grid point locations.

Finally, as is noted by the zone identification in fig. 17, the region to the lower left of the hole does not have a grid on it. Figure 10 shows a typical isochromatic fringe pattern in this region and as can be seen, the fringe locations can be determined quite accurately. Unfortunately the principal stress directions in this region were quite

difficult to determine. Once they were determined it was apparent that, if the determination was accurate, the principal directions changed rapidly over a small distance. Figure 18 shows a typical isoclinic fringe pattern in this region. An overdetermined solution scheme based on polar coordinates was developed and the stresses computed. In light of the rapid variation of the principal stress directions the calculations were viewed as suspect. Much effort went into this particular problem but to avoid presenting possibly misleading information, no results from this portion of the study are presented.

RESULTS

With the numerical method described in the previous chapter, peak
stresses, stress concentration factors, spatial distributions of
stresses, and other stress-dependent trends could be determined for each
model. With 9 models and 3 components of stress at each finite-dif-
ference grid point, a complete description of the stress distribution in
all models involved an overwhelming amount of information. This infor-
mation is not included in this report, but rather important trends and
peak values are presented. The stress information presented here is
based on gross-section (far-field) stress of 1.97 MPa (286 psi). This
gross-section stress is defined as

$$\sigma_{gross} = \frac{P}{Wt} \tag{31}$$

Thus for the wide models, the applied tensile load was 2224 N (500 lb),
for the medium width models the load was 1668 N (375 lb), and for the
narrower models the load was 112 N (250 lb).

Another stress commonly used in discussing pinned joints, bearing
stress, is used to describe stresses in these models. For clarity in
definition, this stress needs some discussion. For a single hole con-
nector, bearing stress is defined as

$$S = \frac{P}{Dt} \tag{32}$$

In this discussion, since roughly one-half the total load is acting on
each hole, bearing stress is defined to be

$$S = \frac{P}{2Dt} \tag{33}$$

39

This definition is applied to both holes. Even though the gross-section stress was the same for all models tested, the bearing stress was not.

Figures 19, 20, and 21 show the trend, with distance away from the hole-edge, of the σ_y stresses at the net-section. These stresses are associated with net-section failures. The stresses in the figures have been normalized to hole-edge values. The figures are, respectively, for the long, medium length, and short models. For most cases the stresses are shown for a distance of up to 3 hole radii away from the edge. This is done to show the stress gradients. The stresses have been normalized to unity at the hole-edge and the stresses are shown for both the top and bottom holes. In some figures shown some plotting symbols appear to be missing, indicating the stresses were not computed. It may be that the symbol is hidden by other symbols grouped closely together. However, in some cases (e.g. narrow width models of medium length, fig. 20, open circles) computation was stopped a few radii away from the hole. This was due to difficulty in interpreting the principal stress directions in certain regions of the model. In certain models where the stresses did not vary rapidly, the isoclinic fringes were not sharp and distinct. In all cases (except for the region at the lower side of the hole mentioned at the end of the previous chapter) the areas were not of prime interest. From the figures it is obvious there was not much difference from model to model or between the lead hole and the second hole in the stress gradients at the net-section.

Figures 22, 23, and 24 show the spatial behavior of the σ_y stresses on the centerline below the holes. Since these stresses are compres-

sive, they are associated with the crushing or bearing failure of the material around the hole. For the second hole these stresses by definition drop to zero at the free end of the model. For the top hole, these centerline stresses also vanish but become tensile as the second hole is approached. If the distance between the two holes is large enough these tensile stresses become one-half the gross stress. A study of stresses in the region between the isotropic point and the second hole for a long wide model [32] showed these tensile stresses were not perfectly uniform across the width but that they were close to achieving uniformity. A similar study for other model geometries was not conducted.

Figures 25, 26, and 27 are quite interesting. These figures show the normalized σ_x stresses below the second hole. These stresses have been normalized to the maximum value of stress along the centerline. As can be seen, in all cases these stresses go from compressive at the hole edge to tensile within a hole radius of the hole edge. In most cases the maximum tensile stress occurs at the free end while the maximum compressive stress occurs at the hole edge. The compressive stress at the hole edge is felt to be due to friction between the dowel and the hole. Wilkinson [23] noted a similar effect in a study of wooden joints with steel pins. Oplinger and Ganhdi [33] showed that including the effects of friction can change the sign of the hoop stress around the hole. Their study was done for orthotropic materials. The large tensile stress near the free end can lead to the splitting of the joints along the centerline. Such an effect was noted by Matthews [34] during a study of glass-epoxy connectors. The connectors which failed in that study were weak in the width direction but this points out that the

splitting stresses should not be ignored even though they may be small compared with, say, peak net-section stresses.

Figures 28, 29, and 30 illustrate the net-section stress concentration factor, based on the gross stress, for the various models. The stress concentration factor for each hole in each model is computed two ways. The stress concentration factor based on the assumption 50% of the load is reacted at each hole, eq. 33, is shown with open symbols. The stress concentration factor based on the actual percentage of load reacted at each hole, from Table 2, is shown in solid symbols. Since all the loads were close to 50-50, there is not much difference in the two sets of numbers. The solid lines on each figure are hand-faired and represent what are felt to be trends. These will be discussed later.

As can be seen, the stress concentration factor for the lead hole is always greater than the stress concentration factor for the second hole and both stress concentration factors increase with increasing W/D. On these figures stress concentration factors obtained by other investigators for single-hole connectors are indicated. The second-hole stress concentration factors should correspond closely to the single-hole values of other investigators if the gross stress for the single-hole connectors is doubled (halving their stress concentration factors) and the width, W, and the distance to the free end, e, are similar.

Coker, et al. [9] tested a single model with the hole about 12 diameters from the free end. The value of W/D for the connector was about 8. The data for this test are shown on the three figures although it most aptly may belong on the figure of the long model, fig. 28, e/D =

3. Finite element results from the single-hole connector study of Crews, et al. [22] are also shown on the figures. The dashed line is their trend with W/D for a quasi-isotropic material and for a model much longer than the ones tested in this study, namely models with an e/D = 10. For wide joints, however, their study shows e/D does not significantly affect stress concentration factors for e/D > 2 or 3. Thus there is some justification in comparing their results with the present results. De Jong [35] studied infinitely long isotropic and orthotropic single-hole connectors and Ogonowski [5] looked at finite-sized single-hole isotropic and orthotropic connectors with an e/D of 2. Both investigators' pertinent results are shown on the three figures. Nisida, et al. [18] tested models with a W/D of 10 and various values of e/D. On the figures are their values of the stress concentration factors obtained for various values of e/D. On figs. 28, 29, and 30 the data for two tests of Jessop, et al. [13] are shown. From their paper it is not clear what the lengths of their models were.

It might be expected that the wide long model stress concentration factor should not be too different than an infinite plate solution. Comparisons using gross stress for infinitely wide plates are of course meaningless. However, if bearing stress is used (stress at net-section hole edge/S of eq. 33), the long wide model has a bearing-stress stress concentration factor of 0.97. Bickley's [4] infinite plate single connector has a bearing-stress stress concentration factor of 0.81. De Jong computed a value of 0.82. The bearing-stress stress concentration factors for all the cases shown in Figures 28, 29, and 30 can be computed knowing the net-section stress concentration factor and the value

of W/D.

Figures 31, 32, and 33 show the stress concentration factors for the radial compressive stress below the hole, on the joint centerline. The stress concentration factors in these figures are based on the bearing stress for the hole, eq. 33. The data on these figures have no discernable trend with the value of W/D. Although, on the whole, they seem higher for the shorter specimens. Based on the results of other investigators for single-hole connectors, the stress concentration factors for the second hole were not expected to vary much with the geometry of the models. For reasons discussed later, the stress concentration factors for the lead hole were not expected to vary much with model geometry either. Furthermore, it was not expected that the values for the stress concentration factors of the lead hole would be too different from the values for the second hole. On these figures are data for the results of other investigators studying single-pin connectors. Nisida, et al. [18] obtained stress concentration values of 1.02, 1.14, 1.11, and 1.25 for e/D values of 1.0, 1.5, 2.5, and 4.0, respectively. This was for an e/D = 10. Bickley [4] obtained a value of 1.27 for the infinte plate single-hole connectors. Coker, et al. [9] obtained a number slightly less than unity. Crews, et al. [22] did not study the compressive radial stress as extensively as they studied the net-section tensile stress. However, their results for quasi-isotropic materials indicate that for wide specimens (W/D = 20) there is little sensitivity of the stress concentration factor to e/D, ranging from slightly less than unity for e/D = 1.00 to about 1.25 for e/D → ∞. They

44

also show that for long specimens (e/D = 10) the stress concentration factor is about 1.25 for widths W/D = 2 to W/D → ∞. De Jong [35] obtained a value of 1.16 for values of W/D ranging from 2.5 to ∞ for infinitely long specimens.

It should be mentioned that the stress studied directly under the hole is a contact stress. Any irregularities in the surfaces of the two contacting materials can cause extremely high and/or irregular local stresses. Such a situation can be seen in fig. 10. To the right of the semi-circular fringe which straddles the centerline just below the hole there is a smaller semi-circular fringe at the hole edge. This smaller fringe is due to a high localized stress from a surface irregularity on either the pin or the hole. When interpreting fringe values at the hole edge, these surface irregularities can induce fringes which effect the results of stress calculations. This results in essentially a 'noisy' stress calculation. Photoelastic material like PSM-1 is particularly sensitive to these irregularities. This is felt to be the reason for much of the scatter observed in figs. 31-33.

The behavior of another important stress, the shear stress, is shown in figs. 34-36. These figures show the shear stress normalized by the gross stress, τ_{xy}/σ_{gross}, along a line parallel to the centerline, starting at the net-section hole edge and proceeding towards the free end of the joint. This line, or plane if the thickness of the joint is considered, is referred to by some investigators as the shear-out plane. If the shear stresses along this line become excessive, the pins could shear out towards the end of the joint. The figures show these shear stresses for both the lead and second holes. Although the figures

45

appear cluttered, if there is interest in a particular joint geometry, the trend and peak values can be easily picked out. All values of the shear stress tend to reach a maximum within a hole radius of the net-section hole edge. In addition, the second hole seems to have higher peak stresses for all joints. Crews, et al. [22] studied this stress and found that the shear stress divided by the bearing stress reached a maximum value of between 0.5 and 0.75, depending on joint geometry, for a quasi-isotropic material. These findings are consistent with the findings presented in figs. 34-36.

Figures 37-39 show further trends of the shear stress. Each figure has two parts. To the right in each figure is an indication of the locus of points of maximum shear stresses below the lower-most point of the second hole. To the left in each figure, the values of the shear stresses normalized by the gross stress along this locus are shown. As can be seen, for all model geometries, the locus of maximum shear stress occurs on the center line side of the shear-out plane near the hole and then moves outside the shear-out plane as the free end of the joint is approached. From figs. 34-36 and figs. 37-39, it appears the maximum τ_{xy} shear stress under the hole does not occur on the shear-out plane but occurs somewhat closer to the joint center line.

DISCUSSIONS AND CONCLUSIONS

As the result of this study, a technique has been developed for the investigation of double-lap, double-pin joints. This technique is based on the use of transmission photoelastic models of the joints. Methods were developed for making the models, for loading them, and for translating the photoelastic data into stress information. All of these phases of the technique involved either extending previously published methods or developing new approaches. The techniques developed were specialized to this particular study but certainly can be used as a basis for other photoelastic work. More important than the development of a new technique, though, was the acquisition of valuable engineering information regarding joints.

The existence of a photoelastic isotropic point, and its relation to the load sharing between the two pins, is a unique discovery. It is felt that this technique can be used to study the load sharing between pins when one pin is deliberately made to be much smaller or much larger than the hole. This would represent the situation where one pin in a connector is accidently missized. It may be possible to determine what degree of missizing is required in a model to have the load proportioning be, for example, 30-70 instead of 50-50. In addition, it is felt the photoelastic isotropic point may have value in actual metal or composite connectors. Such a point probably exists in photoelastic reflective coatings and these coatings could be applied to actual joints. Determining the redistribution of the load from one pin to

another as the hole elongates during the fatigue of a multiple-pin joint may be possible with the coating technique.

The trends in peak values of the stresses for the various joint geometries provide other engineering information. This information is presented in figs. 21-39. While figs. 21-23 show net-section stress gradients normalized to the hole-edge stress value, considering both the gross stress value of 1.97 MPa (286 psi) used for all models and the net-section stress concentration factor of figs. 28-30, actual stress values can be determined. Since there is little difference between the stress gradients among the models or between the lead hole and second hole, failure criteria based on the average stress over some characteristic distance from the hole edge would not seem to be dependent on model geometry. That would lend credibility to idea that these characteristic distances are material properties [3], a phenomena observed when testing composite specimens with holes.

While the net-section stress gradients show little sensitivity to model geometry, the net-section stress concentration factors, figs. 28-30 do. There is particular sensitivity of the stress concentration factors to the numerical value of W/D. The solid lines in figs. 28-30, as stated before, are hand-faired straight lines through the data determined from this experiment. There really was not enough data to justify a least-square fit and in the region a straight line was felt to be a good estimate of the true relation in this region. The single-pin connectors studies of other investigators seemed to cluster around the straight-line fit of the data in this study with Crews et al.'s data

[22] being on the upper end. Their analysis assumed a frictionless but flexible steel pin whereas de Jong [35] assumed a perfectly rigid frictionless pin. Ogonowski [5], as mentioned before, used the radial cosinusoidal distribution over one half the hole opening. It is felt that friction would have a small effect, if any, on the net-section stress concentration factor. All the friction effects between the hole and the pin take place on the circumference of the hole below the net-section location. In the experiments of other investigators, the results are for single-pin connectors about the stiffness of plexiglass and with pins as stiff or only slightly stiffer than the joint material. The pins in all the studies were of some kind of plastic. The results of Nisida et al. [18] seem to be out of line with the other investigator's data. In addition to providing stress concentration factors for double-pin joints, figs. 27-29 are a good summary of pertinent work on single-hole connectors and show a comparison among recent investigations.

As expected, the stress concentrations factors for the lead holes are higher than the stress concentration factors for the second holes and obviously dictate the design of a joint if net-section tension failure is a concern. There does not seem to be an obvious trend of stress concentration factors with model length, although the stress concentration factors for the second holes of the shorter joints are less than the stress concentration factors for the second holes of the other joints. If indeed the stress concentration factors are lower, it is due to the close proximity of the lead hole in this short joint

49

design rather than the short distance to the free edge. This can be said because the distance from the second hole to the free end is the same for the medium length models and the short models and the medium length model's stress concentration factors for the second hole are about the same as the stress concentration factors for the longer model's second holes. Why the stress concentration factors for the lead hole of the medium length model with a W/D of 6 is low (fig. 29, squares) is a puzzle.

It is interesting to note that even for the narrow models with the shorter distance from the second hole to the free end, the σ_y stress was actually zero at the outside edge of the second hole net-section (figs. 20 and 21, closed circles). This indicates that even for these models, material and weight could be saved by rounding the free-end, starting at the net-section with the rounding radius.

Like the net-section stress gradients, the stress gradients below the hole along the joint center lines are all similar. The gradients appear to be insensitive to model geometry. It appears that the longer models are longer than needed both between the holes and from the second hole to the free end. The compressive stresses are very low for at least a hole radius from the free end. In addition, as mentioned before, the compressive stresses below the lead hole become tensile as the second hole is approached. There is no need for the stresses to become uniform in this region and so the lengths can be made shorter and thus provide a lighter joint.

The lack of any discernable geometric effects on the bearing stress

stress concentration factors below the holes, figs. 31-33, also empha-
sizes the fact the shorter joint is as effective as either of the other
designs. It is felt the bearing stress at the lower diameter of the
hole is primarily a function of hole diameter, and of course pin tol-
erance in the hole. This bearing stress is such a localized phenomena
that other geometric characteristics of the joint produce only a second-
order effect on the bearing stress. Since all models have the same hole
size, and ostensibly the same pin/hole tolerance, the bearing-stress
stress concentration factors for all holes, lead and second, should be
about the same. The fact that the lead hole has 50% of the load passing
by really should not affect the bearing stress for that hole. The lead
hole can be considered as the algebraic sum of a single-pin connector,
for the portion of the load reacted by it, and an open hole tensile
strip, for the portion of the load passing by it. The open-hole con-
nector has no bearing stress and so the bearing stress at the bottom of
the lead hole is due to the single-pin connector effect reacting one
half the load, the same as the second hole. Therefore the lead hole and
the second hole should be no different when it comes to bearing stress.
Actual hole size can be important and probably does effect the bearing
stress more than any other geometric parameter of the joint. Globally,
the problem of determining joint stresses is a linear elastic problem.
However, the interaction of the hole and pin is nonlinear and so actual
hole size, as opposed to some value of W/D, is important. Since in this
study all holes were of the same size, not much can be said about this
issue. This area needs further investigation. However, for holes in the

51

19-25 mm range (0.75 to 1.00 in.), a bearing-stress stress concentration factor of 1.5 would give conservative design for both holes. As with the net-section stress concentration factors, figs. 31-33 provide a good comparison of recent investigations.

Examination of the shear stresses below and near the holes, figs. 34-39, reveal some interesting trends. For all geometries, the shear stresses at the lead hole were less than the corresponding stresses at the second hole. In addition, it appears that the wider the joint, the larger the value of τ_{xy}/σ_{gross}, both along the shear-out plane, figs. 34-36, and along the maximum shear locus, figs. 37-39. At first thought it would seem that the narrow joint would produce higher stresses because the load must pass the hole via a narrow piece of net-section material. However, for a given σ_{gross}, wider joints lead to higher total loads which must be reacted by the hole. This obviously is what leads to the higher shear stress. The distance from the second hole to the free end did not seem to have a large influence on the shear stress. As seen in figs. 37-39, the locus of maximum shearing stress below the hole is not quite coincident with the shear-out plane. The shear stress on the joint centerline is zero and so there are large shear stress gradients on lines perpendicular to the joint centerline. This is more pronounced in regions within a hole radius of the bottoms of the holes. The maximum shear stress locus obviously proceeds into the section below the hole that was difficult to analyze. It is felt that interrogation of existing photoelastic data in this region could lead to a completion of the locus to the hole edge.

REFERENCES

1. Hyer, M. W. and Lightfoot, M. C., "Ultimate Strength of High-Load Capacity Composite Bolted Joints," ASTM STP-674 Composite Materials: Testing and Design, Fifth Conference, 1979, p. 118-136.

2. Hyer, M. W., Perry, J. A. and Lightfoot, M.C., "Load Transfer in Composite Bolted Joints," AIAA Paper 80-0779-CP, presented at 21st SDM Meeting, Seattle, Washington, May 1980.

3. Whitney, J. M. and Nusimer, R. J., "Stress Failure Criteria for Laminated Composites Containing Stress Concentrations," Journal of Composite Materials, Vol. 8, July 1974, p. 253-265.

4. Bickley, W. G., "The Distribution of Stress Round a Circular Hole in a Plate," Phil. Trans. Royal Soc. (London), Vol. 227 A, July 1928, p. 383-415.

5. Ogonowski, J. M., "Analytical Study of Finite Geometry Plates with Stress Concentrations, paper no. 80-0778, Proceedings of 21st SDM Conference, AIAA/ASME/ASCE/AHS, p. 694-698 (part 2), 1980.

6. Knight, R. C. "The Action of a Rivet in a Plate of Finite Breadth," Phil. Mag., Series 7, Vol. 19, No. 127, March 1935, p. 517-540.

7. Theocaris, P. S., "The Stress Distribution in a Strip Loaded in Tension by Means of a Central Pin," Trans. ASME, Journal of Applied Mechanics, Vol. 23, No. 1, March 1956, p. 85-90.

8. Fisher, J. W. and Struik, J. H., A Guide to Design Criteria for Bolted and Riveted Joints. New York: John Wiley & Sons, Inc., 1974.

9. Coker, E. G. and Filon, L. N. G., A Treatise on Photoelasticity. Revised by Jessop, H. T. Cambridge, England: Cambridge University Press, 1957, p. 524-530.

10. Frocht, M. M. and Hill, H. N., "Stress-Concentration Factors Around a Central Circular Hole in a Plate Loaded Through Pin in the Hole," Journal of Applied Mechanics, Vol. 7, No. 1, March 1940, p. A-5 -A-9.

11. Jessop, H. T., and Snell, C. and Holister, G. S., "Photoelastic Investigations in Connections with the Fatigue Strength of Bolted Joints," The Aeronautical Quarterly, Vol. 6, Part 3, August 1955, p. 230-239.

12. Jessop, H. T., Snell, C. and Holister, G. S., "Photoelastic Investigation on Plates with Single Interference-Fit Pins with Load Applied to Plate only," The Aeronautical Quarterly, Vol. 7, Part 4, November 1956, p. 297-314.

13. Jessop, H. T., Snell, C. and Holister, G. S., "Photoelastic Investigations on Plates with Single Interference-Fit Pins with Load Applied (a) to Pin Only and (b) to Pin and Plate Simultaneously," The Aeronautical Quarterly, Vol. 9, Part 2, May 1958, p. 147-163.

14. Lambert, T. H. and Brailey, R. J., "The Influence of the Coefficient of Frinction on the Elastic Stress Concentration Factor for a Pin-Jointed Connection," The Aeronautical Quarterly, Vol. 13, Part 1, February 1962, p. 17-29.

15. Lambert, T. H. and Brailey, R. J., "The Use of an Interference-Fit Bushing to Improve Fatigue Life of a Pin-Jointed Connection," The Aeronautical Quarterly, Vol. 13, Part 3, August 1963, p. 275-284.

16. Cox, H. L. and Brown, A. F. C., "Stresses Round Pins in Holes," The Aeronautical Quarterly, Vol. 15, Part 4, November 1964, p. 357-372.

17. Theocaris, P. S., "On an Electrical Analogy Method for the Separation of Principal Stresses along Stress Trajectories," SESA Proceedings, Vol. XIV, No. 2, 1957, p. 11-20.

18. Nisida, M. and Saito, H., "Stress Distributions in a Semi-Infinite Plate Due to a Pin Determined by Interferometric Method," Experimental Mechanics, Vol. 6, No. 5, May 1966, p. 273-279.

19. Oplinger, D. W., Parker, B. S. and Katz, A., "Moiré Measurements of Strains and Deformation in Pin-Loaded Composite Plates," Extended Summaries, 1979 Spring Meeting, SESA, 14 Fairfield Drive, Brookfield Center, CT 06805.

20. Garbo, S. P. and Ogonowski, J. M., "Effect of Variances and Manufacturing Tolerances on the Design Strength and Life of Mechanically Fastened Composite Joints," AFFDL-TR-78-179, September 1978.

21. Soni, S. R., "Failure Analysis of Composite Laminates with a Fastener Hole," ASTM STP 749 Joining of Composite Materials, 1981, p. 145-164.

22. Crews, J. H., Jr., Hong, C. S. and Raju, I. S., "Stress-Concentration Factors for Finite Orthotropic Laminates with a Pin-Loaded Hole," NASA TP 1862, May 1981.

23. Wilkinson, T. L., "Stress in the Neighborhood of Loaded Holes in Wood with Application to Bolted Joints," Ph.D. Thesis, University of Wisconsin-Madison, December 1978, available from University Microfilms, Ann Arbor, Michigan.

24. Sampson, R. C., "A Stress-Optic Law for Photoelastic Analsysis of Orthotropic Composites," Experimental Mechanics, Vol. 10, No. 5, May 1970, p. 210-215.

25. Prabhakaran, R., "Fabrication of Birefringent Anisotropic Model Materials," Experimental Mechanics, Vol. 20, No. 9, September 1980, p. 320-321.

26. Post, D., "A New Photoelastic Interferometer Suitable for Static and Dynamic Measurements," SESA Proceedings, Vol. XII, No. 1, 1954, p. 141-202.

27. Dally, J. W. and Erisman, E. R., "An Analytical Separation Method for Photoelasticity," Experimental Mechanics, Vol. 6, No. 10, November 1966, p. 493-499.

28. Dally, J. W. and Riley, W. F., Experimental Stress Analysis, 2nd ed. New York: McGraw Hill Book Co., 1978.

29. Frocht, M. M., Photoelasticity, Vol. 1. New York: John Wiley & Sons, Inc., 1941

30. Berghaus, D. G., "Overdetermined Photoelastic Solution Using Least Squares," Experimental Mechanics, Vol. 13, No. 3, March 1973, p. 97-194.

31. Smith, G. D., Numerical Solution of Partial Differential Equations. Oxford, England: Oxford University Press, 1964.

32. Hyer, M. W., Use of Two-Dimensional Transmission Photoelastic Models to Study Stresses in Double-Lap Bolted Joints: Load Transfer and Stresses in the Inner Lap, Virginia Polytechnic Institute and State University, College of Engineering Report, VPI-E-80-9, March 1980.

33. Oplinger, O. W. and Gandhi, D. R., "Analytical Studies of Structural Performance in Mechanically Fastened Composite Plates," AMMRC-MS-74-8, 1974.

34. Matthews, F. L. and Hirst, I. R., "The Variation of Bearing Strength with Load Direction," Symposium: Jointing in Fibre Reinforced Plastics. Surrey, England: IPC Science and Technology Press Limited, 1978.

35. de Jong, T., "Stresses Around Pin-Loaded Hole in Elastically Orthotropic or Isotropic Plates," Journal of Composite Materials, Vol. 11, July 1977, p. 313-331.

55

Table 1

DIMENSION OF MODELS*

Model	W mm (in.)	E mm (in.)	e mm (in.)	W/D	E/D	e/D
long, wide	178 (7.00)	133 (5.25)	66.7 (2.62)	8	6	3
long, medium width	133 (5.25)	133 (5.25)	66.7 (2.62)	6	6	3
long, narrow	88.9 (3.50)	133 (5.25)	66.7 (2.62)	4	6	3
medium length, wide	178 (7.00)	133 (5.25)	44.4 (1.75)	8	6	2
medium length medium width	133 (5.25)	133 (5.25)	44.4 (1.75)	6	6	2
medium length, narrow	88.9 (3.50)	133 (5.25)	44.4 (1.75)	4	6	2
short, wide	178 (7.00)	88.9 (3.50)	44.4 (1.75)	8	4	2
short, medium width	133 (5.25)	88.9 (3.50)	44.4 (1.75)	6	4	2
short, narrow	88.9 (3.50)	88.9 (3.50)	44.4 (1.75)	4	4	2

*refer to fig. 1 for definition of W, E, D, and e
D = 22.2 mm (0.875 in.) in all cases

Table 2

PERCENTAGE OF LOAD REACTED AT EACH HOLE OF INNER LAP

Model	Percentage of Load at Lead Hole	Percentage of Load at Second Hole
long, wide	52%	48%
long, medium width	53	47
long, narrow	48	52
medium length, wide	45	55
medium length, medium width	48	52
medium length, narrow	48	52
short, wide	55	45
short, medium width	48	52
short, narrow	40	60
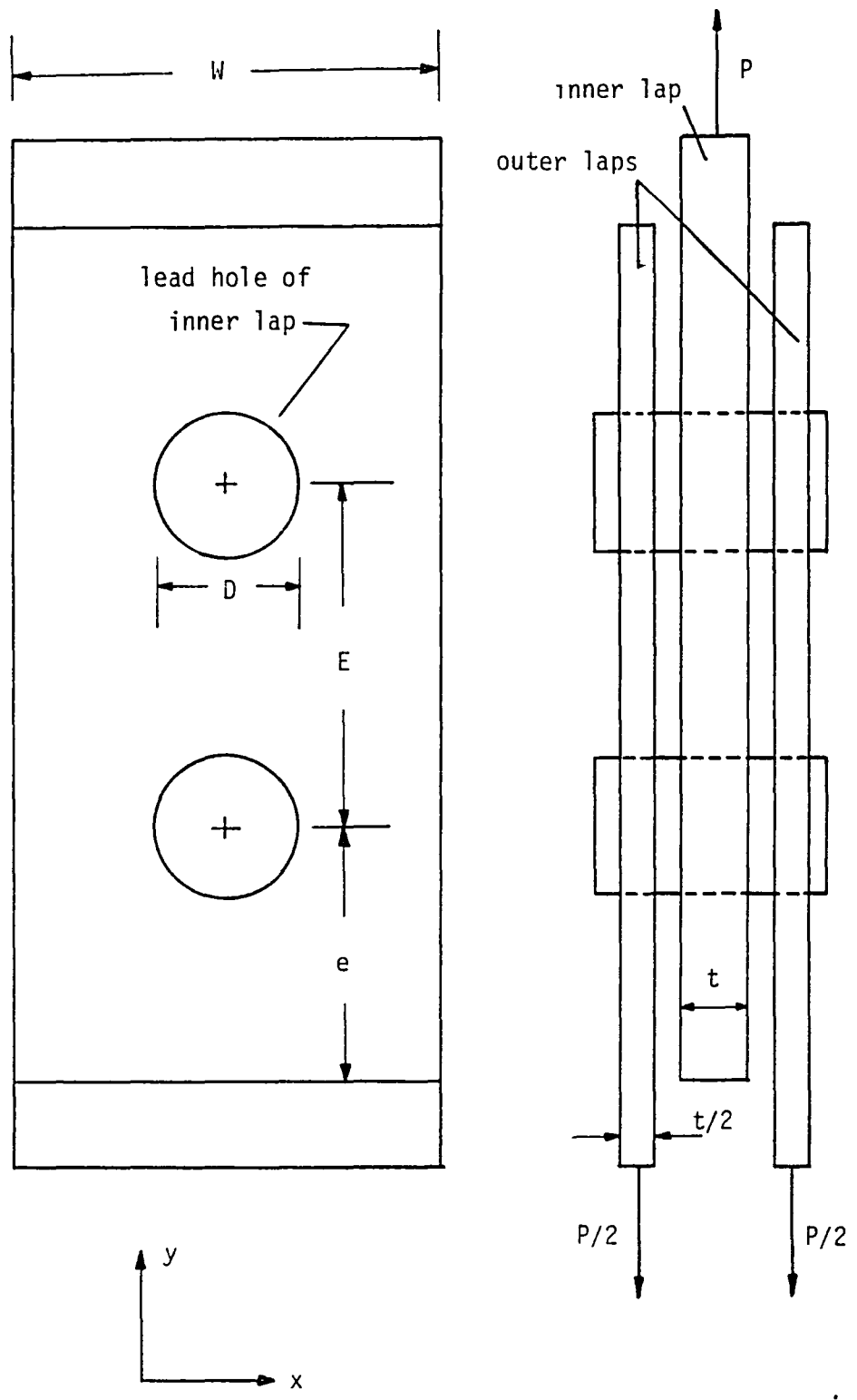
Fig. 1 Joint geometry and nomenclature
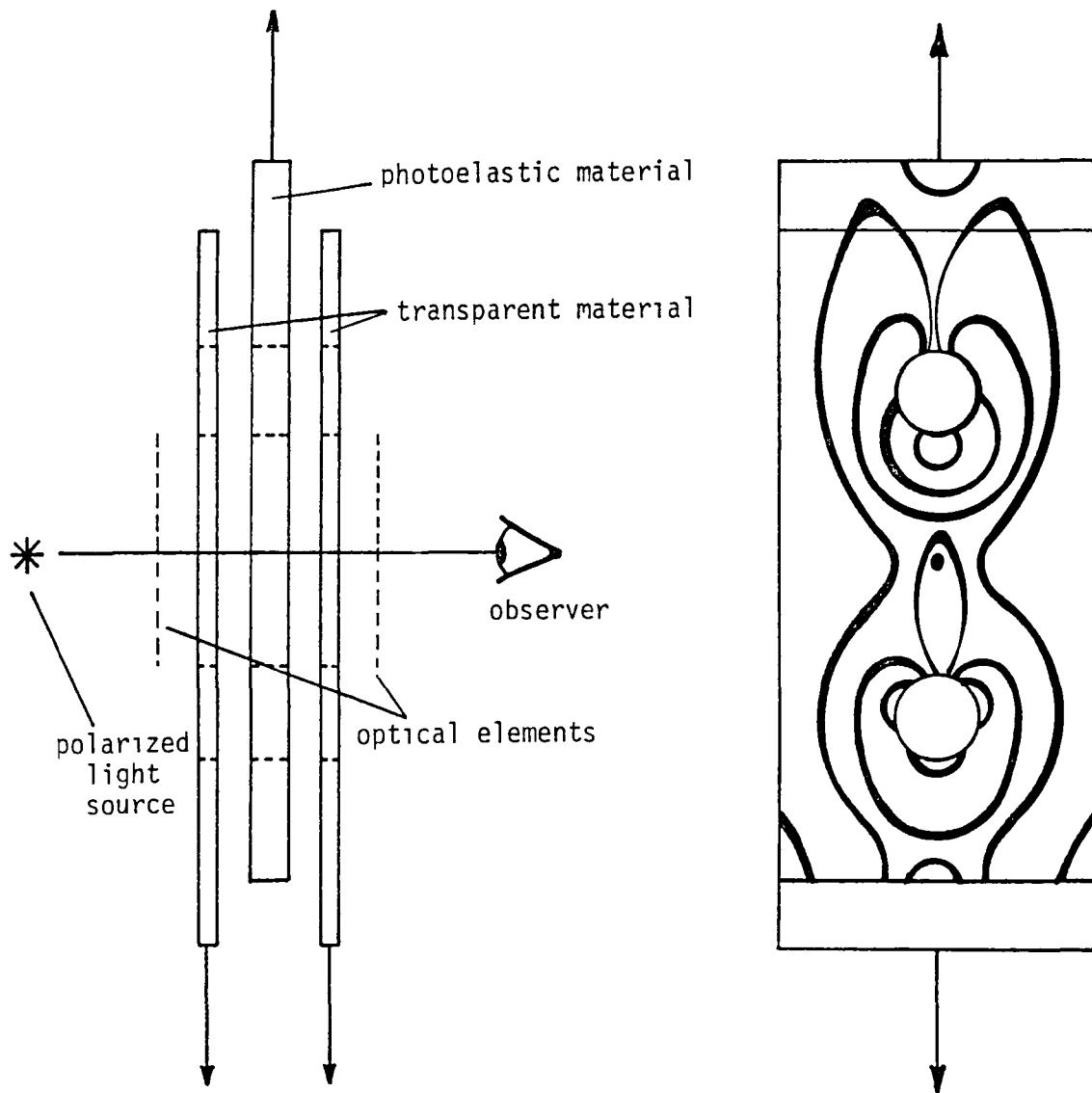
Fig. 2 Design philosophy of photoelastic joint models
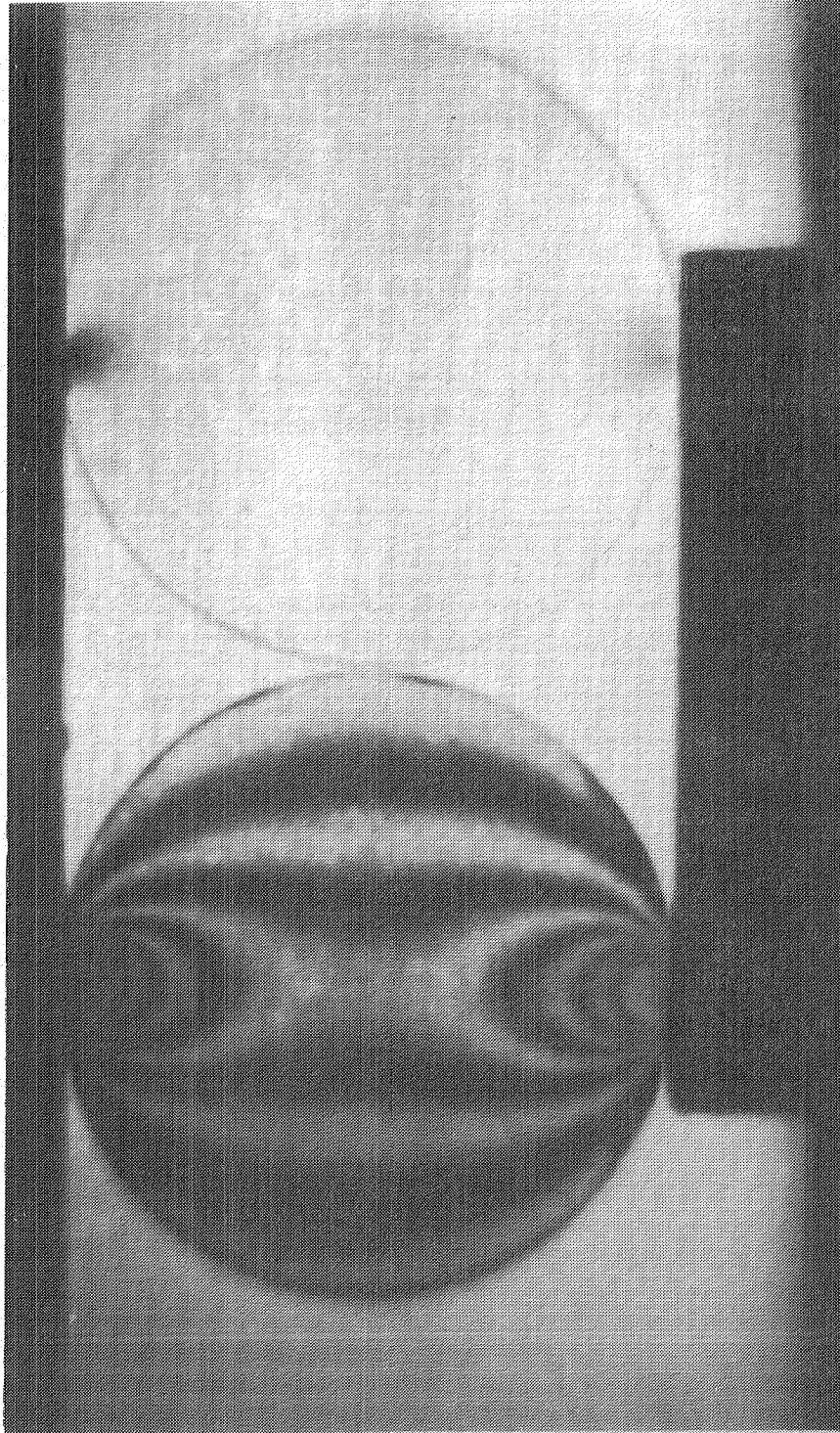
Fig. 3 PSM-1 disk and Acrylite disk subjected
to identical diametral compression loads
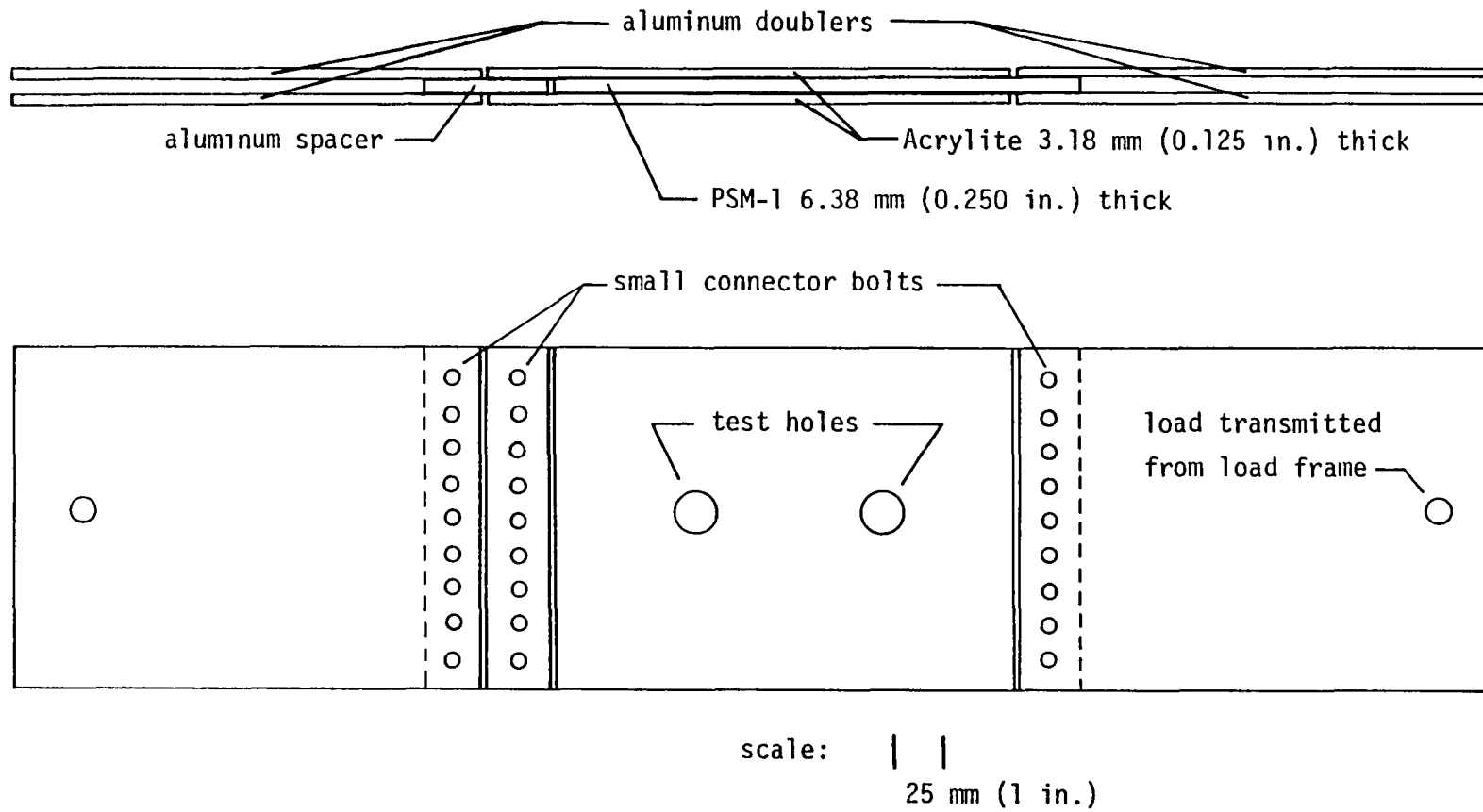
Fig. 4 Geometry of largest model and the load introduction doublers
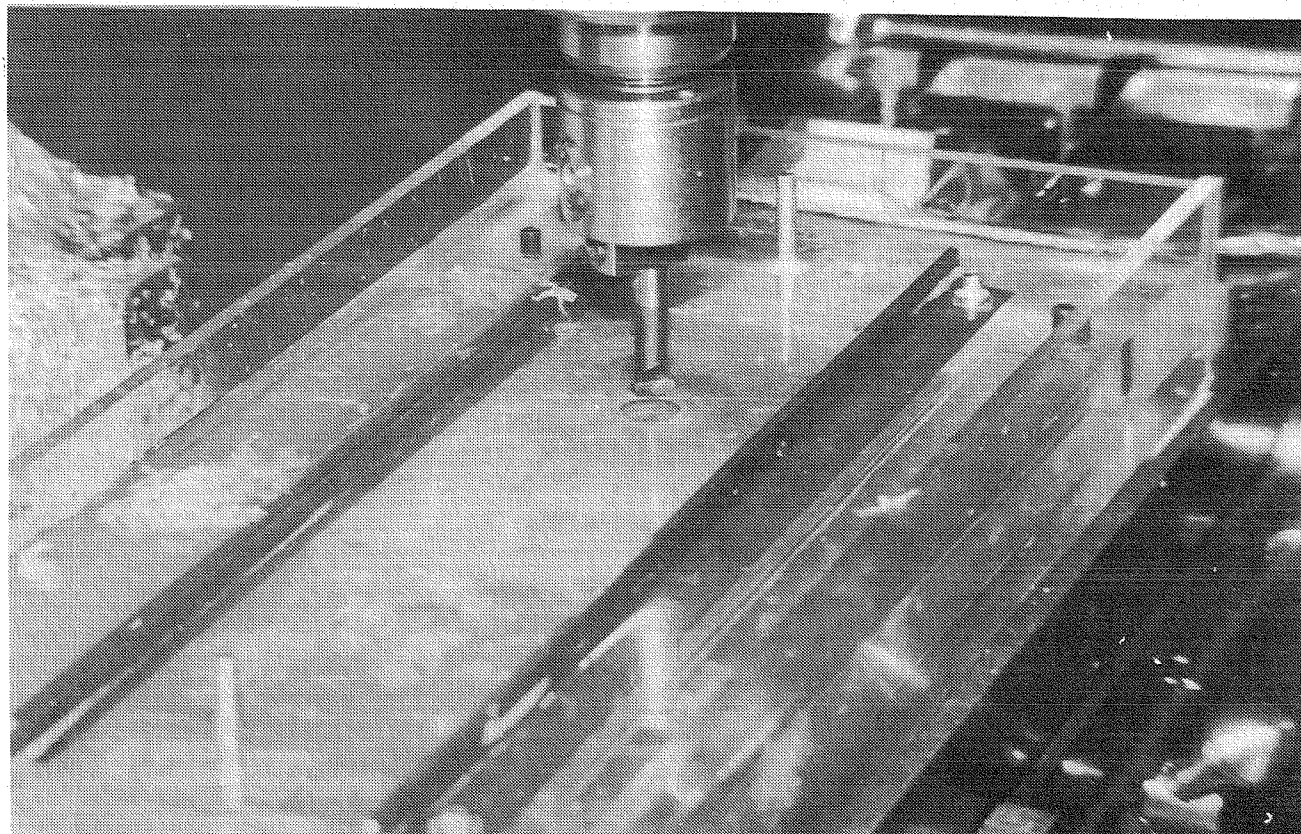
Fig. 5 Machining of the models
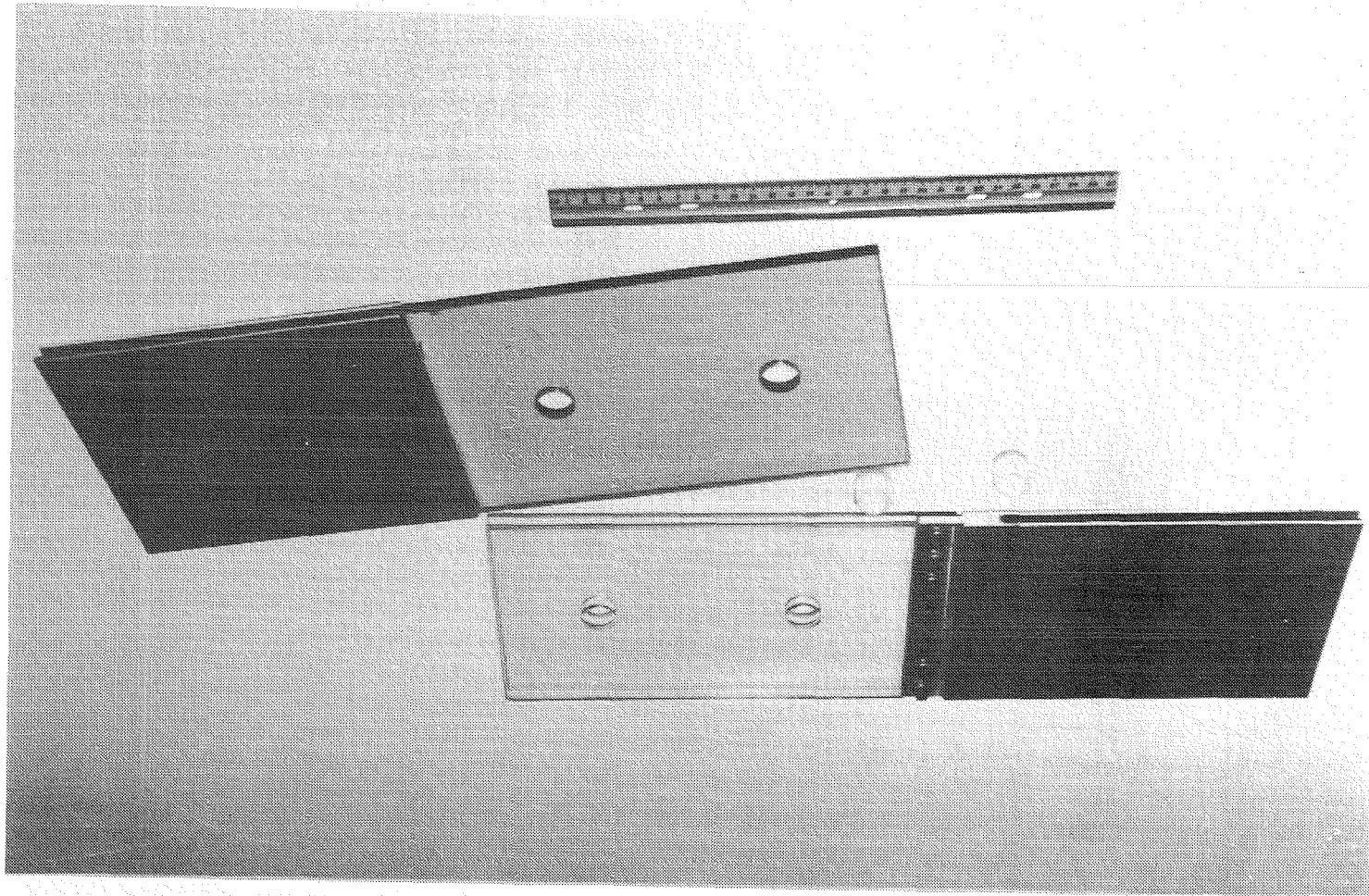
Fig. 6 Long wide model with aluminum doublers
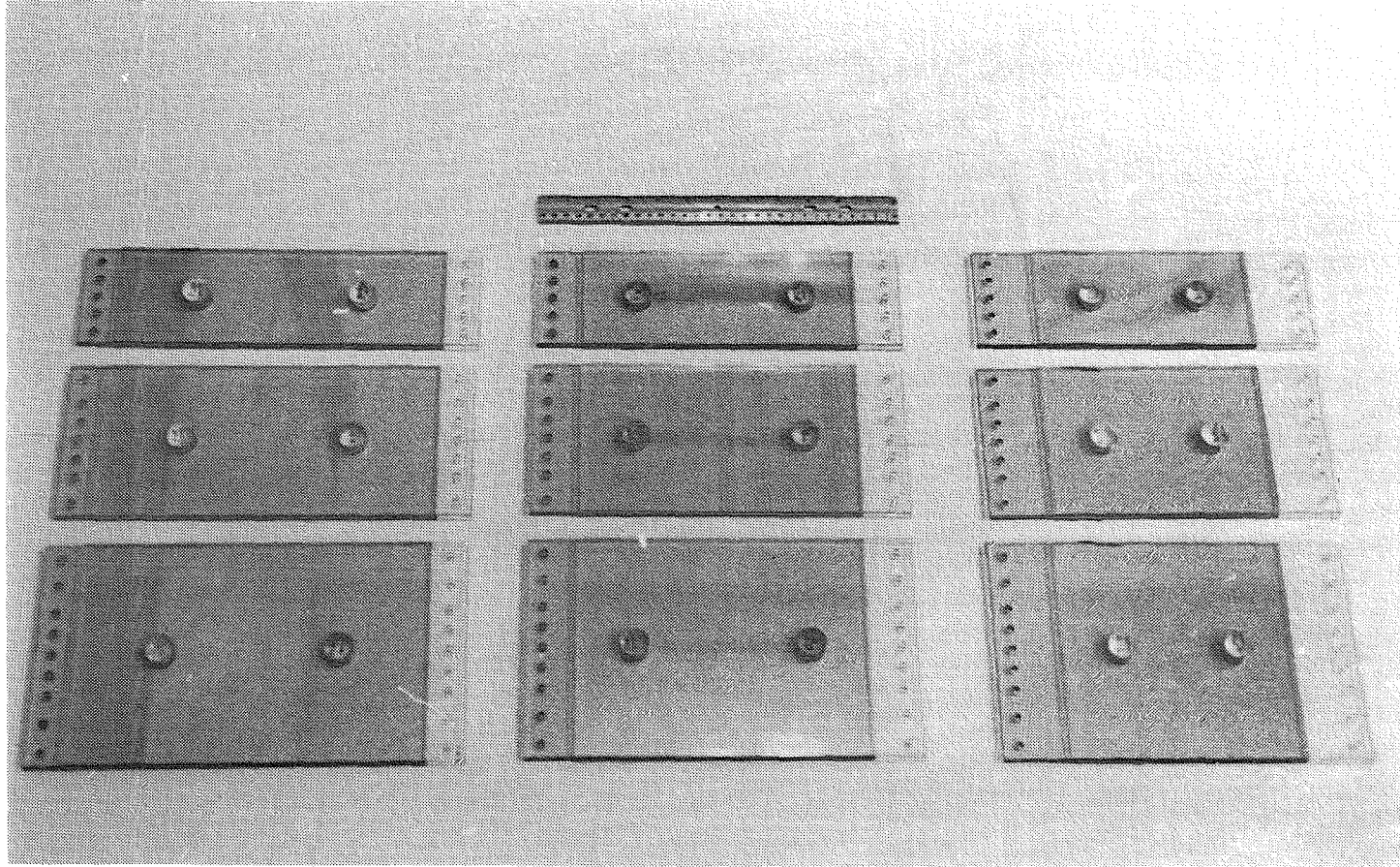
Fig. 7 The nine joint models tested
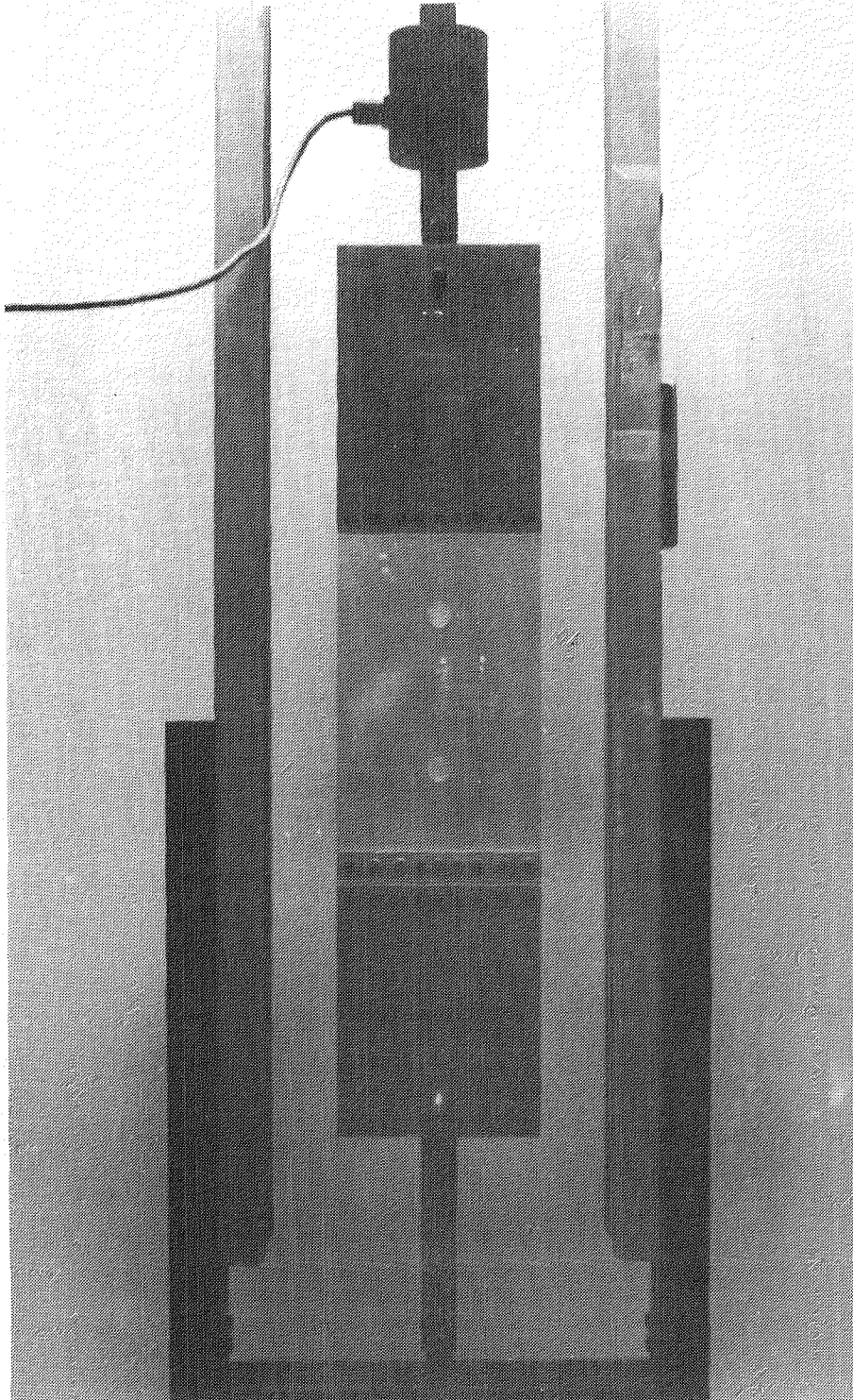
Fig. 8   Long wide model in the loading frame
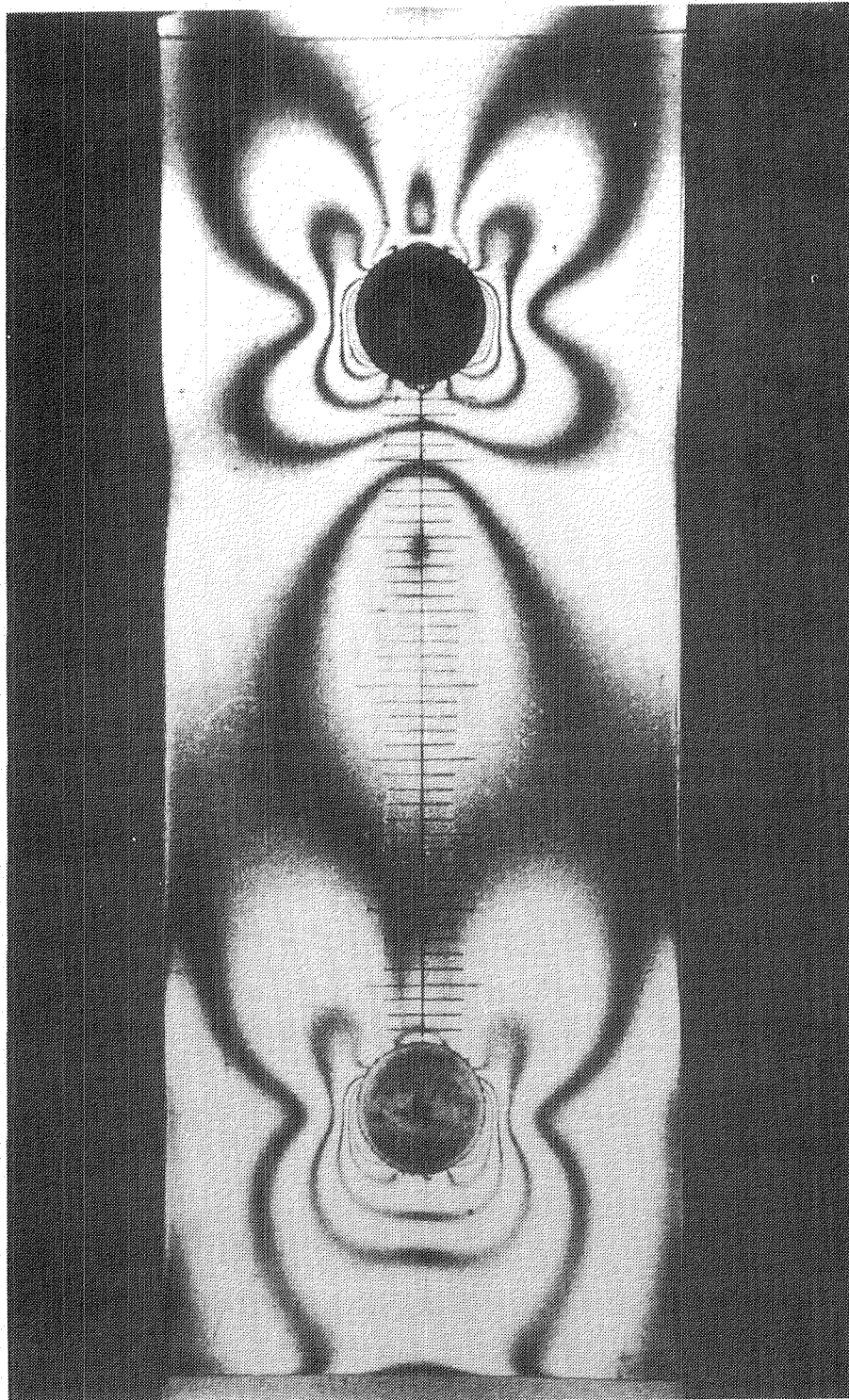
Fig. 9 Typical dark-field isochromatic fringe pattern,
medium length narrow model

singular point

67
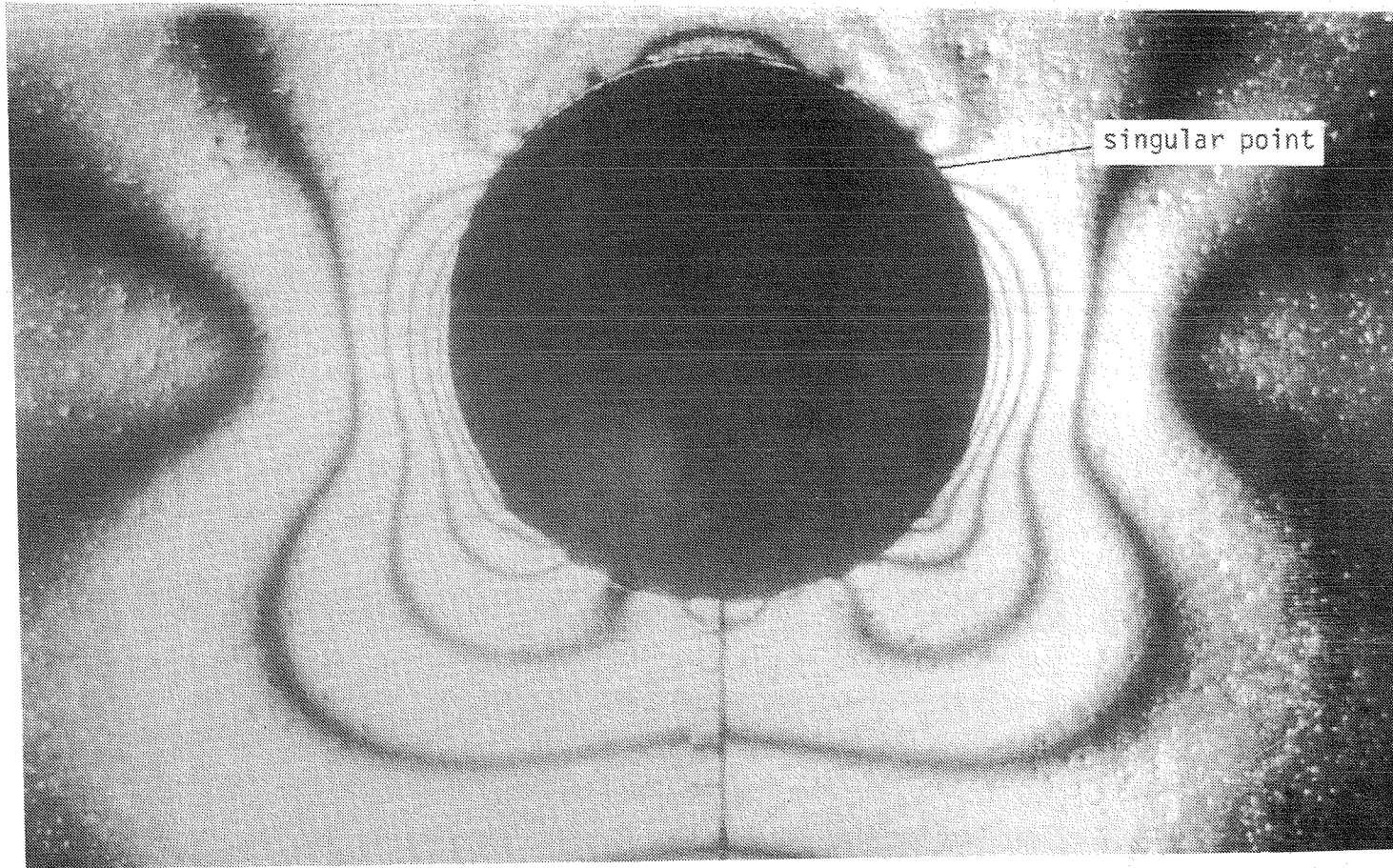
Fig. 10 Close-up view of dark-field isochromatic fringe pattern around lead hole, long narrow model
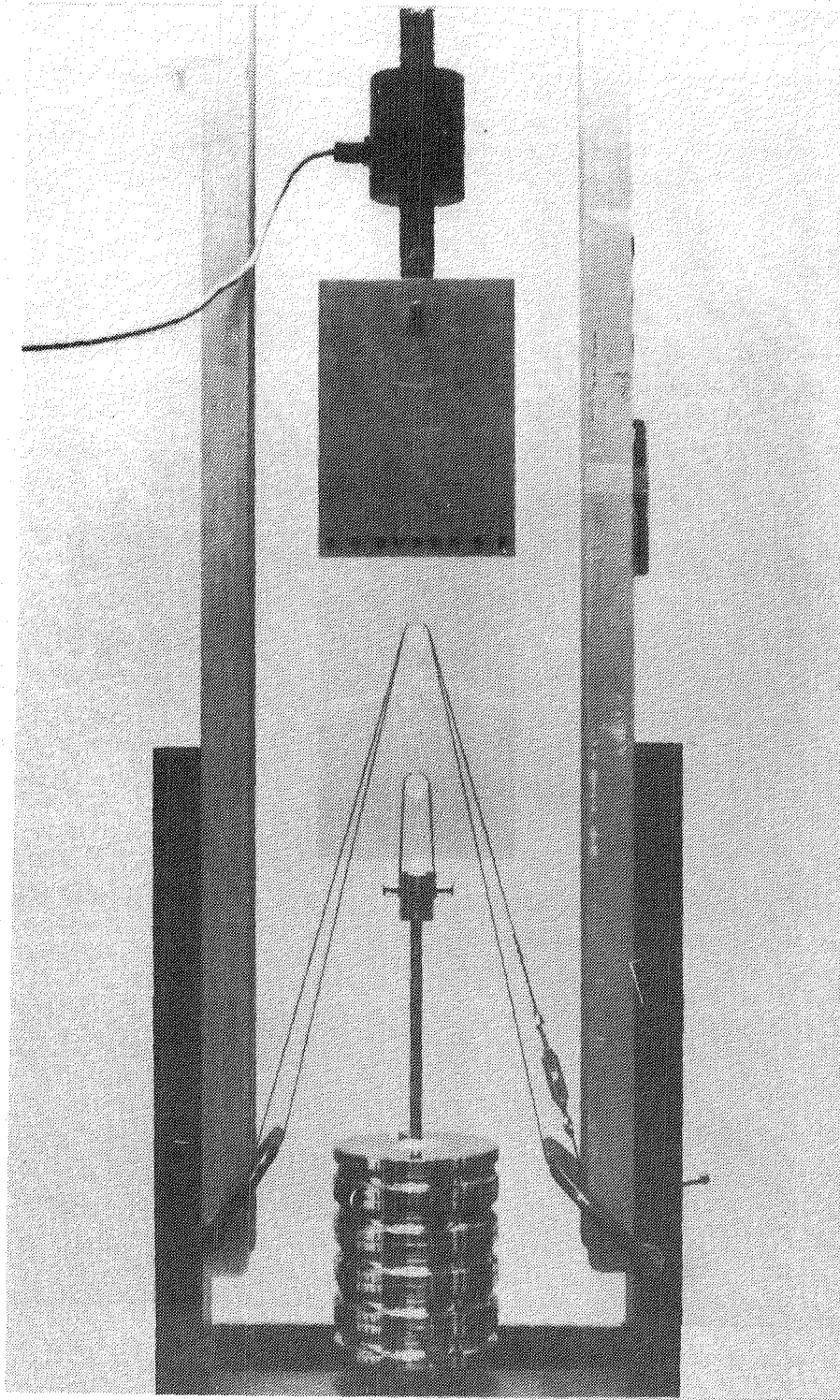
Fig. 11 Apparatus to load each hole independently

68
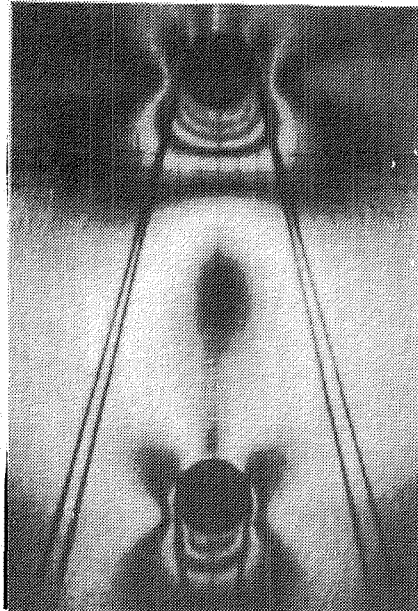
a) P_1=60%, P_2=40%
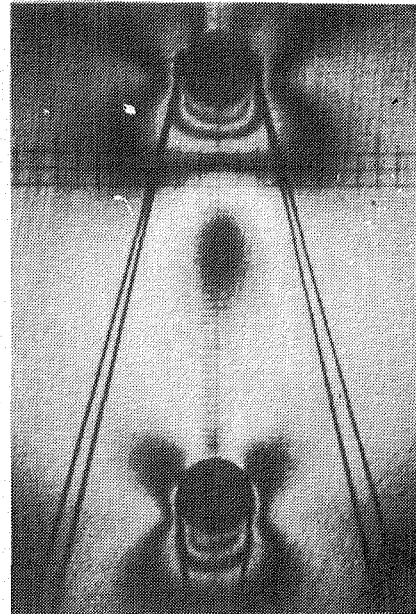
b) P_1=49%, P_2=51%
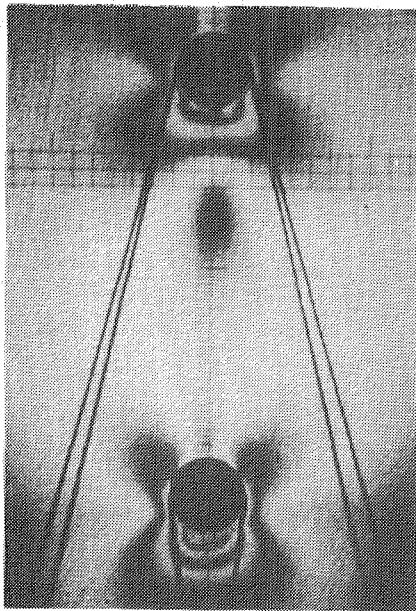
c) P_1=37%, P_2=63%
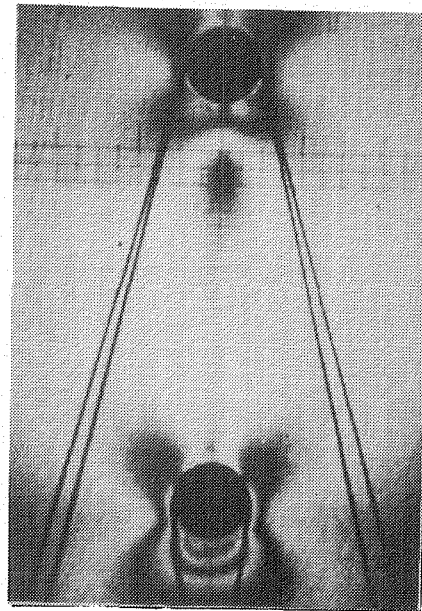
d) P_1=23%, P_2=77%

Fig. 12 Dependence of isotropic point location on percentage of load reacted by each hole (P_1 = top hole, P_2 = bottom hole)

69
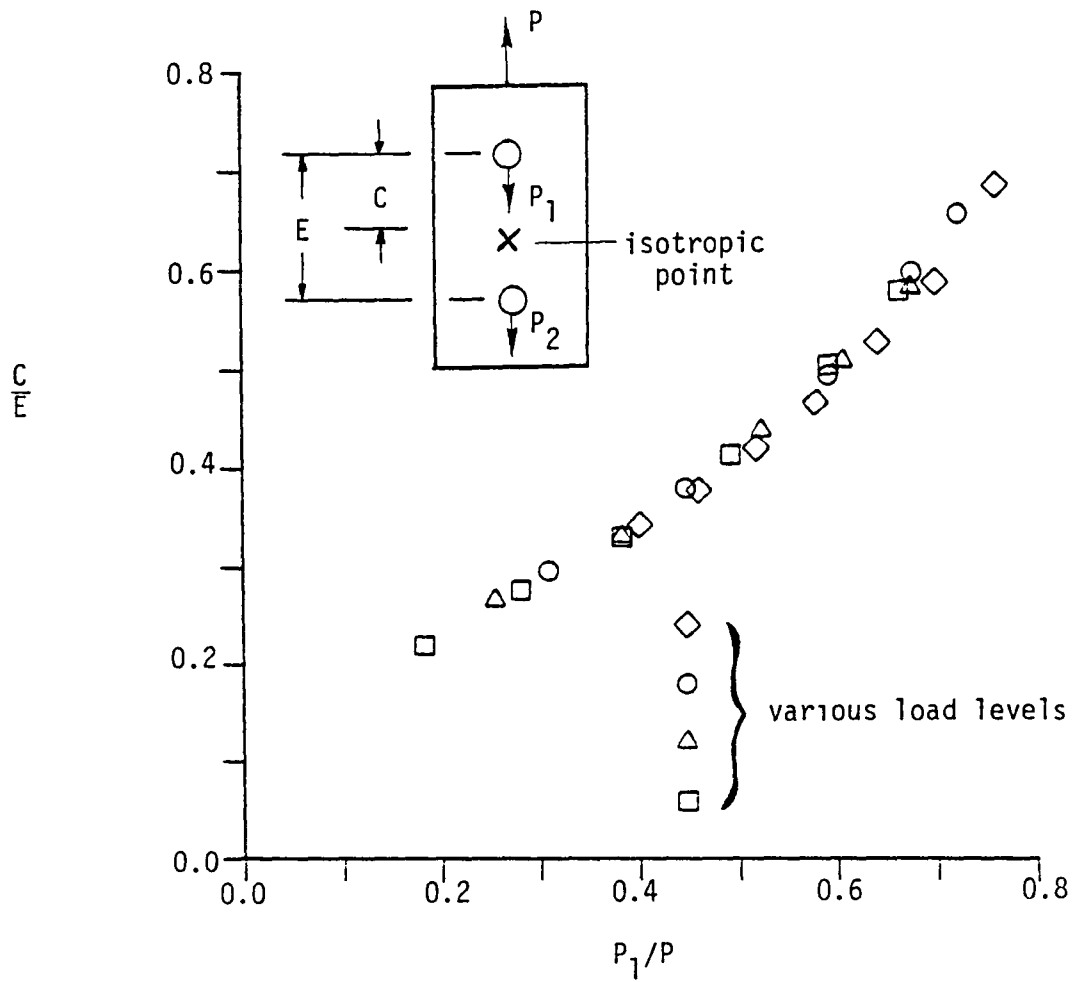
Fig. 13   Isotropic point location as a function of amount of load reacted by each hole
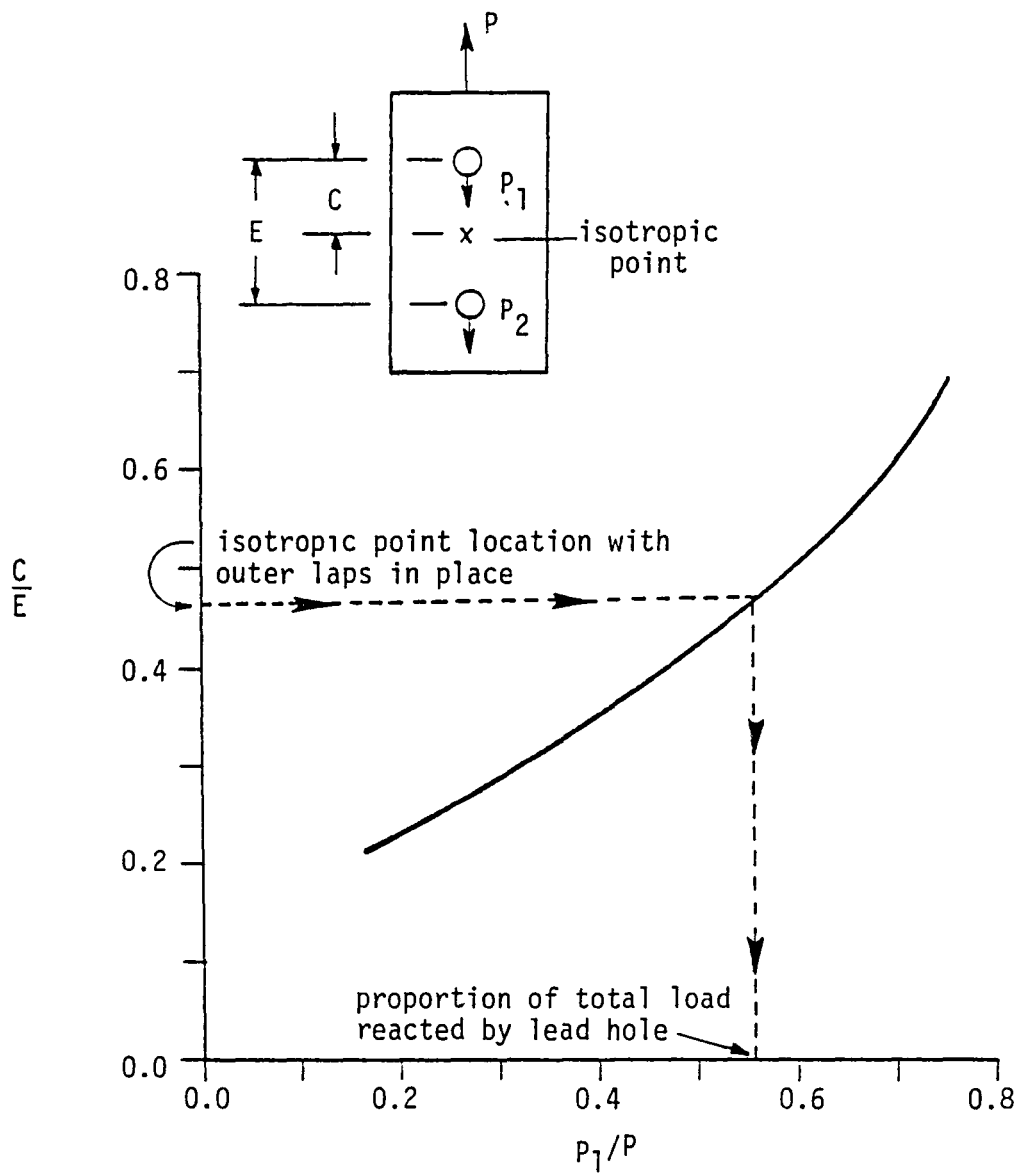
Fig. 14 Determining load proportioning from isotropic point location
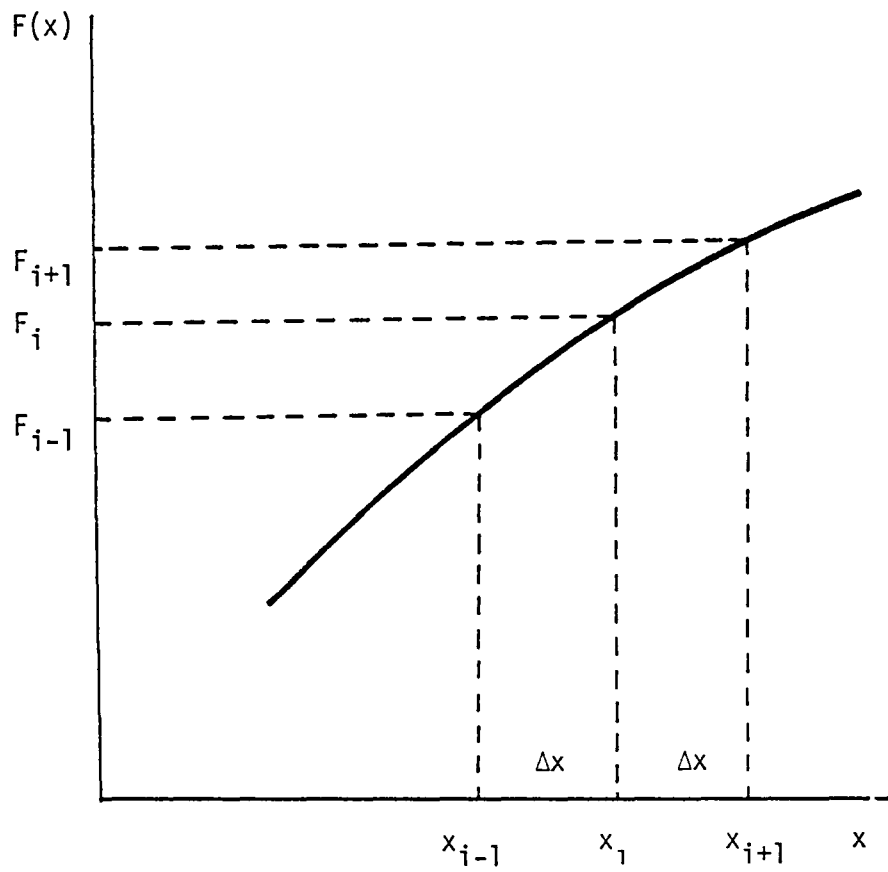
Fig. 15 Discretization of a continuous function

72
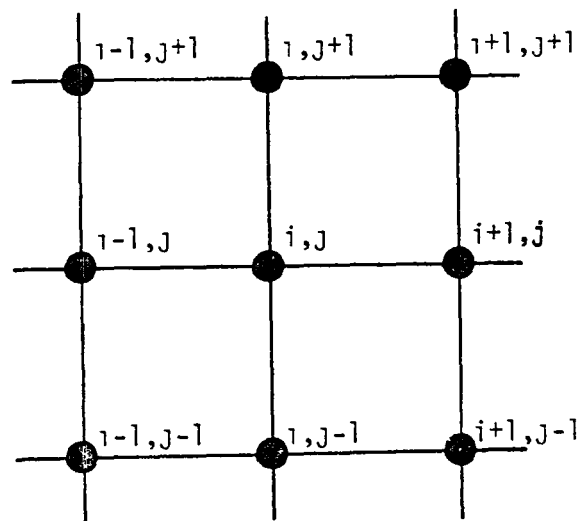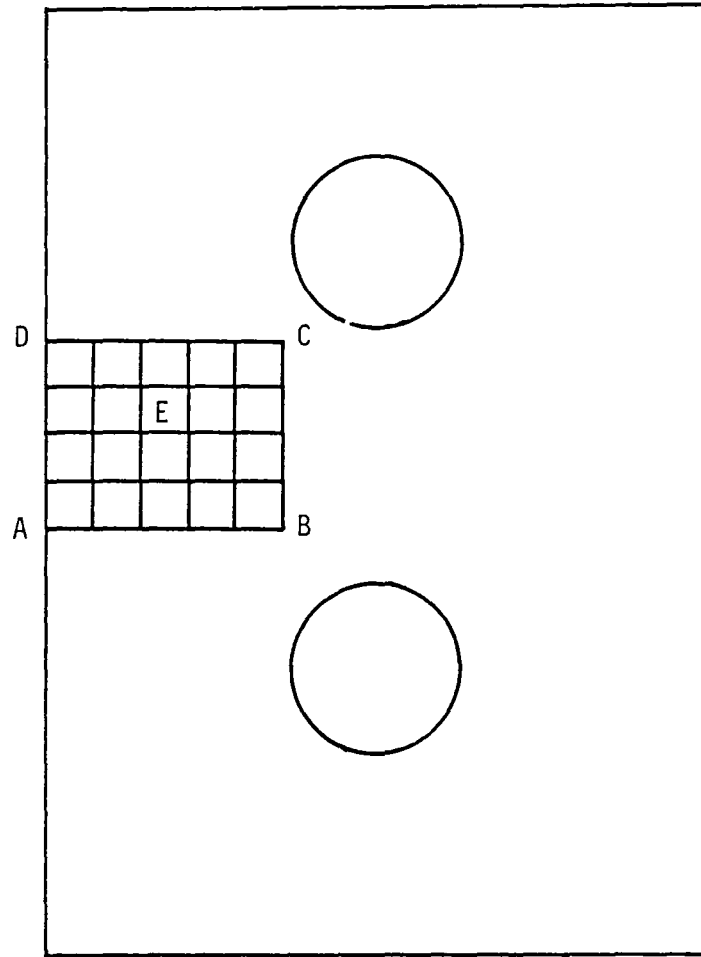
Fig. 16   Two dimensional finite-difference grid on joint model

free edge

zone 4

zone 2

zone 3

zone 5

zone 1

zone 0

centerline
of joint
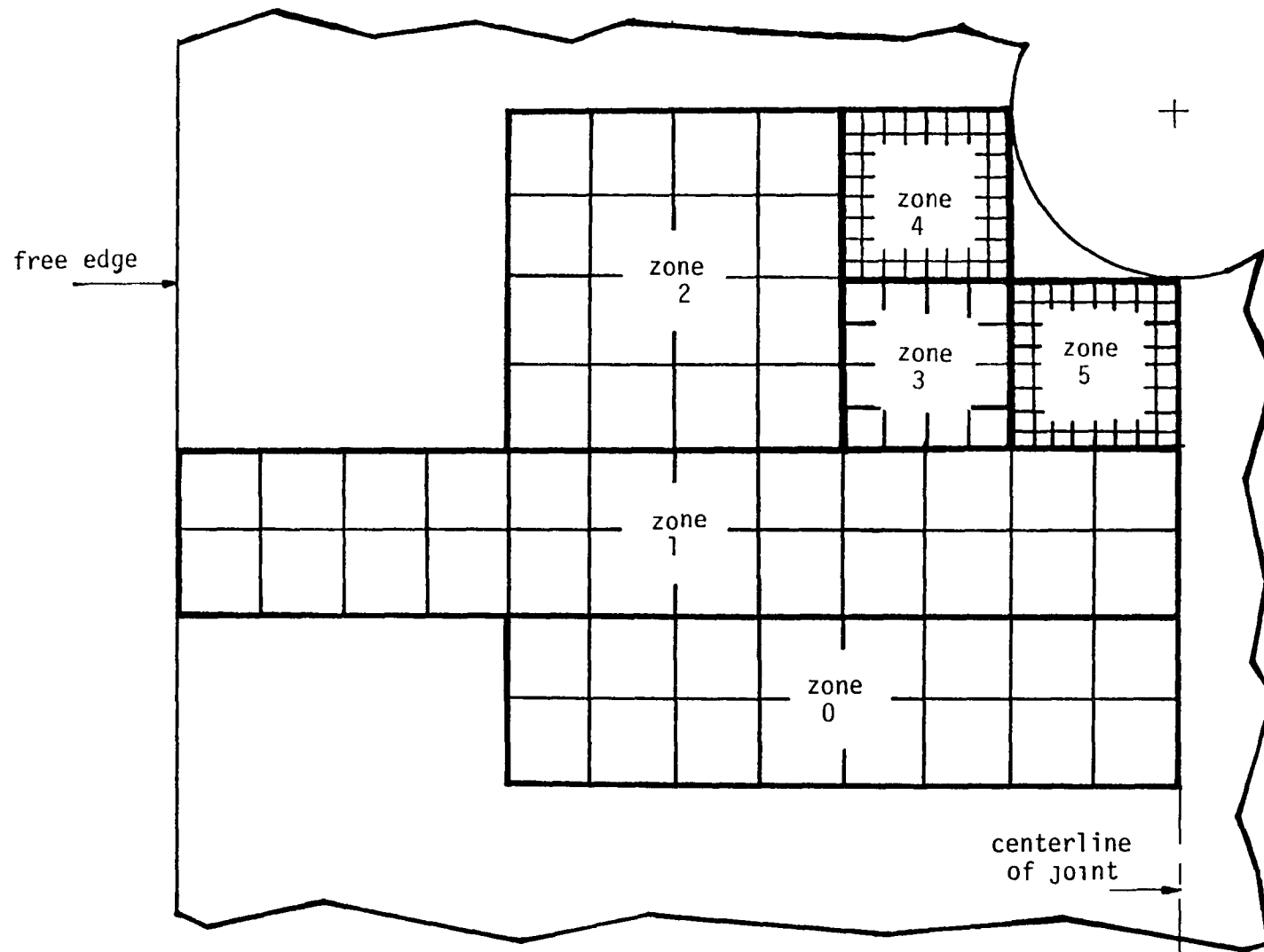
Fig. 17 System of finite-difference zones around hole region
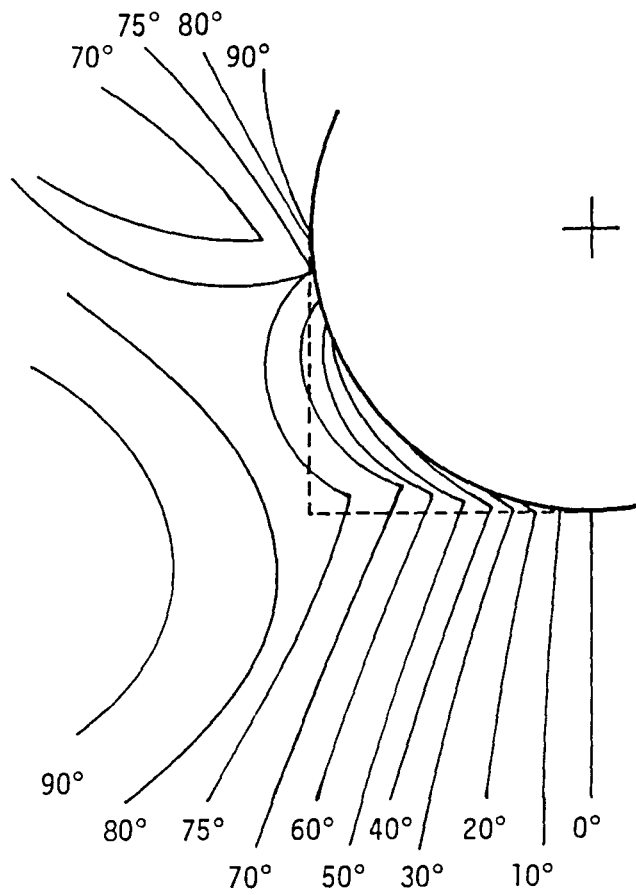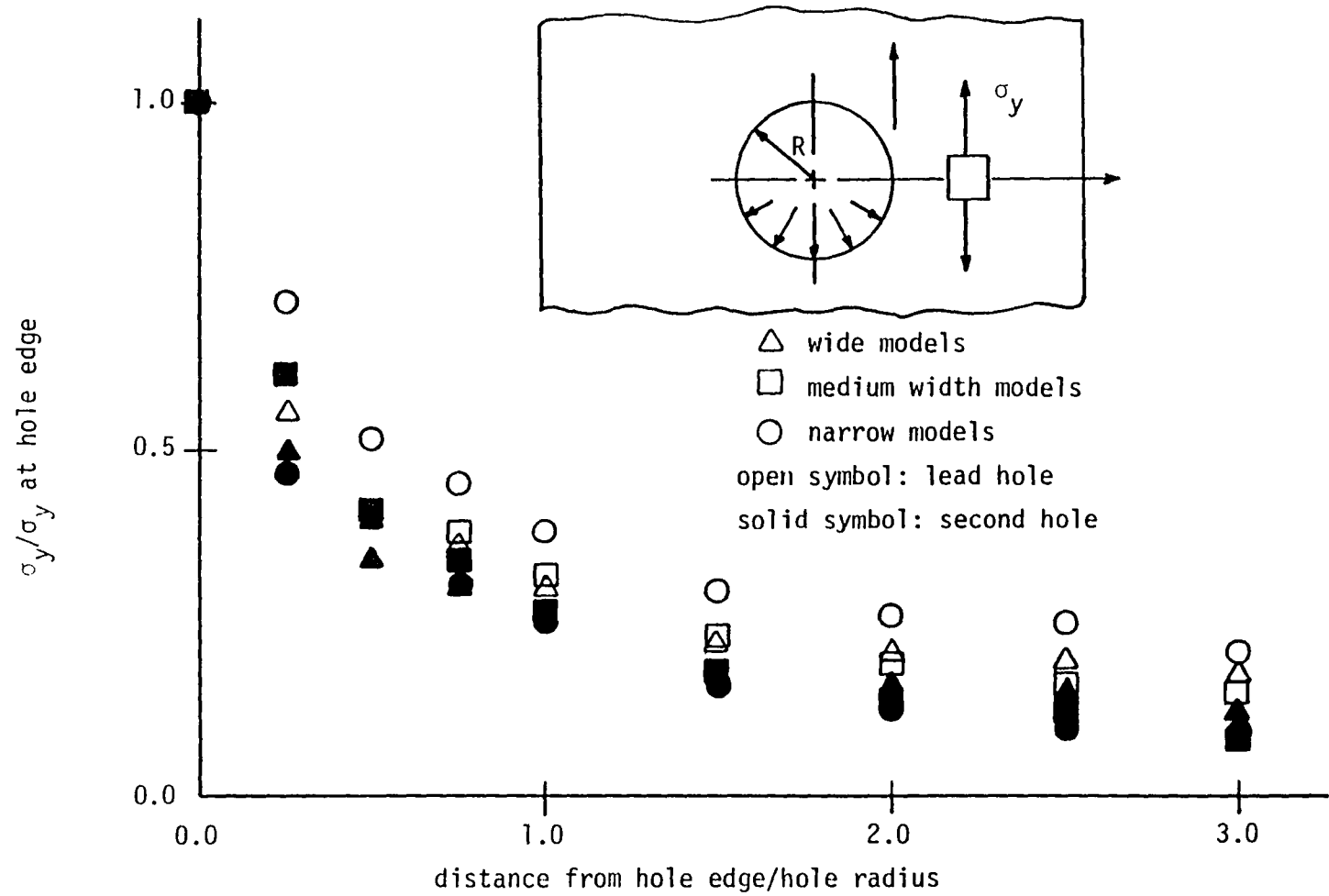
Fig. 18   Isoclinic fringe pattern around hole

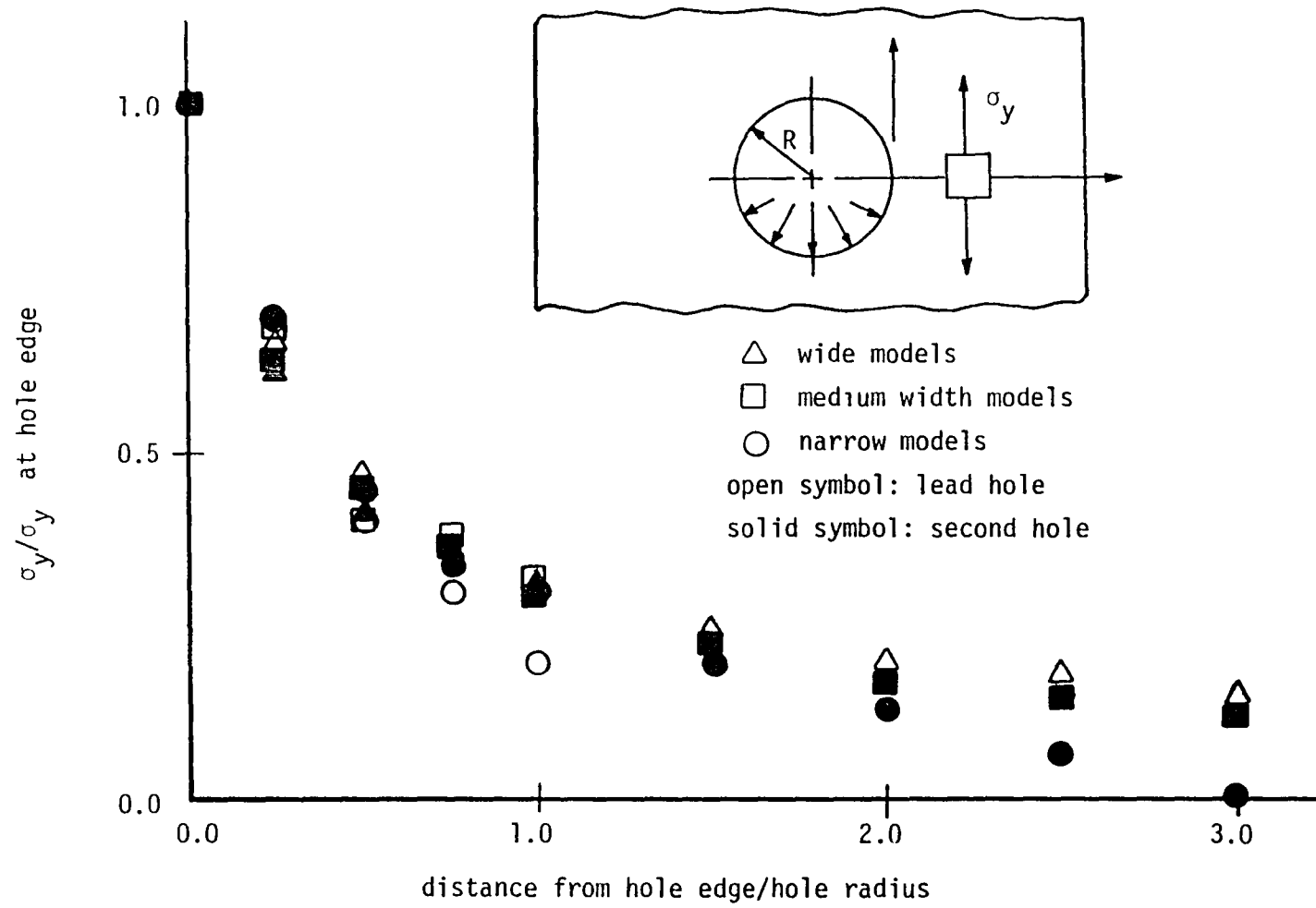Fig. 19 Stress gradients at net-section, long models

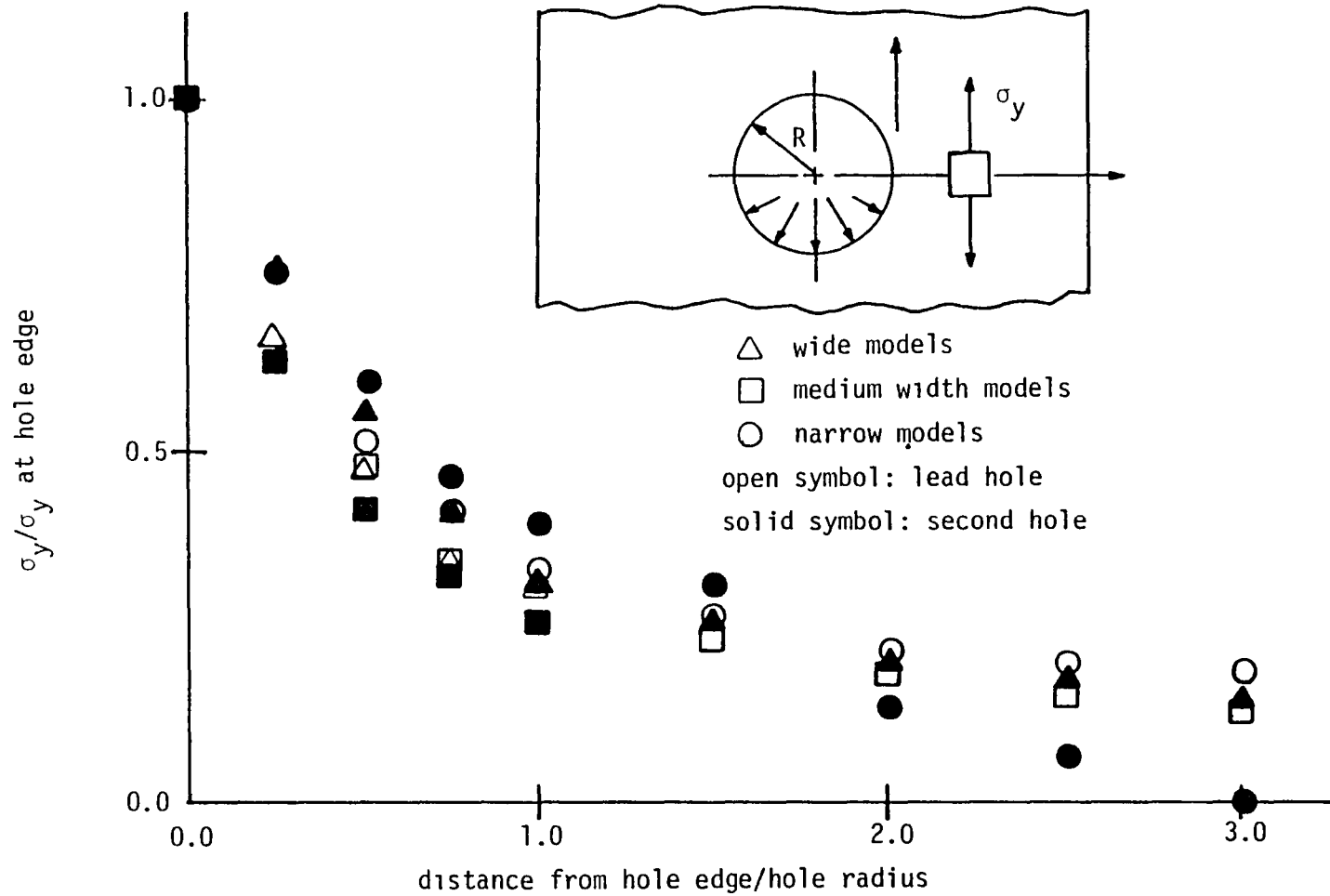Fig. 20 Stress gradients at net-section, medium length models

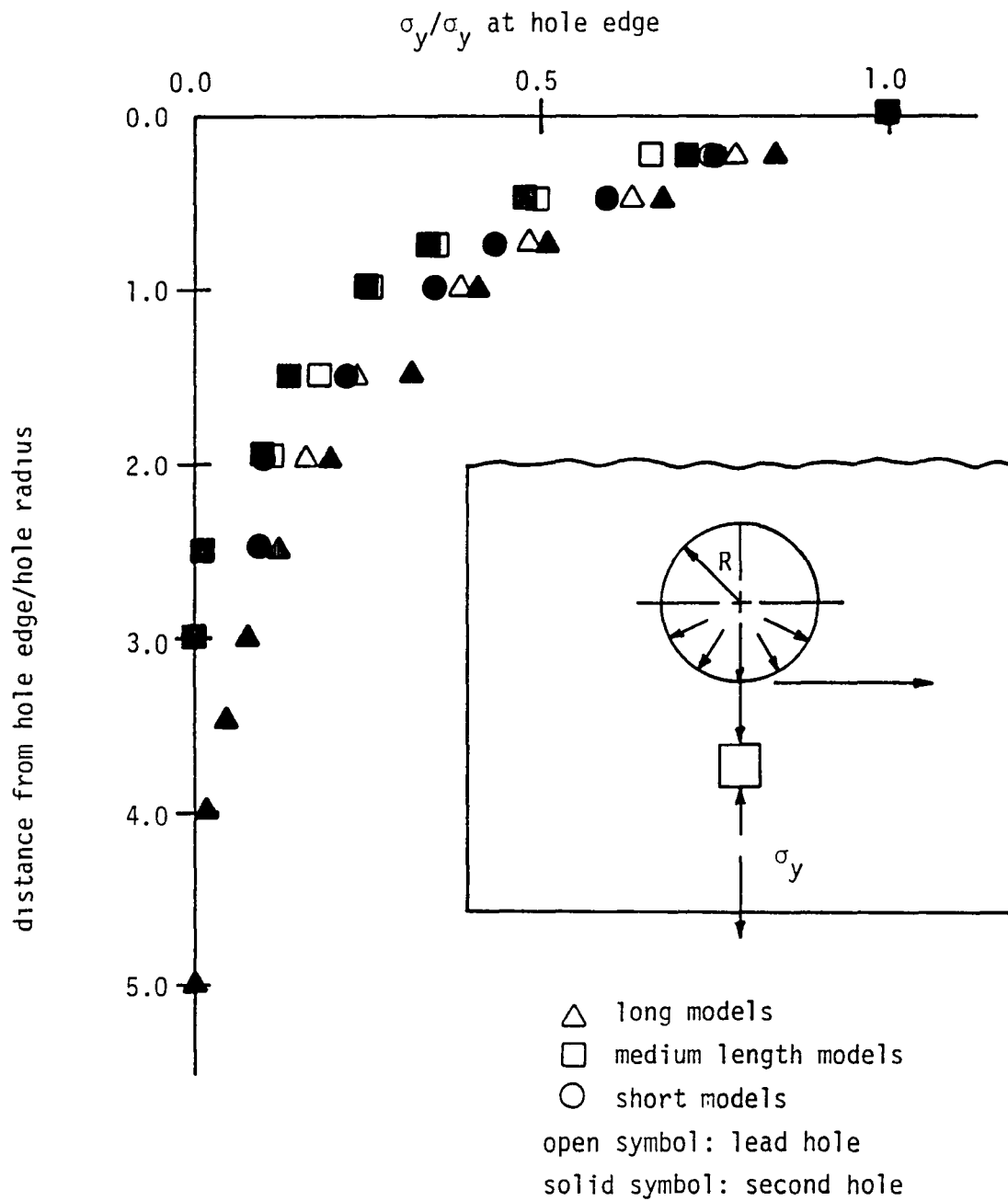Fig. 21 Stress gradients at net-section, short models

78
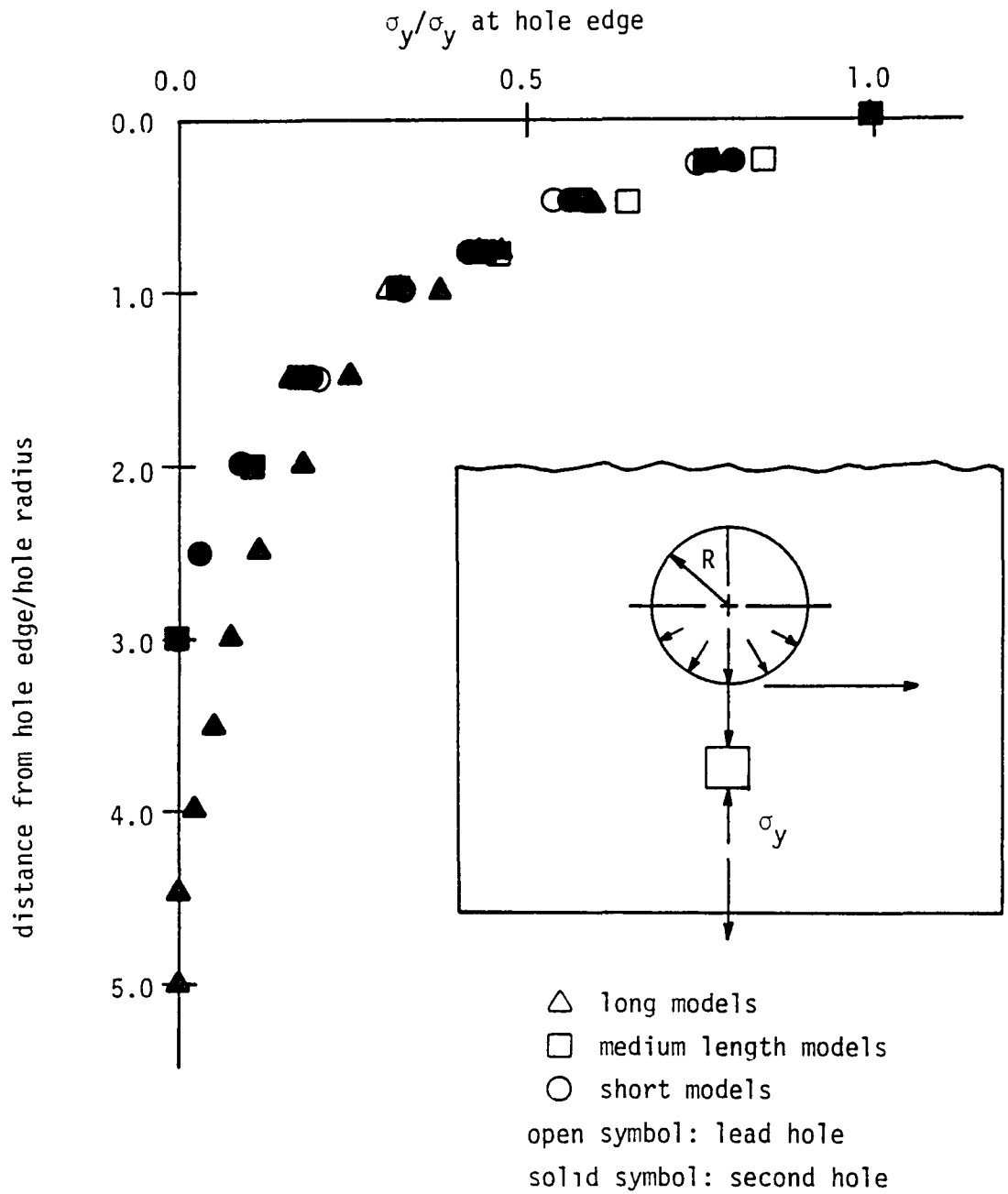
Fig. 22 Stress gradients along centerline, wide models

79

Fig. 23 Stress gradients along centerline, medium width models

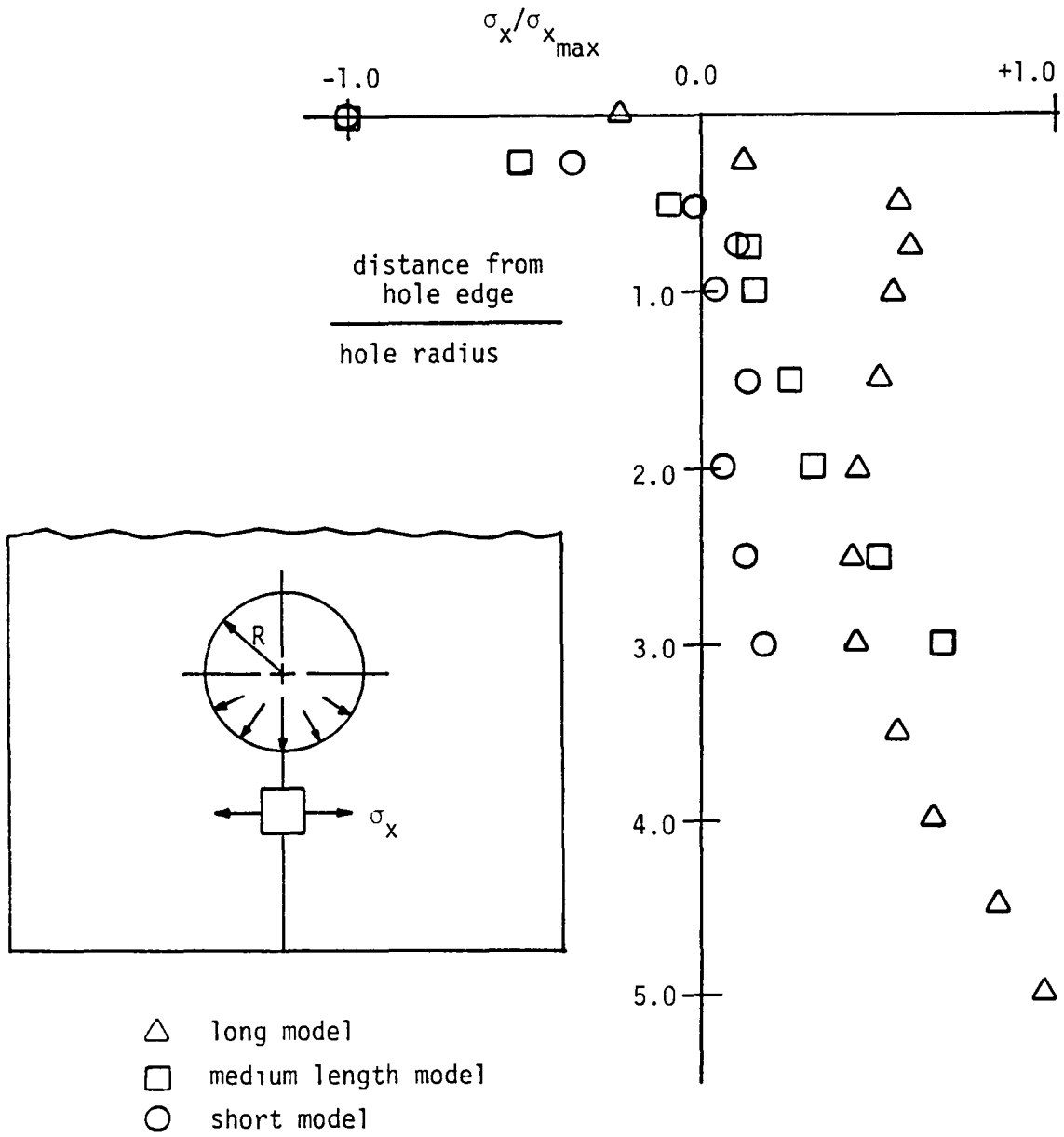Fig. 24 Stress gradients along centerline, narrow models

81

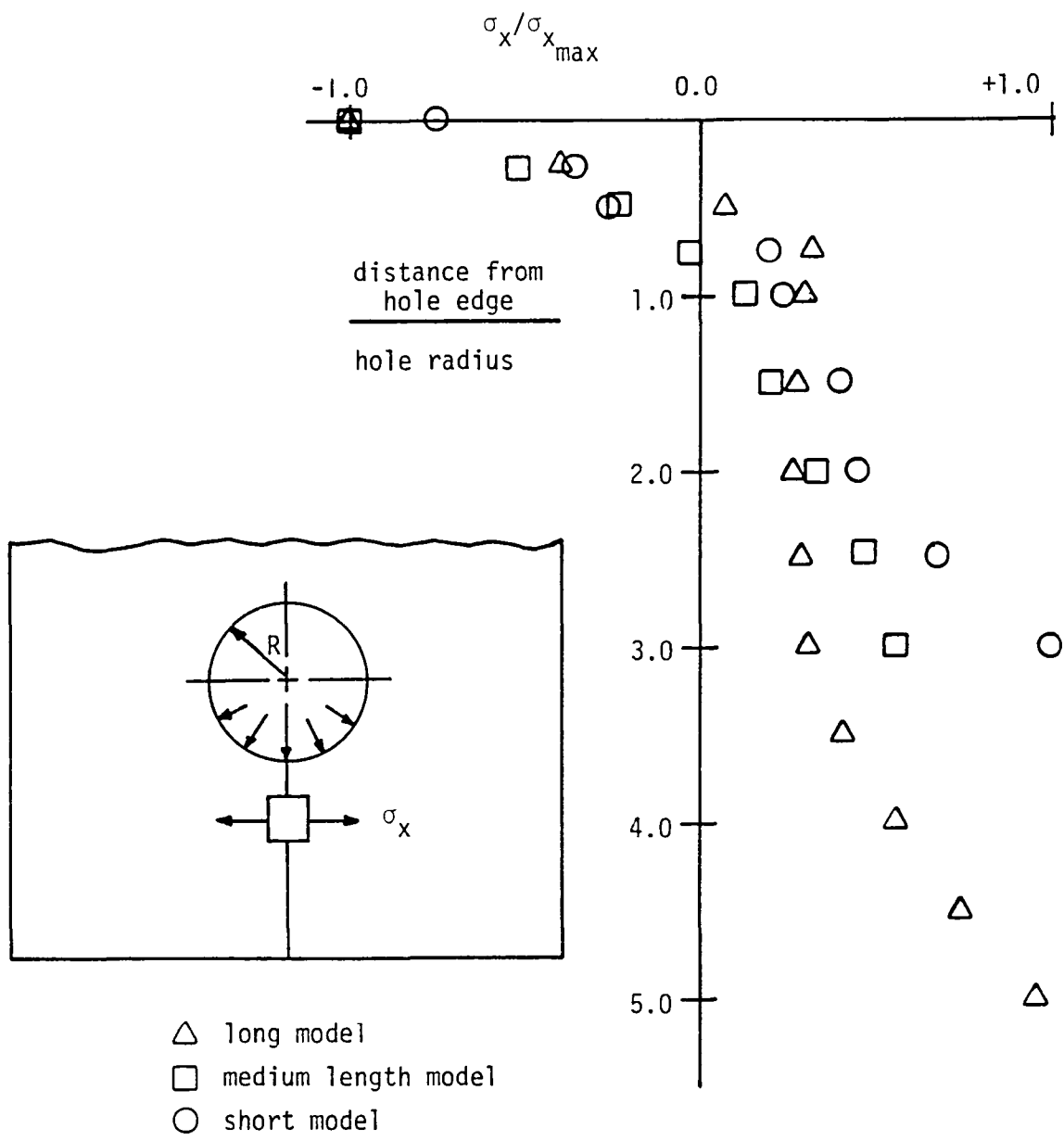Fig. 25   Splitting stress below second hole, wide models

Fig. 26 Splitting stress below second hole, medium width models
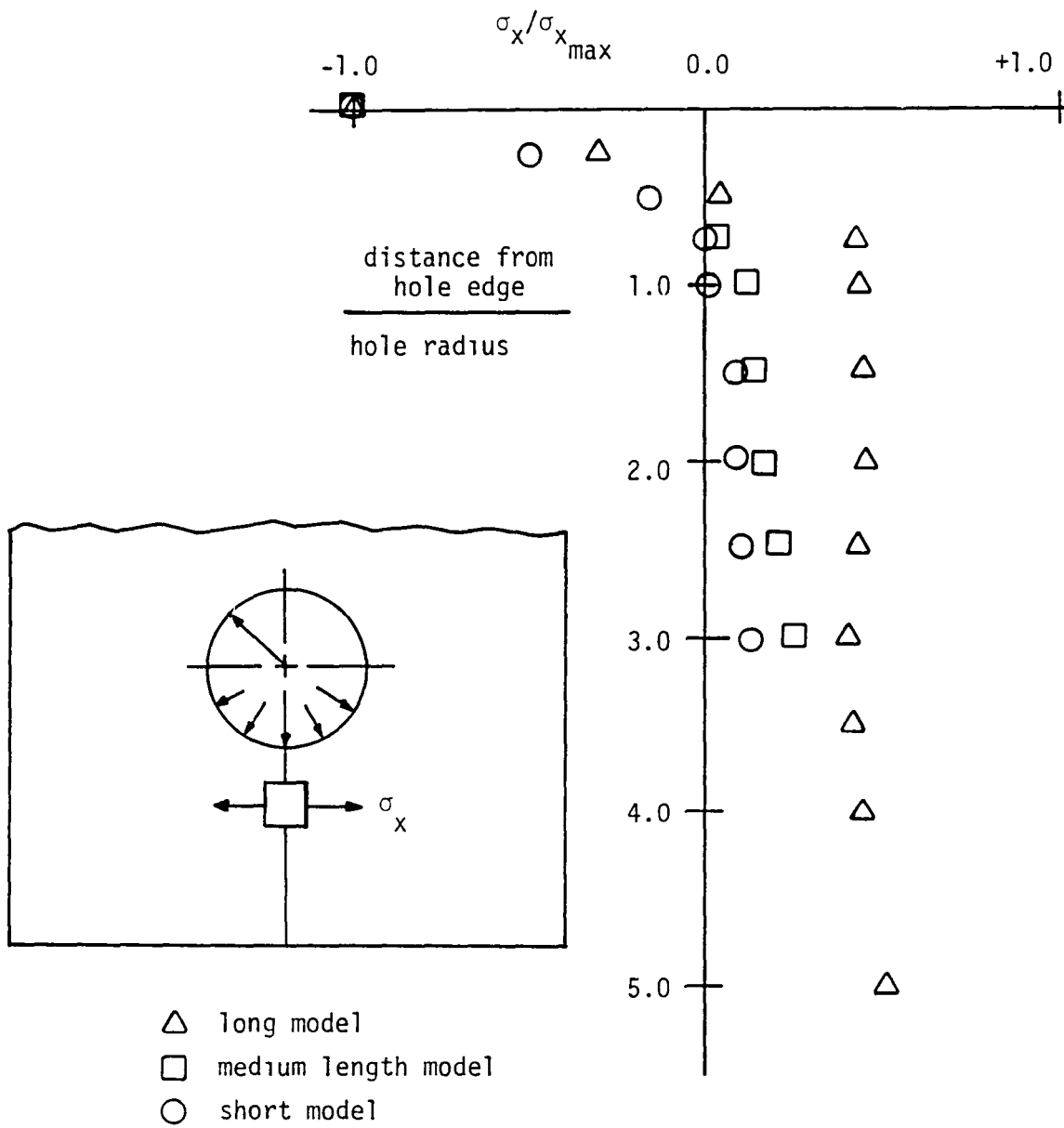
Fig. 27 Splitting stress below second hole, narrow models
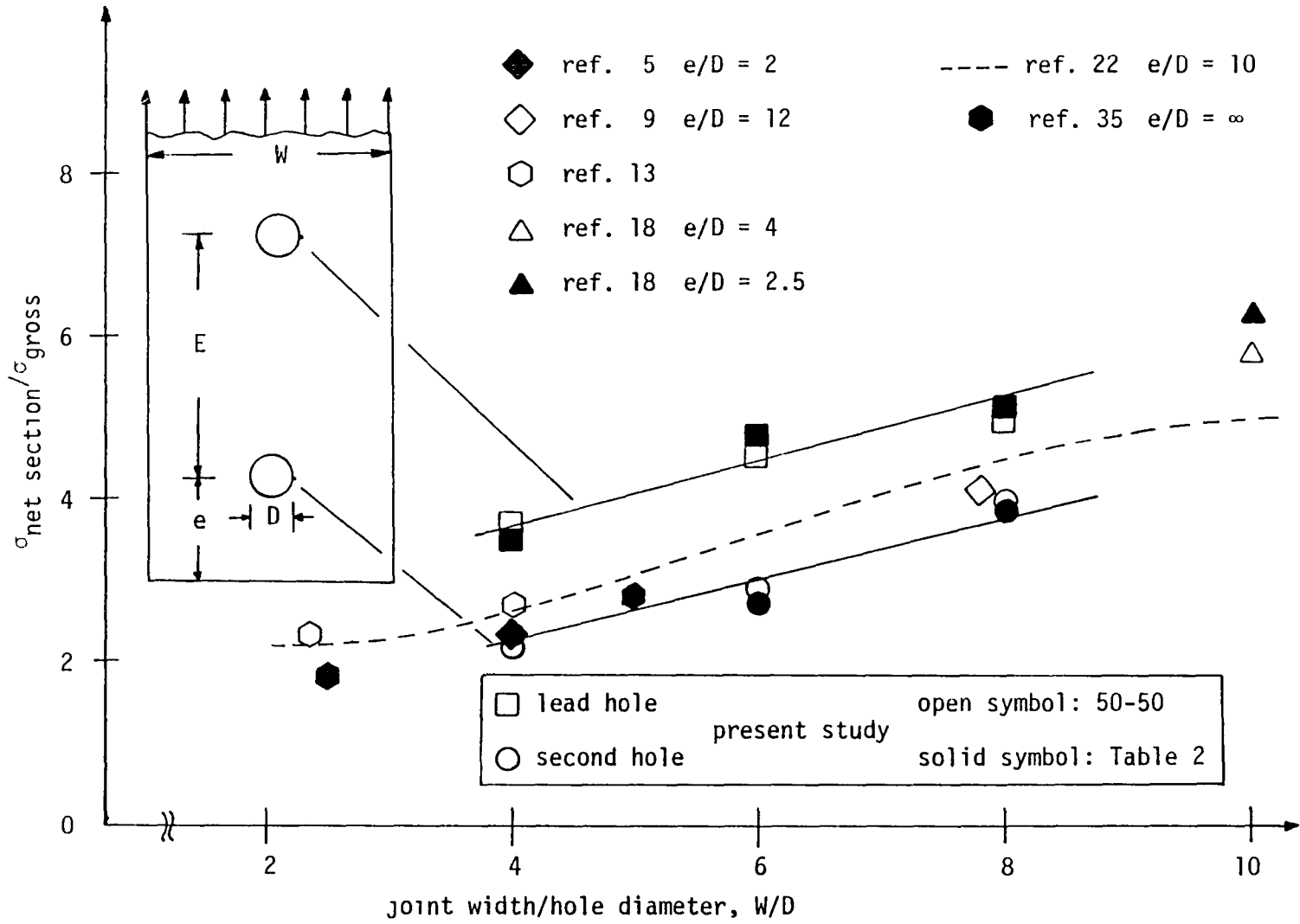
Fig. 28 Net-section stress concentration factors, long models
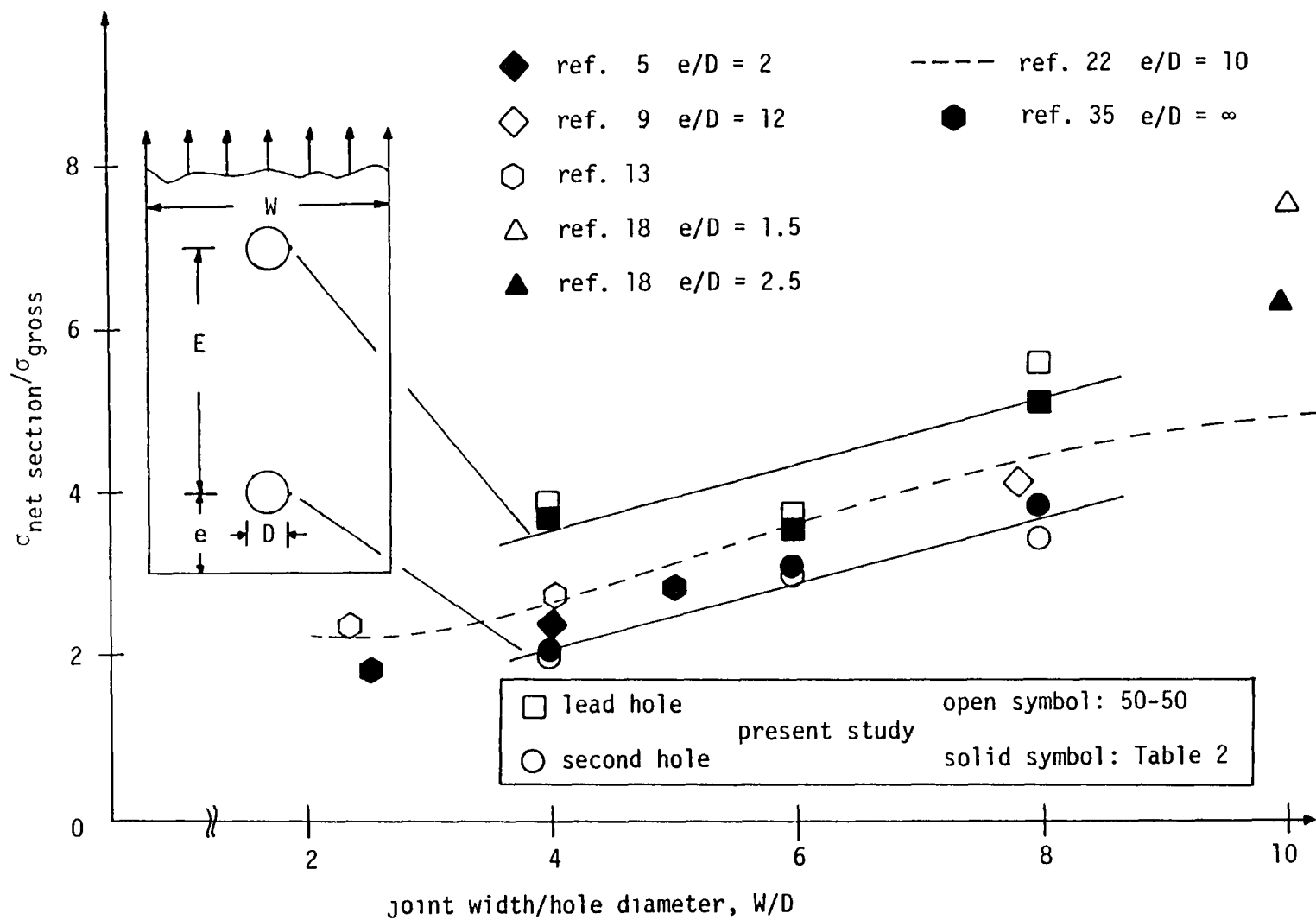
Fig. 29   Net-section stress concentration factors, medium length models
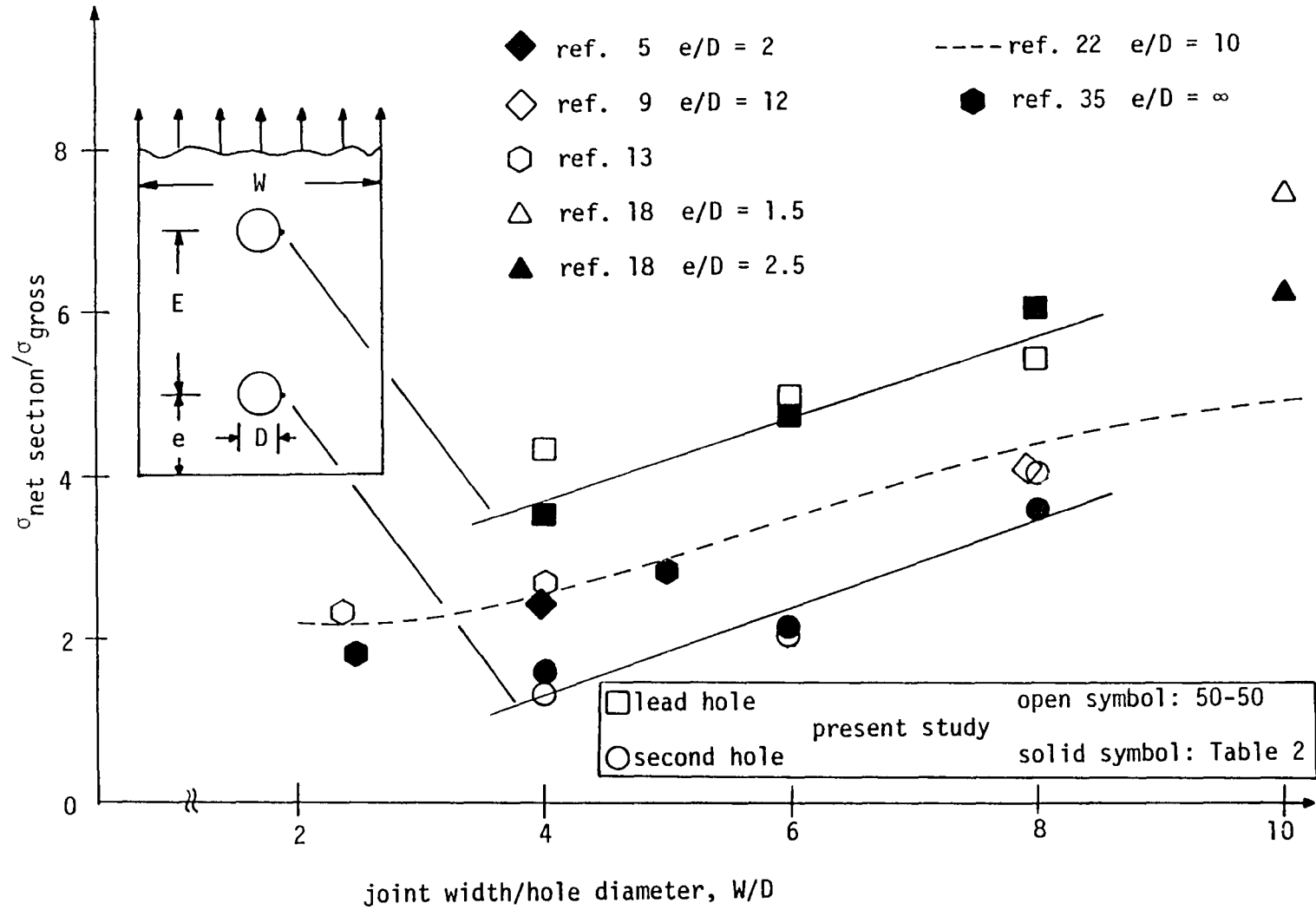
Fig. 30 Net-section stress concentration factors, short models
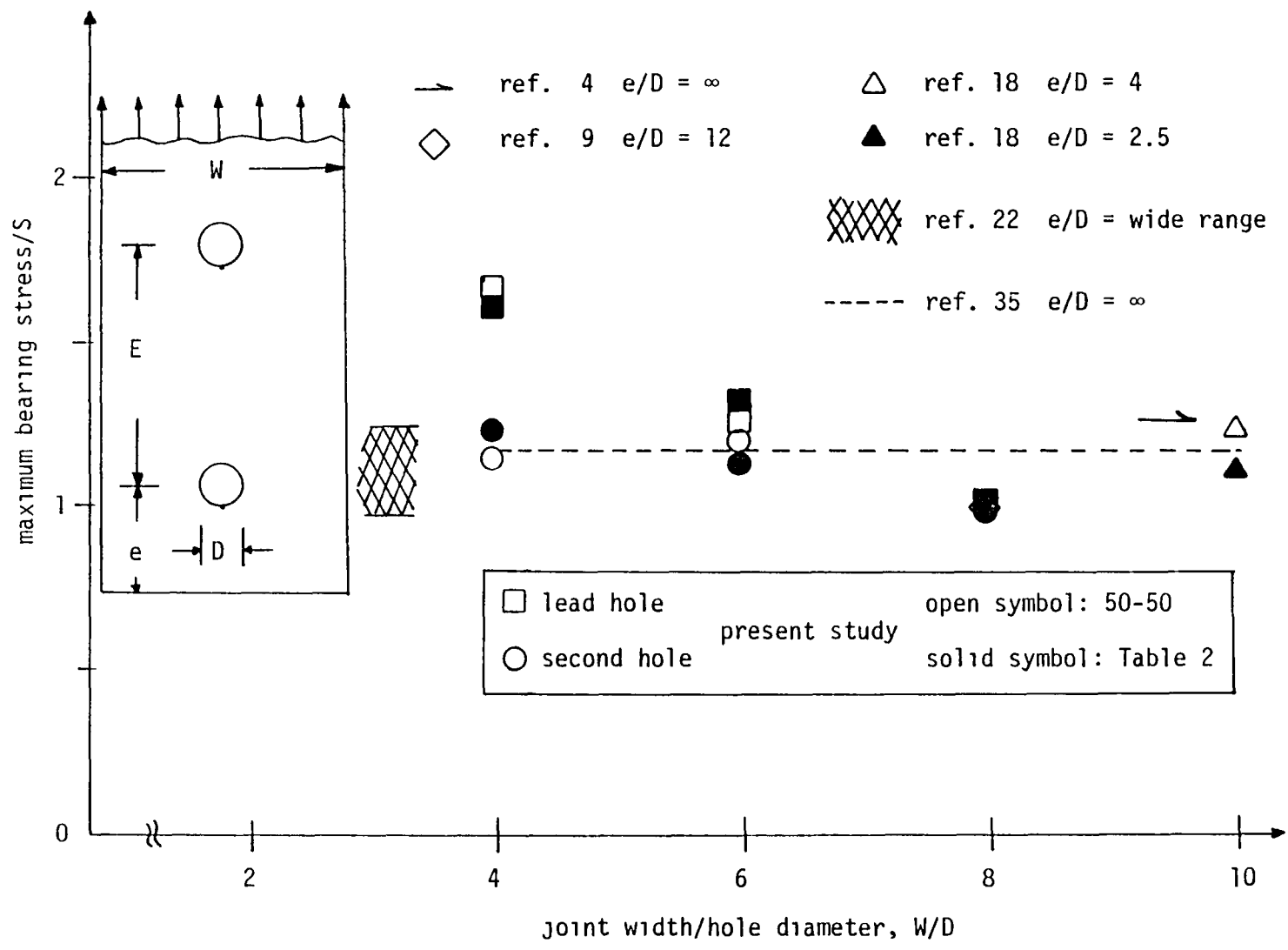
Fig. 31   Bearing stress stress concentration factors, long models
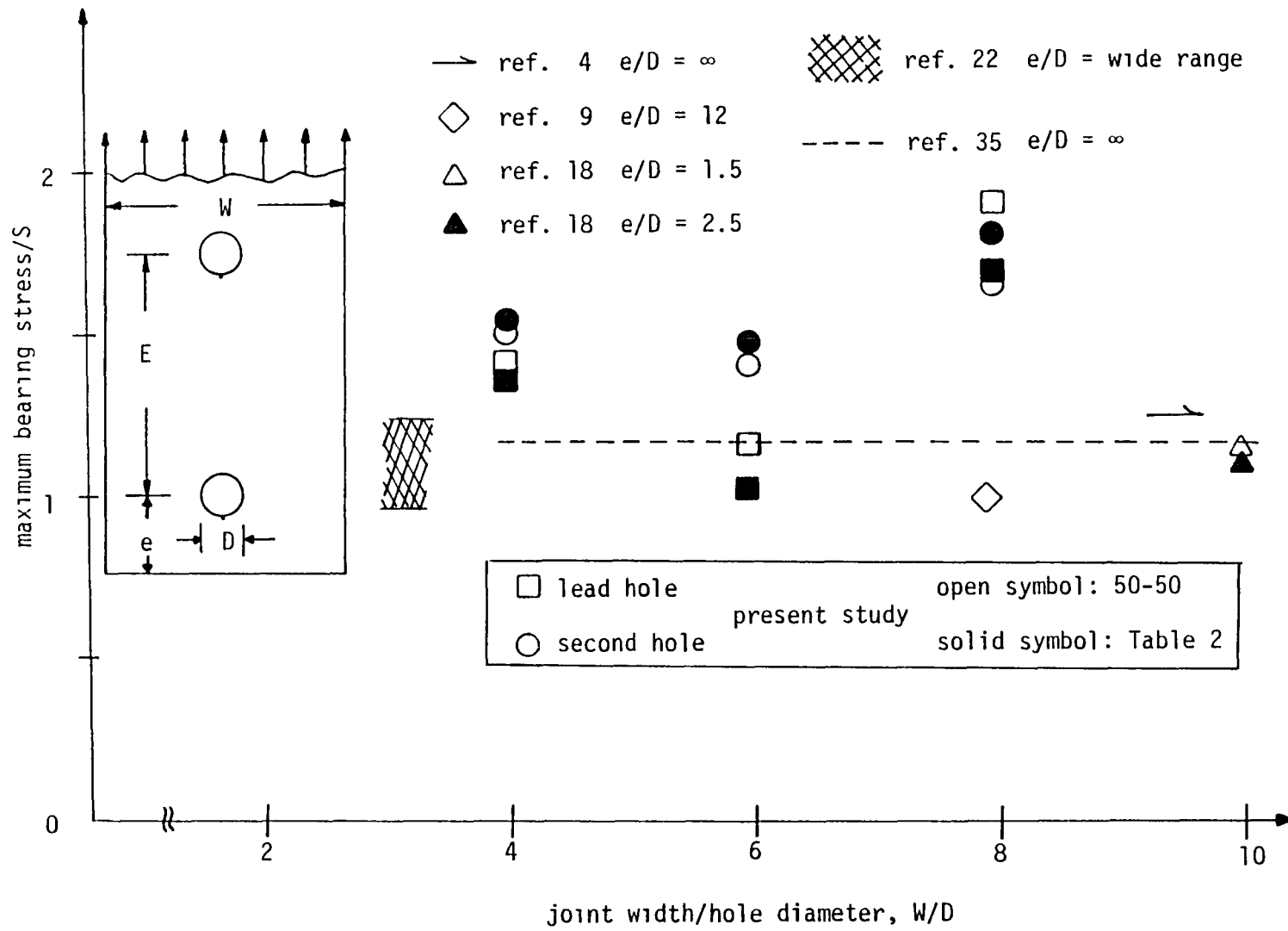
Fig. 32 Bearing stress stress concentration factors, medium length models
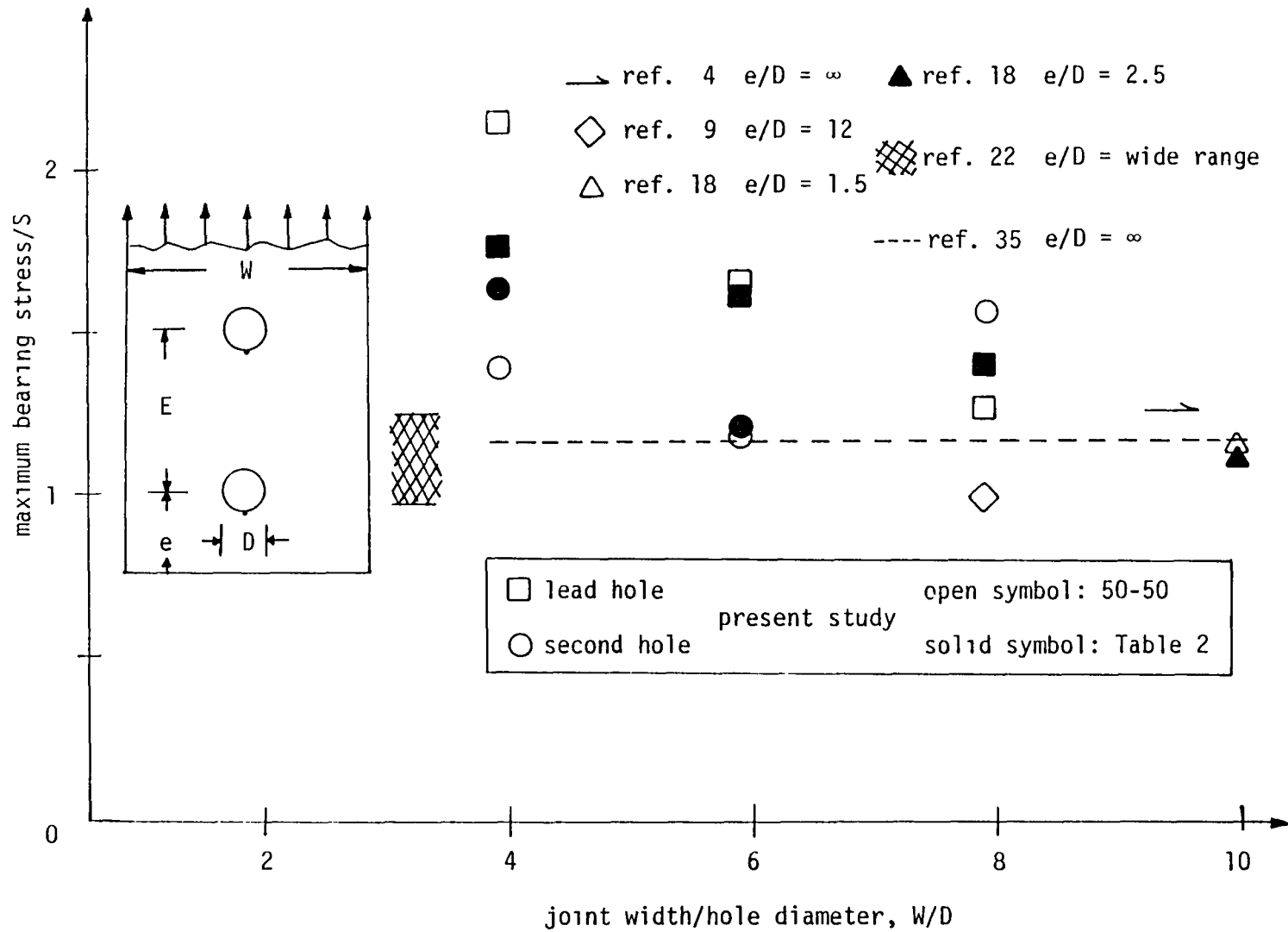
Fig. 33 Bearing stress stress concentration factors, short models
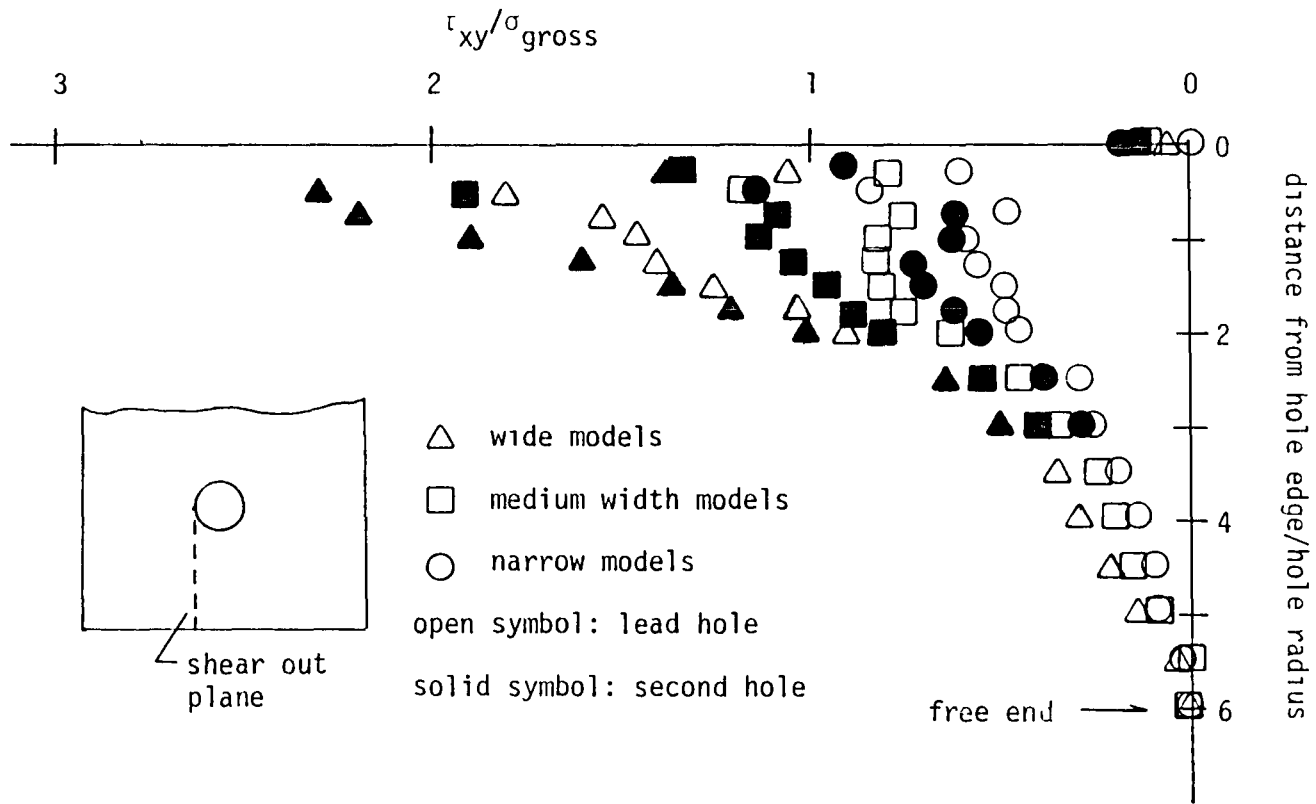
Fig. 34 Shear stress along shear-out plane, long models
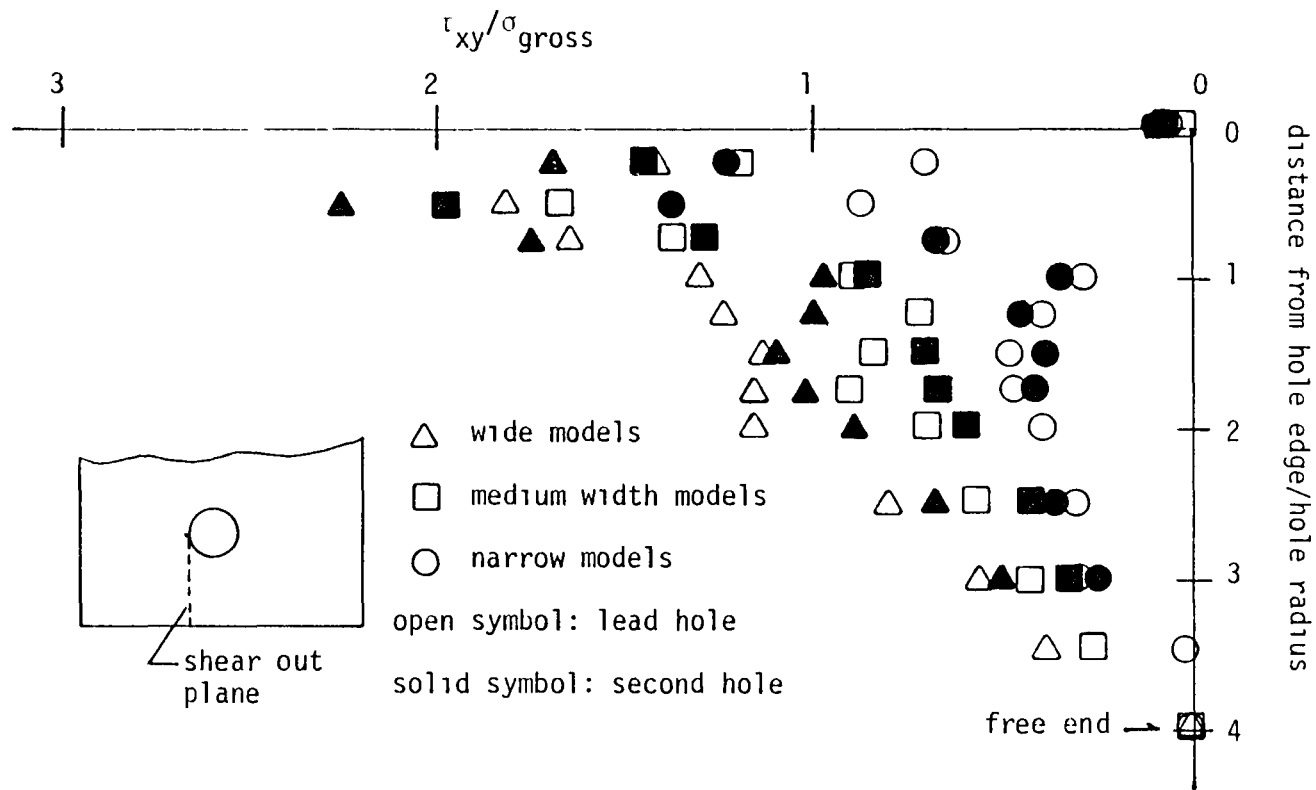
Fig. 35 Shear stress along shear-out plane, medium length models

92
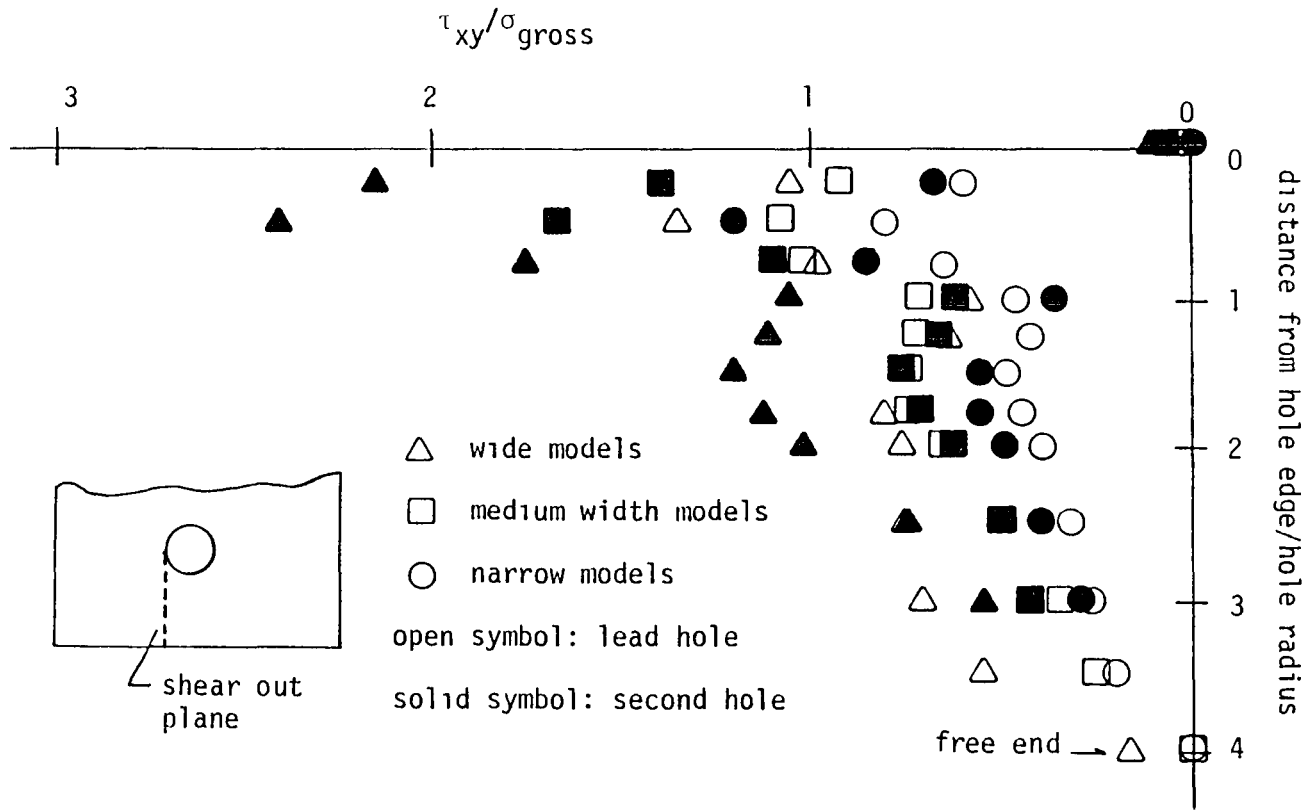
Fig. 36 Shear stress along shear-out plane, short models
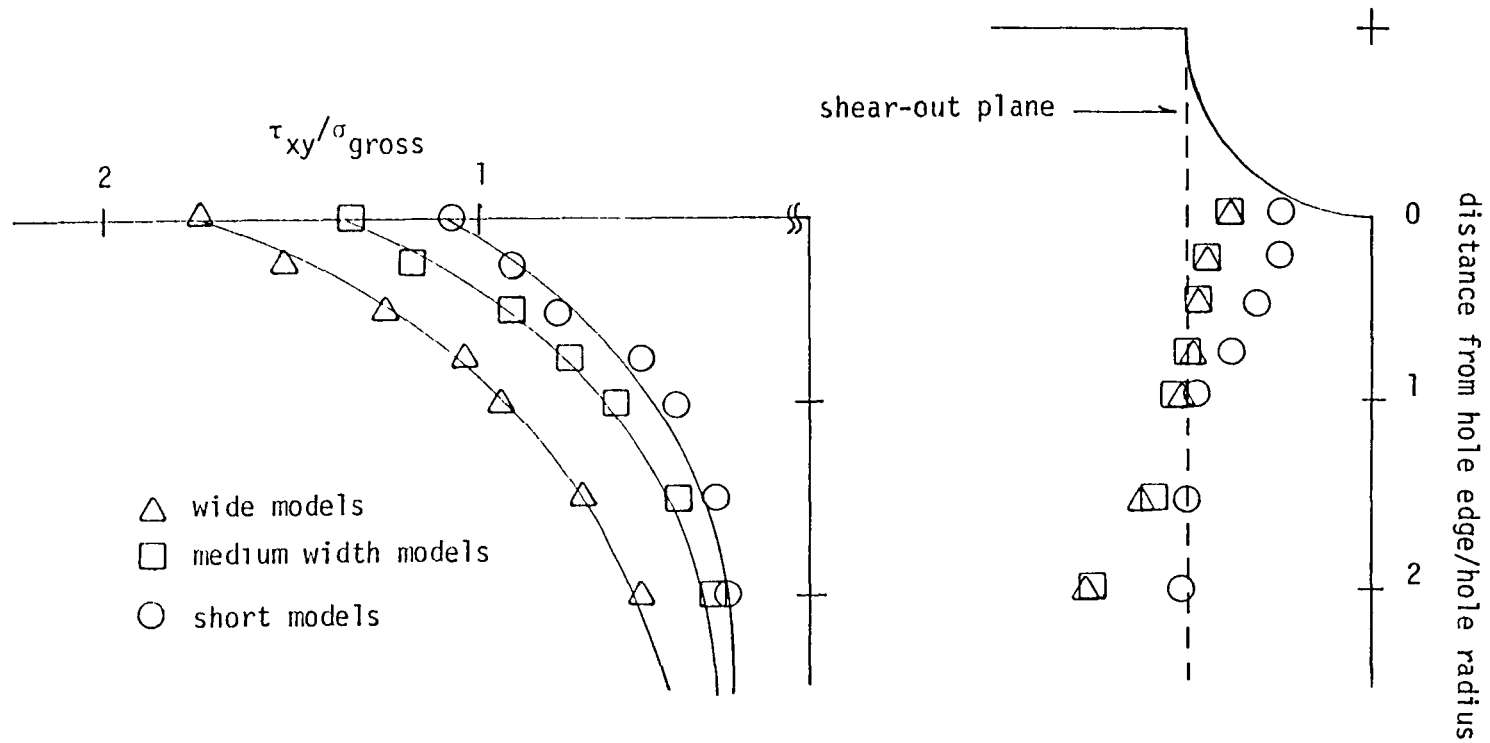
Fig. 37 Shear stress along maximum shear locus, long models

94
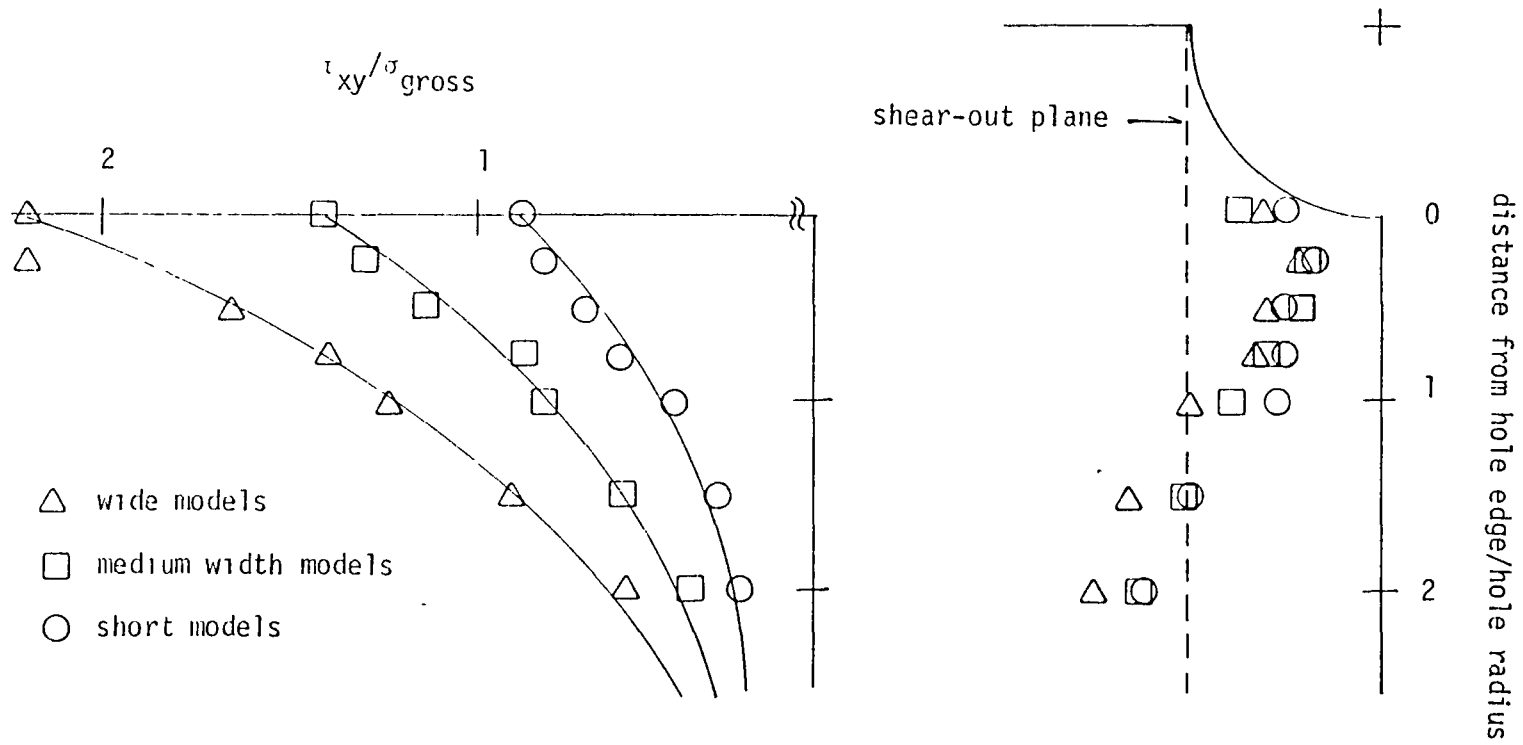
Fig. 38 Shear stress along maximum shear stress locus, medium length models

95

$^{\tau}xy/^{\sigma}gross$

2   1

△ wide models

☐ medium width models

○ short models

shear-out plane ⟶

0

1

2

distance from hole edge/hole radius
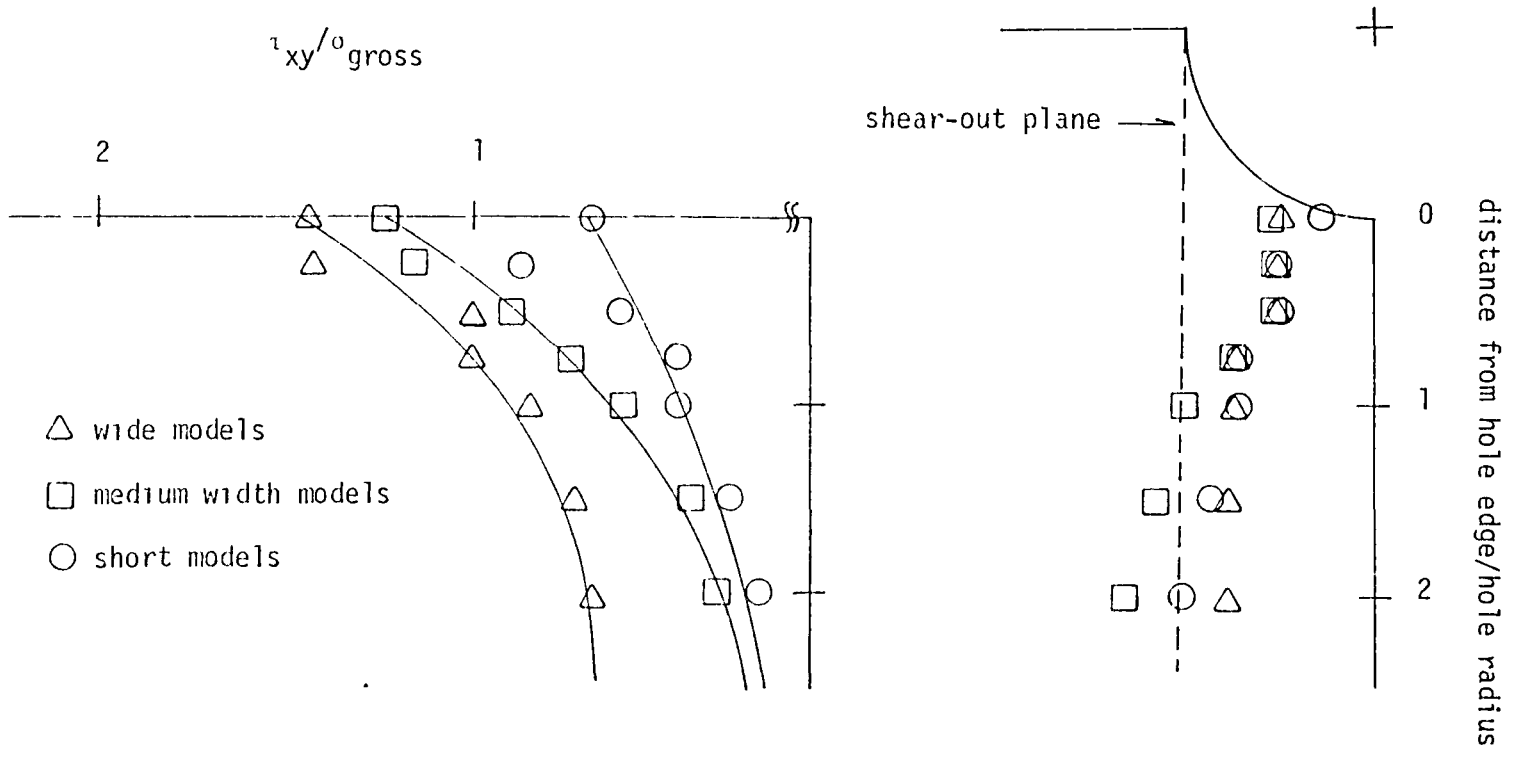
Fig. 39 Shear stress along maximum shear locus, short models

APPENDIX A

BRIEF OVERVIEW OF PHOTOELASTICITY

When light passes from air into a transparent solid, its velocity decreases. Certain transparent materials have the property that if the light vector enters the material in a specific direction the velocity decreases even more than if the light vector were oriented 90° to that direction. Since the phenomenon is related to the orientation of the light vector, polarized light is used so this direction can be controlled. The property of having two propogation velocities in a single material is called birefringence, the prefix 'bi' referring to the two possible speeds. When the light reemerges into the air, certain light wave trains are out of phase with each other because of the different velocities while in the materials. If the reemergent light is viewed with the proper optical elements, these two wave trains can be made to interfere. If the phase shift of these two wave trains is just right, there is destructive interference and no light appears to emerge from the birefringent material. Most all transparent materials exhibit birefringence to some degree. However, there are certain materials that exhibit birefringence which varies strongly when they are subjected to stress. If one of these birefringent materials is stressed so the stresses vary throughout and polarized light is passed through it, an observer will see patterns of dark and light fringes. These fringes correspond to the locus of points where the stress level in the material is such as to cause destructive and constructive interference. Prior calibration will allow determination of those stress levels which cause

interference. Thus the fringe pattern can be interpreted in terms of stresses.

Photoelasticity as just described allows direct measurement of two quantities, (1) difference in principal stresses $(\sigma_1 - \sigma_2)$ and (2), orientation of the principal stresses. In two-dimensional plane stress problems, to completely describe the stress state three quantitites must be known: σ_1, σ_2 and the principal stress direction, or; σ_x, σ_y and τ_{xy}. Photoelasticity does not directly give a third quantity. In many applications the maximum stress occurs at a free boundary where one of the principal stresses is zero. The other principal stress can then be determined directly from the fringe count. When it is required to know the state of stress at a point where neither of the principal stresses is zero, a third piece of information is required. This third piece of information can be obtained experimentally, or it can be the enforcement of one or more of the equations of elasticity. The determination of σ_x, σ_y, and τ_{xy} is referred to as the separation of stresses.

APPENDIX B

ISOCHROMATIC FRINGE NUMBER (N) AND PRINCIPAL
STRESS DIRECTION (θ) NEAR SECOND HOLE IN SHORT NARROW MODEL

The isochromatic fringe information, N, and the isoclinic fringe information, θ, at each point for the short narrow model is presented in this appendix. These data are typical of the data for all models.

For convenience, the data are grouped by the zones used in the finite-difference calculations. The grid points are identified by the letter/number system shown on the accompanying diagram.

zone 5

zone 4

zone 3

zone 2

zone 1

zone 0

Q P O N M L K J I — H G F E D C B A

R   S   T   U

1 2 3 4 5 6 7 8

9 10 11 12 13 14 15 16 17 18 19 20 21

100
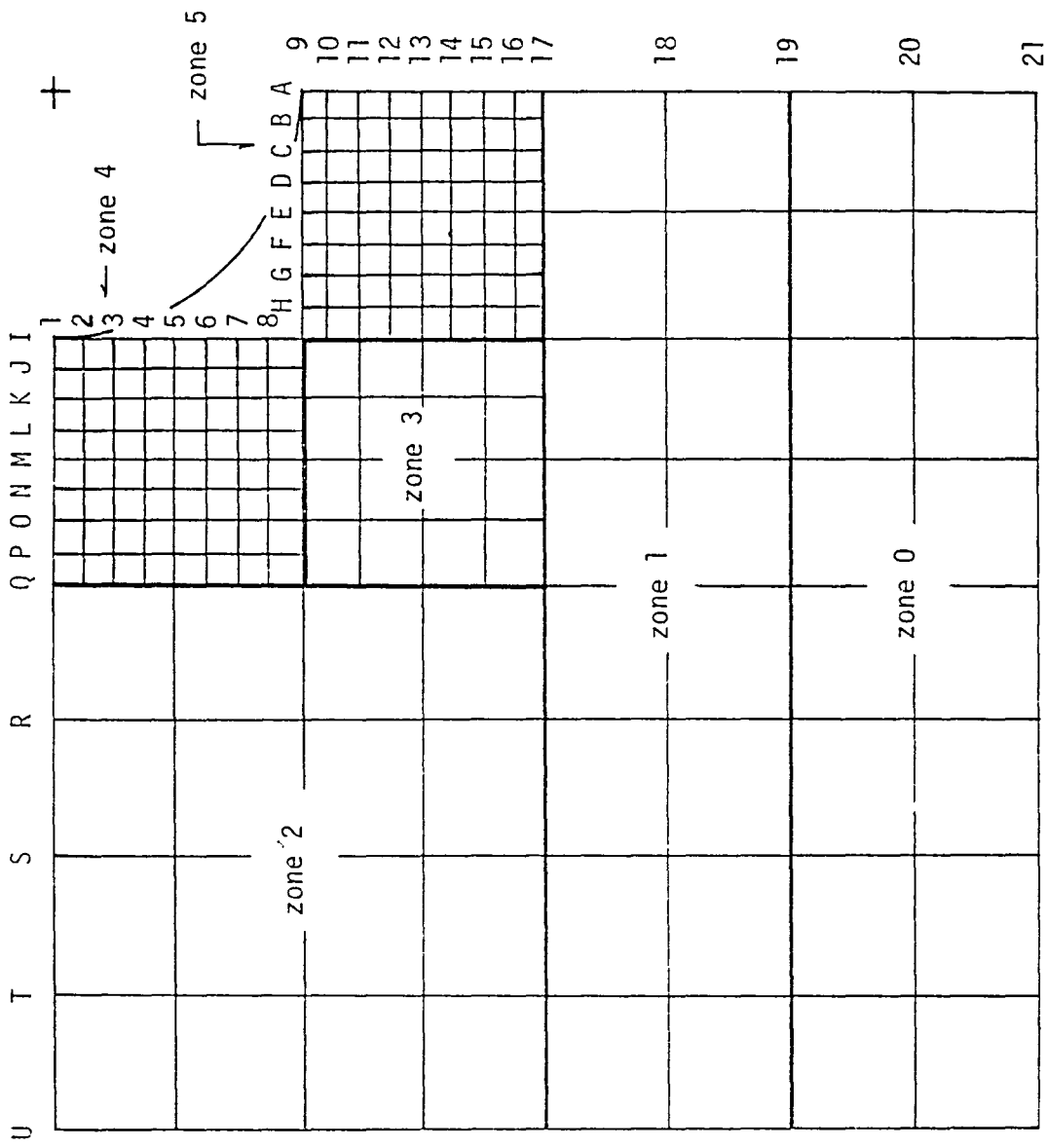
Zone 3		I	K	M	O	Q
9	N	2.91	2.31	1.72	1.43	1.18
	θ	72.10	74.00	79.40	83.60	87.30
11	N	2.40	2.15	1.65	1.40	1.22
	θ	74.50	80.00	85.20	89.50	93.50
13	N	2.13	1.89	1.60	1.39	1.20
	θ	65.20	74.00	78.00	81.00	82.40
15	N	1.87	1.64	1.42	1.27	1.15
	θ	58.20	65.30	70.00	72.40	76.30
17	N	1.63	1.54	1.40	1.27	1.09
	θ	58.20	61.30	66.00	68.50	71.70

Zone 4		I	J	K	L	M	N	O	P	Q
1	N	3.50	2.57	1.85	1.50	1.33	1.16	1.00	0.91	0.87
	θ	90.00	87.80	85.50	83.20	81.00	78.80	76.50	74.20	72.00
2	N	3.91	2.85	2.02	1.58	1.36	1.19	1.04	0.95	0.89
	θ	80.00	70.40	77.60	78.80	78.00	76.70	75.40	74.10	72.80
3	N	4.13	3.04	2.17	1.68	1.42	1.23	1.08	0.98	0.91
	θ	72.30	73.00	73.60	74.30	75.00	74.60	74.30	74.00	73.60
4	N	4.05	3.07	2.28	1.80	1.52	1.30	1.12	1.01	0.95
	θ	66.70	67.50	68.80	70.10	78.50	72.20	73.00	73.70	74.50
5	N	3.79	2.99	2.33	1.90	1.62	1.37	1.17	1.05	0.98
	θ	60.00	62.00	64.00	66.00	68.00	69.80	71.60	73.50	75.30
6	N	3.53	2.88	2.33	1.95	1.68	1.43	1.22	1.09	1.01
	θ	59.00	62.90	66.50	68.70	70.90	72.70	74.60	76.50	78.30
7	N	3.30	2.77	2.31	1.97	1.71	1.45	1.28	1.13	1.04
	θ	58.50	63.80	69.90	71.40	73.70	75.60	77.60	79.50	81.30
8	N	3.10	2.69	2.30	1.98	1.72	1.51	1.35	1.21	1.10
	θ	68.40	68.40	71.50	74.10	76.50	78.00	80.60	82.50	84.30
9	N	2.91	2.62	2.31	1.99	1.72	1.55	1.43	1.31	1.18
	θ	72.10	73.00	74.00	76.70	79.40	81.50	83.60	85.50	87.30

Zone 0		A	E	I	M	Q	R	S	T	U
19	N	1.01	1.07	1.07	0.96	0.74	0.49	0.28	0.10	0.00
	θ	0.00	14.00	31.20	43.20	48.00	52.00	57.00	84.00	90.00
20	N	1.17	1.05	0.91	0.73	0.55	0.37	0.20	0.03	0.00
	θ	0.00	7.00	23.00	35.00	38.00	41.00	42.00	80.00	90.00
21	N	1.63	1.50	1.09	0.73	0.50	0.30	0.01	0.00	0.00
	θ	0.00	0.00	0.00	0.00	0.00	0.00	0.00	0.00	0.00

Zone 1		A	E	I	M	Q	R	S	T	U
17	N	1.74	1.71	1.63	1.40	1.09	0.72	0.40	0.17	0.00
	θ	0.00	30.00	58.00	66.00	71.70	81.50	86.50	90.00	90.00
18	N	1.36	1.33	1.27	1.15	0.92	0.62	0.35	0.16	0.00
	θ	0.00	21.50	38.00	50.50	57.00	63.00	75.00	84.00	90.00
19	N	1.01	1.07	1.07	0.96	0.74	0.49	0.28	0.10	0.00
	θ	0.00	14.00	31.20	43.20	48.00	52.00	57.00	84.00	90.00

Zone 2		Q	R	S	T	U
1	N	0.87	0.65	0.47	0.19	0.00
	θ	72.00	72.00	72.00	90.00	90.00
5	N	0.98	0.68	0.43	0.21	0.00
	θ	75.30	78.50	80.20	90.00	90.00
9	N	1.18	0.77	0.47	0.23	0.00
	θ	87.30	90.00	90.00	90.00	90.00
13	N	1.20	0.82	0.44	0.19	0.00
	θ	82.40	88.00	90.00	90.00	90.00
17	N	1.09	0.72	0.40	0.17	0.00
	θ	71.7	81.50	86.50	90.00	90.00

Zone 5		A	B	C	D	E	F	G	H	I
9	N	3.43	3.18	3.11	3.31	3.52	3.49	3.31	3.10	2.91
	θ	0.00	6.30	36.20	41.60	42.00	50.20	65.50	65.10	72.10
10	N	3.20	3.04	2.98	3.08	3.19	3.14	2.98	2.80	2.63
	θ	0.00	18.00	40.50	57.20	64.20	66.00	68.20	70.00	77.50
11	N	3.00	2.91	2.86	2.88	2.90	2.83	2.70	2.55	2.40
	θ	0.00	13.30	32.33	44.30	56.50	63.90	67.20	71.00	74.50
12	N	2.83	2.78	2.74	2.72	2.69	2.61	2.50	2.38	2.25
	θ	0.00	10.20	28.70	38.20	50.50	67.00	63.80	67.00	71.20
13	N	2.63	2.61	2.58	2.55	2.50	2.44	2.35	2.25	2.13
	θ	0.00	11.40	25.20	33.20	44.20	51.00	58.30	62.10	65.20
14	N	2.37	2.36	2.35	2.33	2.30	2.25	2.20	2.10	2.00
	θ	0.00	10.10	22.30	29.20	40.00	46.90	54.00	57.70	62.10
15	N	2.10	2.11	2.11	2.10	2.09	2.06	2.02	1.95	1.87
	θ	0.00	8.40	18.20	27.00	35.40	42.30	49.30	55.30	58.20
16	N	1.90	1.90	1.91	1.90	1.90	1.88	1.85	1.80	1.75
	θ	0.00	8.50	16.90	23.50	33.60	41.00	45.20	52.30	56.00
17	N	1.74	1.74	1.73	1.72	1.71	1.70	1.68	1.66	1.63
	θ	0.00	7.10	13.60	22.10	31.90	28.10	44.20	48.00	58.20

1 Report No NASA CR-165812	2 Government Accession No	3 Recipient's Catalog No

4 Title and Subtitle Use of Two-Dimensional Transmission Photoelastic Models to Study Stresses in Double-Lap Bolted Joints	5 Report Date November 1981
	6 Performing Organization Code

7 Author(s) M. W. Hyer and D. H. Liu	8 Performing Organization Report No

9 Performing Organization Name and Address Department of Engineering Science and Mechanics Virginia Polytechnic Institute and State University Blacksburg, VA 24061	10 Work Unit No
	11 Contract or Grant No NSG-1621

12 Sponsoring Agency Name and Address National Aeronautics and Space Administration Washington, DC 20546	13 Type of Report and Period Covered Contractor Report April'80 - June'81
	14 Sponsoring Agency Code 505-33-33-07

16 Abstract The results of a study are described which had as goals; (1) the fabricating and testing of photoelastic models of double-lap double-hole joints designed so that the stresses in the inner lap could be determined; (2) the assessment of the effects of joint geometry on the stresses in the inner lap, and; (3) the quantifying of differences in the stresses near the two holes. The two holes were on the centerline of the joint and the joints were loaded in tension, parallel to the centerline. Acrylic slip-fit pins through the holes served as fasteners. Two-dimensional transmission photoelastic models were fabricated by using transparent acrylic outer laps and a photoelastic model material for the inner laps. The sensitivity of the outer lap material to the birefringent effect was about a factor of 20 less than the sensitivity of the inner lap material. Thus the photoelastic fringe patterns visible when the models were loaded were due almost entirely to stresses in the inner lap. Nine models were tested and analyzed, each model having a different geometry. All the models were 13 mm (0.5 in) thick, the thickness being divided evenly between the outer and inner laps. The model widths ranged from 89 to 178 mm (3.5 to 7.0 in.), the hole diameter for all models was 22.2 mm (0.875 in.), and the model lengths ranged from about 10 to about 13 hole diameters.

17 Key Words (Suggested by Author(s)) photoelastic models mechanical fasteners bolted joints quasi-isotropic composite materials stress concentration factors	18 Distribution Statement unclassified - unlimited Subject Category - 39

19 Security Classif (of this report) unclassified	20 Security Classif (of this page) unclassified	21 No of Pages 110	22 Price* A06

End of Document